AIMS Mathematics

http://www.aimspress.com/journal/Math

AIMS Mathematics, 11(7): 22845–22896.
DOI: 10.3934/math.2026921
Received: 25 April 2026
Revised: 07 July 2026
Accepted: 09 July 2026
Published: 28 July 2026

Research article

Integrating XGBoost with the new cotangent-Φ generated family of distributions: a unified frequentist-Bayesian approach with applications

Aijaz Ahmad[1], **Farouq Mohammad A. Alam**[2], **Andaç Batur Çolak**[3], **Aafaq A. Rather**[4,*] **and Mahmoud E. Bakr**[5]

[1] Lincoln University College, Petaling Jaya-47301, Selangor, Malaysia
[2] Department of Statistics, Faculty of Science, King Abdulaziz University, Saudi Arabia
[3] Department of Information Systems and Technologies, Faculty of Computer and Information Sciences, Niğde Ömer Halisdemir University, Niğde 51240, Türkiye
[4] Symbiosis Statistical Institute, Symbiosis International (Deemed University), Pune, India
[5] Department of Statistics and Operations Research, College of Science, King Saud University, P.O. Box 2455, Riyadh 11451, Saudi Arabia

* **Correspondence:** Email: aafaq7741@gmail.com; Tel: +917006131832.

Abstract: This study introduces the cotangent-Φ (NC-Φ) distribution, which establishes a new type of probability distribution for statistical modeling complex real-world data. The proposed method uses trigonometric transformations to systematically manipulate the skewness and tail characteristics of traditional distributions, thus overcoming the difficulties that often arise in existing models. A complete mathematical theory is formulated, with series expansions of the cumulative distribution function and the probability density function. Based on the Weibull distribution, a new cotangent-Weibull distribution (NCWD) is introduced, and its major statistical features are investigated. A machine learning layer was developed to complement the analytical properties of the formulated NCWD. Parameter estimation is carried out in both frequentist and Bayesian approaches, and a Monte Carlo simulation study is conducted to evaluate and compare the performance of the estimators under different sample sizes. The validity of the proposed model is established through applications to three different real-world datasets: the active repair times (in hours) of an aerial communication transceiver, the inter-arrival times between vehicles passing a fixed point on a roadway, and the susceptibility index data of peppermint packages irradiated by gamma and microwave radiation under non-choice packaging conditions. In each scenario, the NCWD outperforms several other competing models in terms of the goodness-of-fit, thus establishing its appropriateness for reliability, transportation, and irradiation data analyses.

Keywords: cotangent function; Weibull distribution; moments; Bayesian analysis; XGBoost; data analysis
Mathematics Subject Classification: 62A86, 62D05, 62F12, 62F25, 62G07, 62L05, 62L10, 62L12

1. Introduction

The implementation of probability distributions to simulate real-world occurrences is widespread and supported by strong theoretical frameworks. The discipline is distinguished by constant progress, with multiple distribution families developed to reflect various occurrences. A popular approach entails complicated models with many parameters; however, the difficulty of estimating these parameters has resulted in a preference for more parsimonious models that maintain the flexibility. This objective has prompted the study of innovative distributions that employ trigonometric functions. As an outcome, in recent years, there has been a substantial and growing scholarly pursuit of generalizing distributions, especially extended families of distributions. Creating extremely flexible distributions is critical to efficiently model data in sectors as diverse as medical, engineering, and finance. In recent years, statisticians have created various novel distributions by employing trigonometric transformations to examine complicated information and identify the best model for forecasting real-world probability. These trigonometric transformations enable extraordinary flexibility and shape modification, since their parameters have a direct impact on the distribution's behavior, with the periodic function determining the curvature of the probability density function. In recent times, the research focus has switched to developing novel generators from established continuous distributions. This method generates novel distributions, which considerably improve the efficacy and diversity of data analyses. Please see the following references to continue study: Aijaz et al. [1–3], proposed several generator families based on various trigonometric functions, demonstrating their versatility through the incorporation of different baseline distributions and extensive model selection criteria. Ali et al. [4] combines the mathematical properties of the Log-Logistic distribution, famous for its suitability to fit heavy tailed data, and the Ailamujia distribution, famous for fitting skewed and unimodal data, employed the quadratic rank transmutation Map (QRTM). Almongy et al. [5] proposed the Marshall-Olkin Alpha Power Lomax distribution, investigated several parameter estimation techniques, and demonstrated its practical usefulness through applications to physics and economics datasets. Similarly Smith et al. [6] compared maximum likelihood and Bayesian estimation procedures for the three parameter Weibull distribution, contributing to the development of efficient statistical inference for lifetime models. SS-transformation based on trigonometric functions is proposed by kumar et al. [7] and Wang et al. [8]. Parameter estimation for the weighted exponential distribution has been given a great deal of consideration in the recent past. For example, Deng et al. [9, 10] have studied the maximum likelihood estimation methods under simple random sampling as well as ranked set sampling schemes.

A large number of studies have explored transformation-based extensions of probability distributions to improve the flexibility and broaden the applicability of classical models. Such developments are motivated by the inability of standard distributions to adequately model complex data characteristics such as skewness, heavy tails, and diverse hazard rate shapes commonly observed in real data. To overcome these limitations, several generalized families have been proposed by introducing additional shape parameters and transformation mechanisms. For example, Rather and Subramanian [11] proposed the exponentiated Garima distribution, while Rather et al. [12] developed the Weighted Erlang-Truncated exponential distribution. Qayoom et al. [13, 14] explored weighted transformation based extensions of probability distributions in order to increase their flexibility while analyzing real-life data. Similarly, Alotaibi et al. [15] introduced the weighted Burhan distribution, and

Qayoom et al. [16] proposed the length-biased Burhan model. Further contributions include the DUS Rayleigh distribution [17], Linear combination of order statistics of exponentiated Nadarajah-Haghighi distribution and their applications [18], the modified flexible Weibull extension [19], and Lomax-based and transformation-based extensions developed in recent studies [17, 20, 21]. Advancements in reliability engineering in recent times have paid great attention towards the analysis of multivariate dependency and environment volatility. Recent literature has come up with a hierarchical Bayesian approach towards multivariate Wiener processes which exhibit dependent degradation features [22]. On the other hand, bivariate Wiener processes that use random scale weight have been developed to deal with asymmetrical degradation paths [23]. Numerical algorithms have revolutionized mathematical modeling. Liu and Xue [24] introduced multistep iterative schemes for nonlinear cases, while Liu et al. [25] introduced diffusion approximation via neural networks of radial basis functions. Localized forms include high order compact polyharmonic splines [27].Y. Liu, Y. Li et al. [26] proposed an RBF-FD numerical scheme for pricing financial derivatives under the Bates model, providing an accurate and efficient approach for handling stochastic volatility and jump dynamics.These works demonstrate the importance of transformation techniques in constructing flexible statistical models for real-world applications.

The aim of this investigation is to describe the innovative sin-generator distributions, a new family of trigonometric function-based generators. The adaptability of this generator is accomplished without the inclusion of extra factors.

Aijaz et al. [28] proposed a new arccosine-based approach to construct probability distributions. The cumulative distribution function is defined by the following expression:

$$F(z;\xi) = 1 - \frac{2}{\pi}\cos^{-1}\left(\frac{\pi^{\Psi(z;\xi)} - \bar{\Psi}(z;\xi)}{\pi}\right), \quad z \in \mathbb{R},\ \xi > 0.$$

Similarly, Alghamdi et al. [29] proposed another distribution in probability theory, titled “A new alpha power Cosine-Weibull model with applications.” They determined some distributional features and then demonstrated its usefulness using data sets from the hydrological and engineering sectors. The cumulative distribution function of this generator is as follows:

$$F(z;\xi) = \frac{\alpha^{\cos\left(\frac{\pi}{2}(1-B(z;\xi))\right)} - 1}{\alpha - 1}, \quad z \in \mathbb{R},\ \alpha > 0,\ \alpha \neq 1.$$

Nanga et al. [30] implemented the tangent function and suggested another generator in the existing research. They applied the Topp-Leone distribution as the foundation model for this generator, which they named the Tangent Topp-Leone Family of Distributions. The cumulative distribution function is defined as follows:

$$F(z;\beta,\xi) = \tan\left[\frac{\pi}{4}\left(1 - (1 - G(z;\xi))^2\right)^{\beta}\right], \quad z \in \mathbb{R},\ \beta > 0.$$

Trigonometric generators currently available primarily alter the central part of the distributions but may not provide sufficient adjustments concerning how the tails behave. The cotangent function’s periodic singularities and rapid decay yield a unique method of providing more flexibility in how the tail behaves, thus allowing greater control over skewness. By introducing the Novel Cotangent-Φ family, this paper addresses a simple yet very flexible generator that provides an extension of classical distributions without adding any extra shape parameters. The Cotangent-Φ generator addresses three significant shortcomings in current statistical modeling practices:

(1) The first of these shortcomings is the limited ability of trigonometric generators (including sine, cosine and tangent) to adequately capture heavy-tailed distributions seen in reliability engineering, financial risk analyses, and extreme event analyses.

(2) The second shortcoming relates to the use of flexible distribution families (such as exponentiated-generated, beta-generated and Kumaraswamy-generated), that use additional shape parameters, thus creating complications in estimating the parameters, the risk of overfitting the data, and lowering the interpretability of results.

(3) The last identified shortcoming is the need for a highly flexible, yet parameter parsimonious, distribution. Many existing probability distributions can only model a narrow band of hazard rate shapes, while real-world engineering systems exhibit non-monotonic behaviors related to failure. Examples of non-monotonic failure behaviors include early high failure rates (infant mortality), constant failure rates during useful-life periods, and increasing failure rates during the later life due to wear out. Most existing generators based on trigonometric functions cannot model all three phases of failure concurrently.

This paper offers a unique probability generator that makes use of the cotangent function, with the goal of increasing the flexibility in complicated data processing. The key advantage is the ability to acquire greater flexibility without introducing additional parameters. To demonstrate its utility, we applied it to the Weibull distribution. The result is a remarkably adaptable model; its probability density function can take on a variety of shapes, from right-skewed to heavy-tailed, leptokurticand fat tailed patterns. Additionally, we found that its hazard rate follows non-monotonic trends, which immediately suggests uses in a wider array of modeling contexts than standard models allow. Ultimately, this work is driven by the practical challenge of creating a probabilistic tool that is both simple to use and highly versatile, thereby aiming to provide a tangible upgrade for analytical work. The cumulative distribution function (CDF) of the cotangent-Φ family is defined as follows.

Assume Z as a random variable with a CDF expressed by $F(z;\zeta)$, where ζ symbolizes the parameter vector. The cumulative distribution function for the proposed cotangent-Φ family of distributions is constructed as follows:

$$F(z;\zeta) = \int_{\frac{\pi}{2}}^{\frac{\pi}{4}\left(2-e^{-\frac{\bar{\Phi}(z;\zeta)}{\Phi(z;\zeta)}}\right)} -\csc^2(y)\,dy = \cot\left(\frac{\pi}{4}\left(2-e^{-\frac{\bar{\Phi}(z;\zeta)}{\Phi(z;\zeta)}}\right)\right), \quad z \in \mathbb{R}. \tag{1.1}$$

Novelty of the proposed novel cotangent-Φ family

(1) Conventional trigonometric function based probabilistic models have been the most expressive approaches, thereby employing the sine, cosine, or tangent mapping directly to the base CDF $\Phi(z;\zeta)$. However, the CDF proposed in the paper is unique in terms of the mechanism, which makes use of the following function:

$$\frac{\bar{\Phi}(z;\,\zeta)}{\Phi(z;\,\zeta)}.$$

This embedding introduces additional flexibility and tail sensitivity at the distributional level, thus distinguishing it from conventional trigonometric-based generators.

(2) The exponential component of the form

$$e^{-\frac{\bar{\Phi}(z;\,\zeta)}{\Phi(z;\,\zeta)}}$$

plays the role of a stabilizing transformation that tempers the explosive growth of the reverse odds ratio, thus preserving its asymptotic behavior. The exponential reverse odds interaction is not employed by existing trigonometric families.
(3) The cotangent transformation adds a curvature that is qualitatively different for sine, cosine, and tangent transformation. This latter transformation adds a tail behavior. It is more of a shape intensifier than just a reshaper. It offers the possibility of distribution to be left and right skewed, having heavy tail behaviors and hazard shapes in flexible ways.
(4) One major novelty introduced with the proposed CDF is that there are no added parameters to its family, unlike the case with most probability generators. The proposed probability distribution increases the flexibility with respect to its distribution through a simple composition, thereby establishing various merits with identifiability reduced, which is more appropriate for smaller sample settings.

Regarding Eq (1.1), the related probability density function (PDF) is provided by the following:

$$f(z;\zeta) = \frac{\pi}{4}\frac{\phi(z;\zeta)}{(\Phi(z;\zeta))^2}e^{-\frac{\bar{\Phi}(z;\zeta)}{\Phi(z;\zeta)}}\csc^2\left(\frac{\pi}{4}\left(2 - e^{-\frac{\bar{\Phi}(z;\zeta)}{\Phi(z;\zeta)}}\right)\right), \quad z \in \mathbb{R}. \tag{1.2}$$

The baseline cummulative distribution function is expressed by $\Phi(z;\zeta)$, and $\bar{\Phi}(z;\,\zeta) = 1 - \Phi(z;\,\zeta)$ is dependent on the parameter vector ζ. Therefore, we determine certain dependability aspects of the stated generator in a generalized form. The reliability function is labeled as $R(z;\zeta)$, the hazard rate function (HRF) is labeled as $h(z;\zeta)$, the reverse HRF is labeled as $r(z;\zeta)$, and the cumulative HRF is labeled as $H(z;\zeta)$:

$$\begin{aligned}
R(z;\zeta) &= \bar{F}(z;\zeta) = 1 - \cot\left(\frac{\pi}{4}\left(2 - e^{-\frac{\bar{\Phi}(z;\zeta)}{\Phi(z;\zeta)}}\right)\right),\\
h(z;\zeta) &= \frac{f(z;\zeta)}{R(z;\zeta)} = \frac{\pi\,\phi(z;\zeta)\,e^{-\frac{\bar{\Phi}(z;\zeta)}{\Phi(z;\zeta)}}\csc^2\left(\frac{\pi}{4}\left(2 - e^{-\frac{\bar{\Phi}(z;\zeta)}{\Phi(z;\zeta)}}\right)\right)}{4\,(\Phi(z;\zeta))^2\left(1 - \cot\left(\frac{\pi}{4}\left(2 - e^{-\frac{\bar{\Phi}(z;\zeta)}{\Phi(z;\zeta)}}\right)\right)\right)},\\
r(z;\zeta) &= \frac{f(z;\zeta)}{F(z;\zeta)} = \frac{\pi}{2}\,\frac{\phi(z;\zeta)}{(\Phi(z;\zeta))^2}\,e^{-\frac{\bar{\Phi}(z;\zeta)}{\Phi(z;\zeta)}}\,\sin\left(\frac{\pi}{2}\left(2 - e^{-\frac{\bar{\Phi}(z;\zeta)}{\Phi(z;\zeta)}}\right)\right),\\
H(z;\zeta) &= -\ln[\bar{F}(z;\zeta)] = -\ln\left\{1 - \cot\left(\frac{\pi}{4}\left(2 - e^{-\frac{\bar{\Phi}(z;\zeta)}{\Phi(z;\zeta)}}\right)\right)\right\}.
\end{aligned}$$

Another interesting function of the provided distribution is the quantile function, which is derived by inverting Eq (1.1) and can potentially be leveraged to evaluate the median, Bowley's skewness, and Moor's kurtosis, besides other aspects, as follows:

$$Q(u;\zeta) = Q_*\left(1 + \log\left(2 - \frac{4}{\pi}\cot^{-1}(u;\zeta)\right)\right)^{-1}, \quad u \in (0,1),$$

where Q_* is the quantile function corresponding with $\Phi(z;\zeta)$.

1.1. Cumulative distribution function symbolized as a linear form

Now, we transform the CDF to a linear form that could potentially be employed to derive a plethora of statistical features. Therefore, we employ the subsequent Taylor series of the cotangent function. By implementing the subsequent series expansion to the CDF in Eq (1.1), we get the following:

$$\cot(y) = \sum_{p=0}^{\infty} \frac{(-1)^p B_{2p}}{(2p)!} y^{2p-1}, \quad 0 < |y| < \pi.$$

$$F(z;\zeta) = \sum_{p=0}^{\infty} \frac{(-1)^p B_{2p}}{(2p)!} \left(\frac{\pi}{4}\right)^{2p-1} \left(2 - e^{-\frac{\bar{\Phi}(z;\zeta)}{\Phi(z;\zeta)}}\right)^{2p-1}, \tag{1.3}$$

where B_{2p} denotes the Bernoulli numbers.

Now, by employing the following generalized bionomial theorem, we have

$$(1-u)^{a-1} = \sum_{q=0}^{\infty} (-1)^q \binom{a-1}{q} u^q, \quad |u| < 1.$$

$$F(z;\zeta) = \sum_{p,q=0}^{\infty} \frac{(-1)^{p+q} 2^{2p-q} B_{2p}}{(2p)!} \left(\frac{\pi}{2}\right)^{2p-1} \binom{2p-1}{q} e^{-q\frac{\bar{\Phi}(z;\zeta)}{\Phi(z;\zeta)}}. \tag{1.4}$$

Onwards, by utilizing the following Taylors expansion's to Eq (1.4), we have

$$e^{-my} = \sum_{r=0}^{\infty} \frac{(-1)^r}{r!} (my)^r,$$

$$(1-u)^s = \sum_{s=0}^{\infty} (-1)^s \binom{r}{s} u^s, \quad |u| < 1,$$

$$F(z;\zeta) = \sum_{p,q,r,s=0}^{\infty} \frac{(-1)^{p+q+r+s} 2^{2p-q} B_{2p}}{(2p)!} \left(\frac{\pi}{2}\right)^{2p-1} \binom{2p-1}{q} \binom{r}{s} \frac{q^r}{r!} (\Phi(z;\zeta))^{s-r} = \sum_{p,q,r,s=0}^{\infty} \mathit{\Lambda}_{pqrs} (\Phi(z;\zeta))^{s-r}, \tag{1.5}$$

where

$$\mathit{\Lambda}_{pqrs} = \frac{(-1)^{p+q+r+s} 2^{2p-q} B_{2p}}{(2p)!} \left(\frac{\pi}{2}\right)^{2p-1} \binom{2p-1}{q} \binom{r}{s} \frac{q^r}{r!}.$$

Now, to develop the linear form of the PDF, we differentiate (1.5), which leads to the following:

$$f(z;\zeta) = \sum_{p,q,r,s=0}^{\infty} \mathit{\Lambda}_{pqrs} (s-r) \phi(z;\zeta) (\Phi(z;\zeta))^{s-r-1} = \sum_{p,q,r,s=0}^{\infty} \Delta_{pqrs} \phi(z;\zeta) (\Phi(z;\zeta))^{s-r-1}, \tag{1.6}$$

where

$$\Delta_{pqrs} = \mathit{\Lambda}_{pqrs}(s-r).$$

1.2. Extremum evaluation

To derive the extrema of the PDF and HRF for the established generator, we employ logarithmic differention. For a more accurate analysis, we utilize the second derivative test to validate the nature of these extrema (i.e., whether they fall under maxima or minima). We perform differentiation to determine the first derivative of the provided PDF expression as follows:

$$\frac{d}{dz}(\log f(z;\zeta)) = \frac{\phi'(z;\zeta)}{\phi(z;\zeta)} - \frac{2\phi(z;\zeta)}{\Phi(z;\zeta)} + \frac{\phi(z;\zeta)}{\Phi^2(z;\zeta)}\left[1 + \frac{\pi}{2}e^{-\frac{\bar{\Phi}(z;\zeta)}{\Phi(z;\zeta)}}\cot\left(\frac{\pi}{4}\left(2 - e^{-\frac{\bar{\Phi}(z;\zeta)}{\Phi(z;\zeta)}}\right)\right)\right].$$

To locate the turning points, we set

$$\frac{d}{dz}(\log f(z;\zeta)) = 0,$$

and let $z*$ symbolize the critical points found by evaluating this equation. To determine whether these points are maxima, minima, or points of inflection, we evaluate the second derivative at each z^*. In particular,

$$\kappa_1 = \left.\frac{d^2}{dz^2}\log(f(z;\zeta))\right|_{z=z_0}.$$

If $\kappa_1 < 0$, then it reveals a local maximum, if $\kappa_1 > 0$, then it reveals a local minimum, and if $\kappa_1 = 0$, then it suggests a feasible point of inflection. By adopting an identical approach for the HRF of the specified generator, we obtain the following:

$$\begin{aligned}\frac{d}{dz}\log h(z;\zeta) = {}& \frac{\phi'(z;\zeta)}{\phi(z;\zeta)} - \frac{2\phi(z;\zeta)}{\Phi(z;\zeta)} + \frac{\phi(z;\zeta)}{\Phi^2(z;\zeta)} + \frac{\phi(z;\zeta)}{\Phi^2(z;\zeta)}\frac{\pi}{2}e^{-\frac{\bar{\Phi}(z;\zeta)}{\Phi(z;\zeta)}} \\ & \times\left[\cot\left(\frac{\pi}{4}\left(2 - e^{-\frac{\bar{\Phi}(z;\zeta)}{\Phi(z;\zeta)}}\right)\right) - \csc\left(\frac{\pi}{2}\left(2 - e^{-\frac{\bar{\Phi}(z;\zeta)}{\Phi(z;\zeta)}}\right)\right)\right].\end{aligned}$$

To put

$$\frac{d}{dz}\log(h(z;\zeta)) = 0$$

and evaluate the resultant equation, we may find the crucial points. The crucial points are denoted as z_*. The HRF at these points can be classified as a local maximum, local minimum, or point of inflection dependent on κ_2, which is defined as

$$\kappa_2 = \left.\frac{d^2}{dz^2}\log(h(z;\zeta))\right|_{z=z_*},$$

and the category relies on whether if $\kappa_2 < 0$, then it indicates maxima, if $\kappa_2 > 0$ then it indicates minima, or if $\kappa_2 = 0$, then it suggests point of inflection.

Through the evaluation of extrema for the PDF and HRF, we are able to perform the following:
(1) Determine the number and location of modes in the PDF (or peaks) and whether or not the HRF is monotonic (or non-monotonic);
(2) Determine if this model is appropriate for this type of application (for example, for early-failure models and for wear-out periods);

The Weibull distribution is a generalization of the exponential and Rayleigh distributions, rendering it extremely adaptable and broadly applicable. These characteristics render it particularly valuable for reliability analyses and life data modeling. The CDF of the Weibull distribution, symbolized by $\Phi(z;\zeta)$, is stated as follows:

$$\Phi(z;\zeta) = 1 - e^{-\psi_1 z^{\psi_2}}, \qquad z > 0,\ \psi_1, \psi_2 > 0. \tag{1.7}$$

The notation $\zeta = \psi_1, \psi_2$ specifies a vector of parameters associated with $\Phi(z;\zeta)$.

The linked PDF is described as follows:

$$\phi(z;\zeta) = \psi_1 \psi_2 z^{\psi_2 - 1} e^{-\psi_1 z^{\psi_2}}, \qquad z > 0,\ \psi_1, \psi_2 > 0. \tag{1.8}$$

Furthermore, the HRF for the survival function $\bar{\Phi}(z;\zeta) = 1 - \Phi(z;\zeta)$ and the probability density function $\phi(z;\zeta)$ of the Weibull distribution, indicated as $h(z;\zeta)$, is described as follows:

$$h(z;\zeta) = \psi_1 \psi_2 z^{\psi_2 - 1}, \quad z > 0.$$

When $\psi = 1$, the Weibull distribution approaches the exponential distribution, thereby demonstrating a uniform failure rate with no fluctuations in failure likelihood over the period. When $\psi = 1$, the Weibull distribution transforms into the Rayleigh distribution, characterized by a growing failure rate, as observed in wear-out or disintegration processes. If $\psi = 1$, then the distribution exhibits a dropping failure rate, thereby demonstrating that failures are more likely in the beginning phases of life, thus emphasizing weaknesses.

The versatile nature of the Weibull distribution renders it a significant tool for statisticians and investigators, permitting them to symbolize an extensive spectrum of occurrences. As research progresses, the Weibull distribution remains a cornerstone for understanding real-world systems and improving predictive modeling methods. Notwithstanding its numerous advantages, the Weibull distribution is not without flaws. One significant drawback is its inherent constraint to monotonic hazard functions, which means it can only describe scenarios in which the hazards rate constantly grows, falls, or remains constant over time. Although this attribute is effective in simpler circumstances, it becomes a substantial barrier when dealing with more complex real-world scenarios. The Weibull distribution's inflexibility in dealing with non-monotonic phenomena severely restricts its effectiveness. When analysts employ a Weibull fit to such data, the constraints of the model might result in glaring errors and false findings.

The vast quantity of knowledge meticulously described and highlighted in recent literature has sparked our curiosity and prompted us to establish a novel probabilistic methodology, as indicated in Eq (1.1). In this instance, we employ the Weibull distribution as a foundational model to carefully examine the important features of the aforementioned generator.

2. Novel cot-Weibull distribution and statistical properties

In this part, we discuss the novel cot-generator and utilize the tailored Weibull distribution as the foundational framework to build the NCWD, thus proving the framework's versatility. Additionally, we consider its statistical features. By putting Eq (1.7) into Eq (1.1), we get the CDF for the suggested distribution as follows:

$$F(z;\psi_1,\psi_2) = \cot\left(\frac{\pi}{4}\left(2 - e^{-(e^{\psi_1 z^{\psi_2}} - 1)^{-1}}\right)\right), \quad z > 0,\ \psi_1, \psi_2 > 0. \tag{2.1}$$

Figure 1 depicts the CDF for the NCWD model, which has a stringent $(0, 1)$ constraint for all analyzed parameter combinations. This offers clear pictorial proof that the function meets the necessary criteria for a suitable cumulative distribution function.

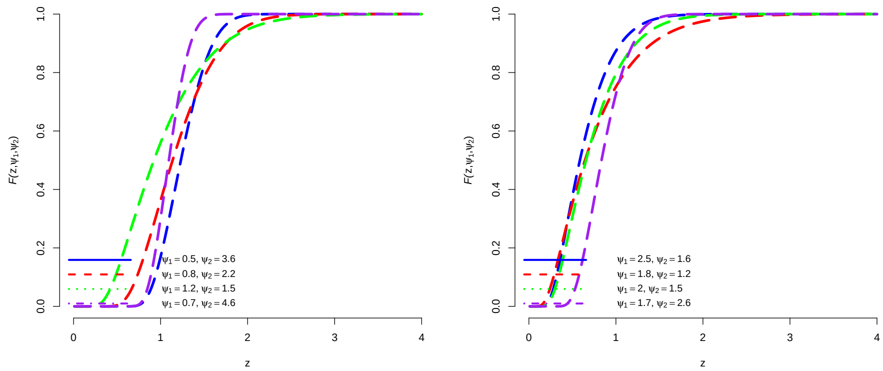

Figure 1. CDF plots of NCWD for distinct parameter choices.

The associated PDF of (2.1) is described as follows:

$$f(z; \psi_1, \psi_2) = \frac{\pi}{4} \frac{\psi_1 \psi_2 z^{\psi_2 - 1} e^{-\psi_1 z^{\psi_2}}}{(1 - e^{-\psi_1 z^{\psi_2}})^2} e^{-(e^{\psi_1 z^{\psi_2}} - 1)^{-1}} \csc^2\left(\frac{\pi}{4}\left(2 - e^{-(e^{\psi_1 z^{\psi_2}} - 1)^{-1}}\right)\right), \quad z > 0,\ \psi_1, \psi_2 > 0. \tag{2.2}$$

The parameters ψ_1 and ψ_2 have meanings almost identical to the ones in the classical Weibull distribution function. Particularly, ψ_1 is a scale parameter, which defines the total life time scale, whereas ψ_2 is a shape parameter, which determines the dynamics of the HRF. By means of the suggested NCWD family of distributions, it is possible to generate almost all kinds of hazard rate shapes without adding new parameters to the model.

Figure 2 demonstrates the PDF of the NCWD, exhibiting a wide range of flexible geometries. These include right-skewed, heavy-tailed, leptokurtic, and fat-tailed forms, depending on the parameter selected. The distribution is unimodal throughout, with noticeable differences in the peak amplitude and tail decay. This intrinsic adaptability distinguishes the NCWD as a strong model appropriate for a wide range of statistical applications that demand complicated data structures.

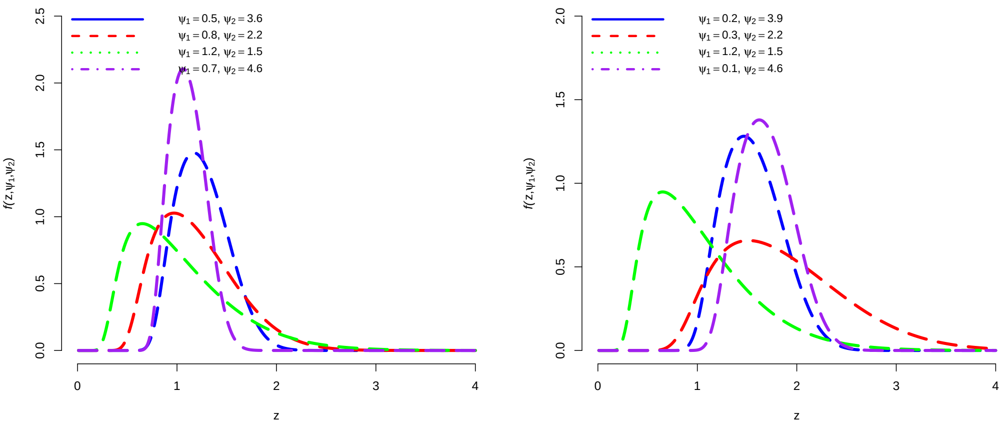

Figure 2. PDF plots of NCWD for distinct parameter choices.

2.1. Moments

Moments are frequently employed in statistics to summarize distributions, estimate parameters, and analyze data behaviors. Each moment yields distinct insights, ranging from center tendency (mean) to extreme outcomes (kurtosis). The k^{th} moment is defined as follows:

$$\mu_k' = \mathbb{E}(z^k) = \int_0^{\infty} z^k f(z; \psi_1, \psi_2)\, dz. \tag{2.3}$$

We derive by inserting Eq (1.6) into Eq (2.3) as follows:

$$\begin{aligned}
\mu_k' &= \sum_{p,q,r,s=0}^{\infty} \Delta_{pqrs} \int_0^{\infty} z^k \phi(z;\zeta)(\Phi(z;\zeta))^{s-r-1}\, dz \\
&= \sum_{p,q,r,s=0}^{\infty} \Delta_{pqrs}\, \psi_1\psi_2 \int_0^{\infty} z^{k+\psi_2-1} e^{-\psi_1 z^{\psi_2}} (1-e^{-\psi_1 z^{\psi_2}})^{s-r-1}\, dz \\
&= \sum_{p,q,r,s,t=0}^{\infty} (-1)^t \binom{s-r-1}{t} \Delta_{pqrs}\, \psi_1\psi_2 \int_0^{\infty} z^{k+\psi_2-1} e^{-\psi_1(t+1) z^{\psi_2}}\, dz.
\end{aligned}$$

Under the substitution $\psi_1\,(t+1)\, z^{\psi_2} = y$ with $0 < y < \infty$, we have the following:

$$\mu_k' = \sum_{p,q,r,s,t=0}^{\infty} (-1)^t \binom{s-r-1}{t} \Delta_{pqrs} \frac{\psi_1}{(\psi_1(t+1))^{(k+\psi_2)/\psi_2}} \int_0^{\infty} y^{k/\psi_2} e^{-y}\, dy.$$

After evaluating the above integral, we obtain the following:

$$\mu_k' = \sum_{p,q,r,s,t=0}^{\infty} (-1)^t \binom{s-r-1}{t} \Delta_{pqrs} \frac{\psi_1}{(\psi_1(t+1))^{(k+\psi_2)/\psi_2}} \Gamma\left(\frac{k}{\psi_2}+1\right),$$

where $\Gamma(.)$ denotes a gamma function.

The moment-generating function (MGF) is a function that provides a simple way to calculate moments (such as mean and variance) of a random variable. The MGF of a distribution is expressed by $M_Z(t)$, which is defined as follows:

$$\begin{aligned}
M_Z(t) = \mathbb{E}(e^{tz}) &= \int_0^{\infty} e^{tz} f(z; \psi_1, \psi_2)\, dz \\
&= \sum_{k=0}^{\infty} \frac{t^k}{k!} \int_0^{\infty} z^k f(z; \psi_1, \psi_2)\, dz \\
&= \sum_{k=0}^{\infty} \frac{t^k}{k!} \mathbb{E}(z^k) \\
&= \sum_{p,q,r,s,t,k=0}^{\infty} (-1)^t \binom{s-r-1}{t} \Delta_{pqrs} \frac{t^k}{k!} \frac{\psi_1}{(\psi_1(t+1))^{(k+\psi_2)/\psi_2}} \Gamma\left(\frac{k}{\psi_2}+1\right).
\end{aligned}$$

Another essential notion in moments is the probability-weighted moments (PWMs) of a random variable Z. These moments extend standard moments by including weights based on the CDF. PWMs are less sensitive to outliers than traditional moments, causing them to be ideal to fit distributions to heavy-tailed or skewed data:

$$\begin{aligned}\mathbb{E}\left(Z^k\Phi(z)^v\right) &= \int_0^\infty z^k\Phi(z)^v f(z;\zeta)\,dz\\ &= \sum_{p,q,r,s=0}^{\infty}\Delta_{pqrs}\int_0^\infty z^k\phi(z;\zeta)(\Phi(z;\zeta))^{v+s-r-1}\,dz\\ &= \sum_{p,q,r,s=0}^{\infty}\Delta_{pqrs}\,\psi_1\psi_2\int_0^\infty z^{k+\psi_1-1}e^{-\psi_1 z^{\psi_2}}(1-e^{-\psi_1 z^{\psi_2}})^{v+s-r-1}\,dz.\end{aligned}$$

We utilize the following generalization of the binomial theorem:

$$\begin{aligned}(1-u)^{a-1} &= \sum_{t=0}^{\infty}(-1)^t\binom{a-1}{t}u^t, \quad |u|<1,\\ &= \sum_{p,q,r,s,t=0}^{\infty}(-1)^t\binom{v+s-r-1}{t}\Delta_{pqrs}\,\psi_1\psi_2\int_0^\infty z^{k+\psi_2-1}e^{-\psi_1(t+1)z^{\psi_2}}\,dz.\end{aligned}$$

Under the substitution $\psi_1\,(t+1)\,z^{\psi_2} = y$, with $0 < y < \infty$, we have the following:

$$\mathbb{E}\left(Z^k\Phi(z)^v\right) = \sum_{p,q,r,s,t=0}^{\infty}(-1)^t\binom{v+s-r-1}{t}\Delta_{pqrs}\frac{\psi_1}{(\psi_1(t+1))^{(k+\psi_2)/\psi_2}}\int_0^\infty y^{k/\psi_2}e^{-y}\,dy.$$

After evaluating the above integral, we obtain the following:

$$\mathbb{E}\left(Z^k\Phi(z)^v\right) = \sum_{p,q,r,s,t=0}^{\infty}(-1)^t\binom{v+s-r-1}{t}\Delta_{pqrs}\frac{\psi_1}{(\psi_1(t+1))^{(k+\psi_2)/\psi_2}}\Gamma\left(\frac{k}{\psi_2}+1\right),$$

where $\Gamma(.)$ denotes a gamma function.

2.2. *Incomplete moments*

In lifespan models, incomplete moments are critical to evaluate the remaining life expectancy, forecasting failure times, examining survival rates, and modeling asset lifetimes. The incomplete moment is critical in these analyses for assessing risk, improving durability, and evaluating treatments. The m^{th} incomplete moment is determined as follows:

$$I_m(x) = \int_0^x z^m f(z;\psi_1,\psi_2)\,dz. \tag{2.4}$$

Considering Eqs (1.6), (1.8) and Eq (2.4), we can determine

$$I_m(x) = \sum_{p,q,r,s,t=0}^{\infty}(-1)^t\binom{s-r-1}{t}\Delta_{pqrs}\,\psi_1\psi_2\int_0^x z^{m+\psi_2-1}e^{-\psi_1(t+1)z^{\psi_2}}\,dz.$$

By substituting $\psi_1(t+1)z^{\psi_2} = y$ with $0 < z < \psi_1(t+1)x^{\psi_2}$, we have the following:

$$I_m(x) = \sum_{p,q,r,s,t=0}^{\infty} (-1)^t \binom{s-r-1}{t} \Delta_{pqrs} \frac{\psi_1}{(\psi_1(t+1))^{(m+\psi_2)/\psi_2}} \int_0^{\psi_1(t+1)x^{\psi_2}} y^{m/\psi_2} e^{-y}\, dy.$$

Following accomplishing the integral, we obtain the following:

$$I_m(x) = \sum_{p,q,r,s,t=0}^{\infty} (-1)^t \binom{s-r-1}{t} \Delta_{pqrs} \frac{\psi_1}{(\psi_1(t+1))^{(m+\psi_2)/\psi_2}} \gamma\left(\frac{m}{\psi_2} - 1,\ \psi_1(t+1)x^{\psi_2}\right), \tag{2.5}$$

where $\gamma(w; x) = \int_0^x t^{w-1} e^{-t} dt$ denotes a lower incomplete gamma function.

2.3. Quantile function and random number generation

Suppose Z is a random variable with a CDF outlined in Eq (2.1). The quantile function of the NCWD may be obtained through inverting its CDF, according to Eq (2.1):

$$F(z) = q \implies z = F^{-1}(q),$$
$$z = \left(\frac{1}{\psi_1} \ln\left(1 - \frac{1}{\ln\left(2 - \frac{4}{\pi}\cot^{-1}(q)\right)}\right)\right)^{1/\psi_2}.$$

Setting $u = q$ provides random numbers by employing the quantile function. In this instance, u is a random variable with a uniform distribution on the interval $(0, 1)$. Additionally, the quantile function outputs Bowley's skewness and Moors' kurtosis, which are beneficial to determine the extent to which the kurtosis and skewness alter a distribution.

Bowley's skewness is defined as follows:

$$\gamma_3 = \frac{Q_3 + Q_1 - 2Q_2}{Q_3 - Q_1},$$

where Q_1, Q_2, and Q_3 represent the first, second (median), and third quartiles, respectively. The Moors kurtosis based on octiles is stated as follows:

$$\gamma_4 = \frac{(E_7 - E_5) + (E_3 - E_1)}{(E_6 - E_2)},$$

where E_i denotes the i^{th} octile of the distribution. These evaluations offer reliable insights into the distribution's structure and tail behavior.

Table 1 demonstrates that for a fixed value of ψ_1, increasing value of ψ_2 leads to gradual decreases in the mean, variance and standard deviation; for instance, when $\psi_1 = 0.5$, we observe that the mean decreases from 4.2673 to 1.3197 as ψ_2 increases from 0.5 to 3.0. Similarly the variance also sharply decreases, which indicates that the larger value of ψ_2 makes the distribution more concentrated around its central tendency. The skewness values (γ_3) remain mostly positive for several parameter combinations, which indicates that the NCWD distribution is generally right skewed. However, the magnitude of the skewness decreases as ψ_2 increases, which means that the distribution becomes more symmetric. Furthermore, the kurtosis values (γ_4) follow a decline pattern as ψ_2 increases. For smaller values of ψ_2, the kurtosis is relatively larger, which indicates a leptokurtic behavior. As ψ_2 increases the kurtosis decreases and even approaches to negative values in some cases, which shows platykurtic nature of the distribution. Eventually, the coefficient of variation (CV) decreases when ψ_2 increases, which suggests that the relative dispersion of the distribution becomes smaller as ψ_2 increases, thus indicating a more stable and less variable distribution. On the whole, these results show the flexibility of the NCWD distribution, as its shape, spread, and tail behavior can be controlled by the parameters ψ_1 and ψ_2. This flexibility makes the NCWD distribution appropriate to the model of many types of positively skewed data encountered in reliability and survival analyses, and statistical modeling in general.

Table 1. The μ, σ^2, σ, γ_3, γ_4 and CV of NCWD distribution for distinct parameter combinations.

ψ_1	ψ_2	μ	σ^2	σ	γ_3	γ_4	CV
	0.5	4.2673	20.9341	4.5754	1.7920	2.0862	1.0722
	1.5	1.84602	0.84125	0.91720	1.13163	1.59979	0.49685
0.5	2.0	1.54972	0.32774	0.57249	0.81333	0.59861	0.36941
	2.5	1.40483	0.17115	0.41370	0.63183	0.17891	0.29448
	3.0	1.319656	0.104528	0.323309	0.513796	-0.036664	0.244995
	0.5	1.2622	4.2347	2.0578	3.6464	17.7271	1.6304
	1.5	0.88747	0.19443	0.44094	1.13163	1.59979	0.49685
1.5	2.0	0.89473	0.10925	0.33052	0.81333	0.59861	0.36941
	2.5	0.905265	0.071068	0.266586	0.631828	0.178913	0.294484
	3.0	0.914998	0.050252	0.224170	0.513796	-0.036664	0.244995
	0.5	0.73381	1.64654	1.28318	4.65382	33.18920	1.74864
	1.5	0.73259	0.13249	0.36399	1.13163	1.59979	0.49685
2.0	2.0	0.774858	0.081935	0.286243	0.813332	0.598606	0.369413
	2.5	0.806864	0.056458	0.237609	0.631828	0.178913	0.294484
	3.0	0.831331	0.041482	0.203672	0.513796	-0.036664	0.244995
	0.5	0.32836	0.34899	0.59076	5.50180	55.47626	1.79911
	1.5	0.55907	0.07716	0.27778	1.13163	1.59979	0.49685
2.5	2.0	0.632669	0.054623	0.233716	0.813332	0.598606	0.369413
	2.5	0.686062	0.040818	0.202034	0.631828	0.178913	0.294484
	3.0	0.726235	0.031657	0.177924	0.513796	-0.036664	0.244995

3. Ageing indicators

This section provides significant insights on the reliability function, thereby emphasising its broad applications in a variety of scientific disciplines. The reliability function is an essential tool in engineering, statistics, and risk assessments because it allows for the long-term analysis of system performance and failure probabilities. Its adaptability renders it indispensable to ensure the quality, safety, and efficiency in both theoretical and practical settings.

3.1. Reliability function

The survival function, also known as the reliability function, is used to determine the probability that a system or component will keep functioning after a certain time period. It is especially valuable in reliability engineering and survival evaluations to estimate the failure rates and predict lifetimes.

The reliability function, often known as the survival function, for a continuous random variable Z with a cumulative distribution function $F(z)$ is provided by the following:

$$R(z) = \int_{z}^{\infty} f(z)\, dz = 1 - F(z).$$

Therefore, the reliability function for NCWD is stated as follows:

$$R(z; \psi_1, \psi_2) = 1 - \cot\left(\frac{\pi}{4}\left(2 - e^{-(e^{\psi_1 z^{\psi_2}} - 1)^{-1}}\right)\right). \tag{3.1}$$

3.2. Cumulative hazard rate function

In survival analyses, the cumulative HRF evaluates the overall risk over time. The cumulative HRF, which is important in reliability and medical research, quantifies the instantaneous risk at a certain period. The cumulative HRF of a random variable Z is stated as follows:

$$H(z; \psi_1, \psi_2) = -\ln[\bar{F}(z; \psi_1, \psi_2)] = -\ln\left[1 - \cot\left(\frac{\pi}{4}\left(2 - e^{-(e^{\psi_1 z^{\psi_2}} - 1)^{-1}}\right)\right)\right]. \tag{3.2}$$

By differentiating Eq (3.2), we obtain the HRF of NCWD as follows:

$$h(z; \psi_1, \psi_2) = \frac{\pi \psi_1 \psi_2 z^{\psi_2 - 1} e^{-\psi_1 z^{\psi_2}} e^{-(e^{\psi_1 z^{\psi_2}} - 1)^{-1}} \csc^2\left(\frac{\pi}{4}\left(2 - e^{-(e^{\psi_1 z^{\psi_2}} - 1)^{-1}}\right)\right)}{4(1 - e^{-\psi_1 z^{\psi_2}})^2 \left(1 - \cot\left(\frac{\pi}{4}\left(2 - e^{-(e^{\psi_1 z^{\psi_2}} - 1)^{-1}}\right)\right)\right)}.$$

Figure 3 contains plots of the HRF of the NCWD model, which show a great deal of flexibility and diversity of behavior that depend on the values of its two parameters ψ_1 and ψ_2. As seen from the plots below, this model is able to change easily from the bathtub curve (Plot a), strictly decreasing curve (Plot b), strictly increasing curve (Plot c), and unimodal/ upside down bathtub curve (Plot d). Such flexibility allows the NCWD, model to describe a broad variety of practical life data from the cases of systems with infant mortality and/or wear out phases to those of continuously deteriorating assets or only having the rising phase of HRF. Indeed, in the NCWD model, the interpretation of two parameters ψ_1 and ψ_2 significantly depends on the HRF as well as on the life characteristics.

(1) The bathtub curve (Plot a): results when both the parameter values are low ($\psi_1 = 0.2, \psi_2 = 0.05$). In this case, the result is a quick drop-off that becomes leveled out.

(2) The unimodal curve (Plot d): Results when both the parameter values are increased ($\psi_1 = 1.5, \psi_2 = 0.8$). The effect of this interaction results in the hazard function sharply increasing before it slowly falls.

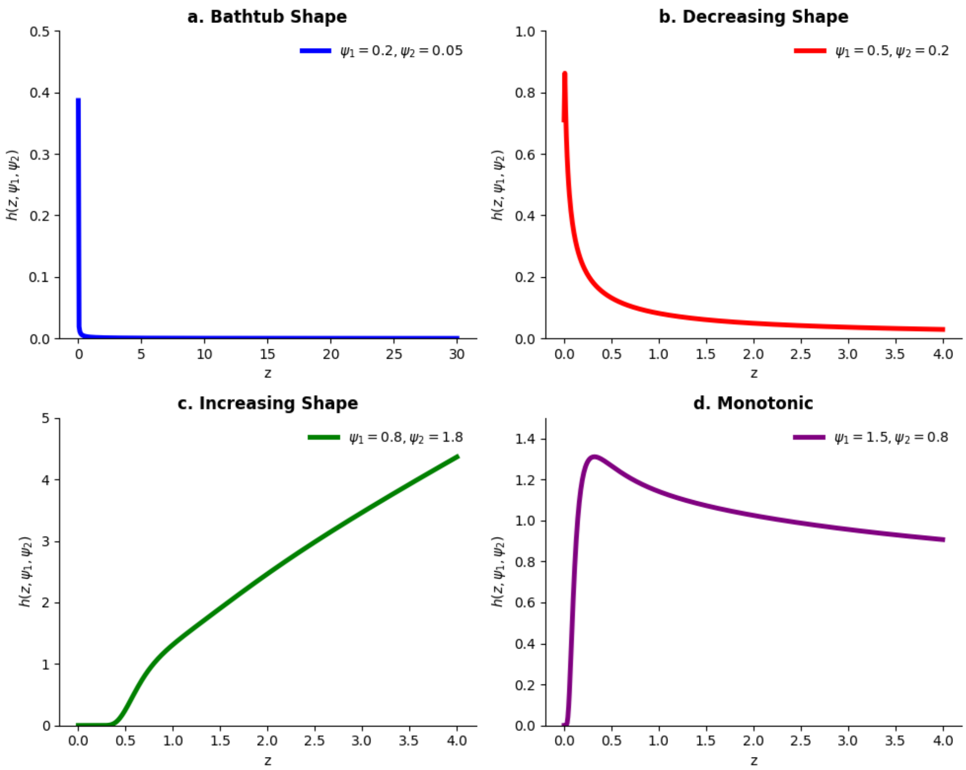

Figure 3. Hazard rate function plots of NCWD for distinct parameter choices.

3.3. *Reverse hazard rate function*

The reverse HRF assesses the chance of an event occurring at a specified time, assuming it has taken place already. This idea is implemented in survival analyses, reliability engineering, and risk assessments to investigate failure times and duration data. The formula for reverse HRF defined below having random variable Z.

$$r(z;\psi_1,\psi_2) = \frac{f(z;\psi_1,\psi_2)}{F(z;\psi_1,\psi_2)} = \frac{\pi\psi_1\psi_2 z^{\psi_2-1} e^{-\psi_1 z^{\psi_2}} e^{-(e^{\psi_1 z^{\psi_2}}-1)^{-1}} \sin\left(\frac{\pi}{2}\left(2 - e^{-(e^{\psi_1 z^{\psi_2}}-1)^{-1}}\right)\right)}{2(1-e^{-\psi_1 z^{\psi_2}})^2}.$$

3.4. *Mean residual function*

The mean residual lifetime (MRL) function determines a component's predicted lifespan after a specific time z, which is important for reliability analyses. This metric facilitates maintenance planning, risk assessments, and optimizing component replacement strategies. The MRL function may be derived from the following definition:

$$m(z;\psi_1,\psi_2) = \frac{1}{R(z;\psi_1,\psi_2)} \int_z^\infty v\, f(v;\psi_1,\psi_2)\, dv - z. \tag{3.3}$$

Now, we determine the following integral:

$$\int_z^\infty v f(v;\psi_1,\psi_2)\, dv = \sum_{p,q,r,s,t=0}^{\infty} (-1)^t \binom{s-r-1}{t} \Delta_{pqrs}\, \psi_1\psi_2 \int_0^x v^{\psi_2} e^{-\psi_1(t+1)v^{\psi_2}}\, dv.$$

By substituting $\psi_1(t+1)z^{\psi_2} = y$, with $\psi_1(t+1)z^{\psi_2} < y < \infty$, we have the following:

$$\int_z^{\infty} v f(v;\psi_1,\psi_2)\,dv = \sum_{p,q,r,s,t=0}^{\infty} (-1)^t \binom{s-r-1}{t} \Delta_{pqrs} \frac{\psi_1}{(\psi_1(t+1))^{(1+\psi_2)/\psi_2}} \int_{\psi_1(t+1)z^{\psi_2}}^{\infty} y^{1/\psi_2} e^{-y}\,dy.$$

By solving the integral, we get the following:

$$\int_z^{\infty} v f(v;\psi_1,\psi_2)\,dv = \sum_{p,q,r,s,t=0}^{\infty} (-1)^t \binom{s-r-1}{t} \Delta_{pqrs} \frac{\psi_1}{(\psi_1(t+1))^{(1+\psi_2)/\psi_2}} \Gamma\left(\frac{\psi_2+1}{\psi_2};\ \psi_1(t+1)z^{\psi_2}\right). \quad (3.4)$$

The desired result follows from substituting Eq (3.4) into Eq (3.3):

$$m(z;\psi_1,\psi_2) = \sum_{p,q,r,s,t=0}^{\infty} (-1)^t \binom{s-r-1}{t} \Delta_{pqrs} \tan\left(\frac{\pi}{4}\left(2 - e^{-(e^{\psi_1 z^{\psi_2}}-1)^{-1}}\right)\right) \times \frac{\psi_1}{(\psi_1(t+1))^{(1+\psi_2)/\psi_2}} \Gamma\left(\frac{\psi_2+1}{\psi_2};\ \psi_1(t+1)z^{\psi_2}\right) - z.$$

Here, $\Gamma(w;x) = \int_x^{\infty} t^{w-1} e^{-t} dt$ denotes the upper incomplete gamma function.

4. Estimations

This section presents the estimation of the parameters of the proposed NCWD distribution using both Non-Bayesian and Bayesian approaches.

4.1. Maximum likelihood estimation

Consider the random samples $z_1, z_2, z_3, ..., z_n$ drawn from NCWD. The initial strategy, known as Maximum likelihood estimation (MLE), denoted as (∇^1), aims to maximize the following likelihood equation:

$$\begin{aligned} \ell = {} & n\log\left(\frac{\pi}{4}\right) + n\log(\psi_1) + n\log(\psi_2) + (\psi_2 - 1)\sum_{i=1}^{n}\log(z_i) - 2\sum_{i=1}^{n}\log\left(1 - e^{\psi_1 z_i^{\psi_2}}\right) \\ & - \psi_1 \sum_{i=1}^{n} z_i^{\psi_2} - \sum_{i=1}^{n}\left(e^{\psi_1 z_i^{\psi_2}} - 1\right)^{-1} + 2\sum_{i=1}^{n}\log\csc\left(\frac{\pi}{4}\left(2 - e^{-(e^{\psi_1 z_i^{\psi_2}}-1)^{-1}}\right)\right). \end{aligned} \quad (4.1)$$

To determine the MLE of $\zeta(\psi_1,\psi_2)$, we initially partially differentiate Eq (4.1) with respect to the parameters ψ_1 and ψ_2. Setting these partial derivatives to zero yields the following:

$$\frac{\partial \log \ell}{\partial \psi_1} = 0 \quad \text{and} \quad \frac{\partial \log \ell}{\partial \psi_2} = 0.$$

However, the resulting equations are nonlinear and hence cannot be explicitly solved. To resolve this, we employ numerical approximation techniques such as the Newton-Raphson approach and the Bisection approach to repeatedly estimate the parameters. These strategies enable us to approach the MLE by improving the initial estimations through consecutive approximations. Interval estimation and hypothesis testing for model parameters necessitate an information array. The observed values are presented in a 2-by-2 array as follows:

$$I(\zeta) = -\frac{1}{n}\begin{bmatrix} \mathrm{E}\left(\frac{\partial^2 \ell}{\partial \psi_1^2}\right) & \mathrm{E}\left(\frac{\partial^2 \ell}{\partial \psi_1 \partial \psi_2}\right) \\ \mathrm{E}\left(\frac{\partial^2 \ell}{\partial \psi_2 \partial \psi_1}\right) & \mathrm{E}\left(\frac{\partial^2 \ell}{\partial \psi_2^2}\right) \end{bmatrix}.$$

The components of the supplied information array can be generated by considering second-order partial derivatives of the equations found in the following:

$$\frac{\partial \log \ell}{\partial \psi_1} = 0 \quad \text{and} \quad \frac{\partial \log \ell}{\partial \psi_2} = 0.$$

As $n \to \infty$, the distribution of $\hat{\zeta}$ approaches a multivariate normal distribution $N(0, I(\hat{\zeta}) - 1)$ distribution to provide approximate confidence intervals for the parameters. Consequently, the estimated $100(1-\phi)\%$ confidence intervals for ψ_1 and ψ_2 are supplied by the following:

$$\hat{\psi}_1 \pm Z_{\phi/2} \sqrt{I^{-1}_{\psi_1\psi_1}(\hat{\zeta})} \quad \text{and} \quad \hat{\psi}_2 \pm Z_{\phi/2} \sqrt{I^{-1}_{\psi_2\psi_2}(\hat{\zeta})},$$

where Z_ϕ denotes the $\phi-$percentile critical value of the standard normal distribution.

4.2. Anderson-Darling estimation

The Anderson-Darling estimator (∇^2) is a minimum distance estimator that determines deviations from symmetry in sample distributions. Notably, the Anderson-Darling test rapidly converges as the sample size improves. This estimator is determined by minimizing the following expression:

$$\begin{aligned} A &= -n - \frac{1}{n}\sum_{i=1}^{n}(2i-1)[\log F(z_i) + \log S(z_i)] \\ &= -n - \frac{1}{n}\sum_{i=1}^{n}(2i-1)\Big[\log\Big(\cot\Big(\frac{\pi}{4}(2 - e^{-(e^{\psi_1 z_i^{\psi_2}}-1)^{-1}})\Big)\Big) + \log\Big(1 - \cot\Big(\frac{\pi}{4}(2 - e^{-(e^{\psi_1 z_i^{\psi_2}}-1)^{-1}})\Big)\Big)\Big]. \end{aligned}$$

4.3. Right-Tail Anderson-Darling estimation

The purpose of right-tail Anderson-Darling estimation (∇^3) is to minimize the equation, thus ensuring the best feasible fit for the right tail of the distribution:

$$\begin{aligned} R &= \frac{n}{2} - 2\sum_{i=1}^{n} F(z_i) - \frac{1}{n}\sum_{i=1}^{n}(2i-1)\log S(z_{n+1-i}) \\ &= \frac{n}{2} - 2\sum_{i=1}^{n}\cot\Big(\frac{\pi}{4}(2 - e^{-(e^{\psi_1 z_i^{\psi_2}}-1)^{-1}})\Big) - \frac{1}{n}\sum_{i=1}^{n}(2i-1)\log\Big(1 - \cot\Big(\frac{\pi}{4}(2 - e^{-(e^{\psi_1 z_{n+1-i}^{\psi_2}}-1)^{-1}})\Big)\Big). \end{aligned}$$

4.4. Cramér-von Mises estimation

The Cramér-von Mises is a minimal distance estimator that has been found to have less bias than other minimum distance estimators. The purpose of the Cramér-von Mises estimation (∇^4) is to minimize the equation that follows:

$$C(z_i) = -\frac{1}{12n} + \sum_{i=1}^{n}\left[F(z_i) - \frac{2i-1}{2n}\right]^2 = -\frac{1}{12n} + \sum_{i=1}^{n}\left[\cot\left(\frac{\pi}{4}(2 - e^{-(e^{\psi_1 z_i^{\psi_2}}-1)^{-1}})\right) - \frac{2i-1}{2n}\right]^2.$$

4.5. Maximum product spacings estimation

Cheng and Amin developed the maximum product spacing (MPS) approach, which was later demonstrated by Ranneby to approximate the Kullback-Leibler (KL) information measurement. This relationship establishes the MPS method as a feasible alternative to the MLE technique. Now, assume the data is sorted in ascending order. Maximizing the following equation yields the maximum product of the spacings estimation (∇^5):

$$T = \frac{1}{n+1}\sum_{i=1}^{n+1}\log E_i, \qquad E_i = F(z_{(i)}) - F(z_{(i-1)}).$$

4.6. Least-Squares estimation

On the other hand, least-squares estimation (∇^6) aims to minimize the equation as follows:

$$LS = \sum_{i=1}^{n}\left[F(z_i) - \frac{i}{n+1}\right]^2 = \sum_{i=1}^{n}\left[\cot\left(\frac{\pi}{4}(2 - e^{-(e^{\psi_1 z_i^{\psi_2}}-1)^{-1}})\right) - \frac{i}{n+1}\right]^2.$$

4.7. Simulation investigation for non-Bayesian estimators

The present investigation aims to assess the efficiency of several estimating methodologies for the parameters of the newly developed NCWD model by employing large simulations ($N = 500$). To accomplish this, we applied the model's quantile function to simulate a variety of datasets. The simulation design utilizes a range of sample sizes ($n = 25, 75, 150, 200, 250,$ and 400) and parameter values to analyze the estimator behavior under different settings. The major purpose is to evaluate the estimators' accuracy and sturdiness. Their performance is quantitatively assessed via well-established statistical indicators such as average absolute biases (BIAS), mean square errors (MSEs), and mean relative errors (MREs), average absolute difference $D_{\max}$, maximum absolute difference $D_{\max}$, and average squared absolute error (ASAE):

$$\text{BIAS} = \frac{1}{N}\sum_{i=1}^{N}|\hat{\zeta} - \zeta|, \qquad \text{MSEs} = \frac{1}{N}\sum_{i=1}^{N}(\hat{\zeta} - \zeta)^2, \qquad \text{MREs} = \frac{1}{N}\sum_{i=1}^{N}\frac{|\hat{\zeta} - \zeta|}{\zeta},$$

$$D_{\text{abs}} = \frac{1}{nN}\sum_{i=1}^{N}\sum_{j=1}^{n}|F(z_{ij} \mid \zeta) - F(z_{ij} \mid \hat{\zeta})|, \quad D_{\max} = \frac{1}{N}\sum_{i=1}^{N}\max_j|F(z_{ij} \mid \zeta) - F(z_{ij} \mid \hat{\zeta})|, \quad \text{ASAE} = \frac{1}{n}\sum_{i=1}^{n}\frac{|z_i - \hat{z}_i|}{z_n - z_1}.$$

where the observations z_i are in ascending order, and $\zeta = \psi_1, \psi_2$. Tables 2–5 provide specifics of simulation results of several parameter estimate approaches for the NCWD distribution. The findings show that, under all circumstances, all estimators are incredibly reliable and yield estimates that are strikingly near to the actual parameter values. The low results for bias, MSE, MRE, and other evaluated metrics demonstrate this great accuracy. Furthermore, as the sample size (n) grows, these error measures steadily decline. It is evident from the ranking presented in Table 6 that the MLE estimator performed the best among all estimators used in the present simulation exercise. Nevertheless, one must not forget that the findings are purely based on an empirical analysis.

Table 2. Numerical values of simulation evaluation for $\psi_1 = 0.6,\ \psi_2 = 0.7$.

n	Est.	∇_1	∇_2	∇_3	∇_4	∇_5	∇_6
30	BIAS(ψ_1)	0.070726[1]	0.073878[3]	0.086571[6]	0.082090[4]	0.073267[2]	0.082885[5]
	BIAS(ψ_2)	0.076908[2]	0.078065[3]	0.092124[5]	0.103050[6]	0.074145[1]	0.091775[4]
	MSE(ψ_1)	0.008054[1]	0.008821[3]	0.011656[6]	0.010885[4]	0.008746[2]	0.010994[5]
	MSE(ψ_2)	0.011039[3]	0.010198[2]	0.014303[5]	0.019098[6]	0.008204[1]	0.013714[4]
	MRE(ψ_1)	0.117876[1]	0.123130[3]	0.144285[6]	0.136817[4]	0.122112[2]	0.138141[5]
	MRE(ψ_2)	0.102544[2]	0.104087[3]	0.122832[5]	0.137400[6]	0.098860[1]	0.122367[4]
	D_{abs}	0.04270[1]	0.04439[2]	0.04826[4]	0.04997[5]	0.04498[3]	0.05058[6]
	D_{max}	0.06764[1]	0.06961[3]	0.07645[4]	0.08157[6]	0.06875[2]	0.07984[5]
	ASAE	0.03581[6]	0.03256[2]	0.03083[1]	0.03562[5]	0.03380[3]	0.03515[4]
	$\sum$ Ranks	18[2]	24[3]	42[4.5]	46[6]	17[1]	42[4.5]
70	BIAS(ψ_1)	0.046027[2]	0.051513[3]	0.061432[6]	0.052954[4]	0.045344[1]	0.056255[5]
	BIAS(ψ_2)	0.044410[1]	0.047911[2]	0.057832[5]	0.062138[6]	0.050043[3]	0.056107[4]
	MSE(ψ_1)	0.003330[1]	0.004074[3]	0.005962[6]	0.004400[4]	0.003415[2]	0.004916[5]
	MSE(ψ_2)	0.003200[1]	0.003617[2]	0.005315[5]	0.005962[6]	0.003775[3]	0.005100[4]
	MRE(ψ_1)	0.076712[2]	0.085854[3]	0.102387[6]	0.088257[4]	0.075573[1]	0.093758[5]
	MRE(ψ_2)	0.059213[1]	0.063882[2]	0.077110[5]	0.082850[6]	0.066725[3]	0.074810[4]
	D_{abs}	0.02812[1]	0.03073[3]	0.03309[6]	0.03230[4]	0.02896[2]	0.03322[5]
	D_{max}	0.04382[1]	0.04764[3]	0.05249[6]	0.05232[5]	0.04528[2]	0.05185[4]
	ASAE	0.01983[4]	0.01849[2.5]	0.01769[1]	0.01988[5]	0.01849[2.5]	0.02014[6]
	$\sum$ Ranks	14[1]	23.5[3]	46[6]	44[5]	19.5[2]	42[4]
100	BIAS(ψ_1)	0.038823[1]	0.041406[3]	0.047058[6]	0.046743[5]	0.041115[2]	0.044743[4]
	BIAS(ψ_2)	0.036200[1]	0.039618[2]	0.046118[4]	0.048759[6]	0.040055[3]	0.047556[5]
	MSE(ψ_1)	0.002355[1]	0.002819[3]	0.003483[6]	0.003388[5]	0.002703[2]	0.003073[4]
	MSE(ψ_2)	0.002088[1]	0.002587[3]	0.003477[4]	0.004051[6]	0.002463[2]	0.003763[5]
	MRE(ψ_1)	0.064705[1]	0.069011[3]	0.078431[6]	0.077905[5]	0.068524[2]	0.074572[4]
	MRE(ψ_2)	0.048267[1]	0.052824[2]	0.061490[4]	0.065012[6]	0.053407[3]	0.063407[5]
	D_{abs}	0.02352[1]	0.02504[3]	0.02576[4]	0.02700[6]	0.02489[2]	0.02615[5]
	D_{max}	0.03652[1]	0.03905[3]	0.04086[4]	0.04282[6]	0.03859[2]	0.04139[5]
	ASAE	0.01570[4]	0.01481[3]	0.01345[1]	0.01574[5]	0.01478[2]	0.01623[6]
	$\sum$ Ranks	12[1]	25[3]	39[4]	50[6]	20[2]	43[5]
200	BIAS(ψ_1)	0.026085[1]	0.028404[2]	0.033883[6]	0.033048[5]	0.028855[3]	0.031810[4]
	BIAS(ψ_2)	0.025908[1]	0.028560[3]	0.030888[4]	0.035709[6]	0.027215[2]	0.034732[5]
	MSE(ψ_1)	0.001043[1]	0.001293[3]	0.001794[6]	0.001716[5]	0.001291[2]	0.001567[4]
	MSE(ψ_2)	0.001113[1]	0.001319[3]	0.001512[4]	0.002055[6]	0.001163[2]	0.001883[5]
	MRE(ψ_1)	0.043476[2]	0.047340[3]	0.056472[6]	0.055081[5]	0.048092[4]	0.001567[1]
	MRE(ψ_2)	0.034544[2]	0.038080[4]	0.041184[5]	0.055081[6]	0.036286[3]	0.001883[1]
	D_{abs}	0.01591[1]	0.01702[2]	0.01877[5]	0.01967[6]	0.01726[3]	0.01873[4]
	D_{max}	0.02501[1]	0.02675[2]	0.02943[4]	0.03139[6]	0.02687[3]	0.02989[5]
	ASAE	0.00979[4]	0.00921[2]	0.00860[1]	0.01005[6]	0.00924[3]	0.00982[5]
	$\sum$ Ranks	14[1]	24[2]	41[5]	51[6]	25[3]	34[4]
300	BIAS(ψ_1)	0.021801[1]	0.023760[3]	0.027495[6]	0.024165[4]	0.022172[2]	0.025094[5]
	BIAS(ψ_2)	0.020453[1]	0.024580[3]	0.026691[5]	0.027691[6]	0.021545[2]	0.026390[4]
	MSE(ψ_1)	0.000764[1]	0.000901[3]	0.001174[6]	0.000903[4]	0.000770[2]	0.000996[5]
	MSE(ψ_2)	0.000671[1]	0.000933[3]	0.001109[5]	0.001213[6]	0.000710[2]	0.001074[4]
	MRE(ψ_1)	0.036336[1]	0.039601[3]	0.045825[6]	0.040275[4]	0.036954[2]	0.041824[5]
	MRE(ψ_2)	0.027271[1]	0.032773[3]	0.035589[5]	0.036922[6]	0.028726[2]	0.035187[4]
	D_{abs}	0.01350[1]	0.01435[4]	0.01531[5]	0.01434[3]	0.01355[2]	0.01539[6]
	D_{max}	0.02098[1]	0.02257[3]	0.02424[5]	0.02310[4]	0.02113[2]	0.02439[6]
	ASAE	0.00727[4]	0.00718[2]	0.00663[1]	0.00750[6]	0.00725[3]	0.00733[5]
	$\sum$ Ranks	12[1]	27[3]	44[5.5]	43[4]	19[2]	44[5.5]
400	BIAS(ψ_1)	0.019076[2]	0.020507[3]	0.024805[6]	0.0224481[4]	0.018766[1]	0.022837[5]
	BIAS(ψ_2)	0.018264[1]	0.019476[2]	0.024076[4]	0.025200[6]	0.019930[3]	0.023551[5]
	MSE(ψ_1)	0.000588[2]	0.000647[3]	0.000978[6]	0.000782[4]	0.000544[1]	0.000812[5]
	MSE(ψ_2)	0.000533[1]	0.000633[3]	0.000890[5]	0.000981[6]	0.000611[2]	0.000876[4]
	MRE(ψ_1)	0.031794[2]	0.034179[3]	0.041342[6]	0.037414[4]	0.031276[1]	0.038061[5]
	MRE(ψ_2)	0.031794[3]	0.025967[1]	0.032101[5]	0.033600[6]	0.026573[2]	0.031401[4]
	D_{abs}	0.01172[2]	0.01240[3]	0.01401[6]	0.01350[4]	0.01132[1]	0.01395[5]
	D_{max}	0.01824[2]	0.01935[3]	0.02208[6]	0.02170[4]	0.01790[1]	0.02195[5]
	ASAE	0.00581[3]	0.00573[2]	0.00544[1]	0.00626[6]	0.00599[4]	0.00612[5]
	$\sum$ Ranks	18[2]	23[3]	45[6]	44[5]	16[1]	43[4]

Table 3. Numerical values of simulation evaluation for $\psi_1 = 0.9,\ \psi_2 = 1.2$.

n	Est.	∇_1	∇_2	∇_3	∇_4	∇_5	∇_6
30	BIAS(ψ_1)	0.103868[3]	0.103230[2]	0.111134[5]	0.115131[6]	0.093167[1]	0.107680[4]
	BIAS(ψ_2)	0.114888[1]	0.128357[3]	0.144888[4]	0.158059[6]	0.118652[2]	0.151435[5]
	MSE(ψ_1)	0.017636[3]	0.016782[2]	0.020492[5]	0.022028[6]	0.013914[1]	0.019451[4]
	MSE(ψ_2)	0.022642[2]	0.026062[3]	0.038388[5]	0.046825[6]	0.021270[1]	0.036153[4]
	MRE(ψ_1)	0.115409[3]	0.114700[2]	0.123482[5]	0.127923[6]	0.103519[1]	0.119644[4]
	MRE(ψ_2)	0.095740[1]	0.106964[3]	0.120740[4]	0.131715[6]	0.098876[2]	0.126196[5]
	D_{abs}	0.04448[1]	0.04646[3]	0.04835[4]	0.05027[6]	0.04535[2]	0.04982[5]
	$D_{\max}$	0.06922[2]	0.07232[3]	0.07702[4]	0.08145[6]	0.06918[1]	0.07944[5]
	ASAE	0.03685[6]	0.03342[2]	0.03162[1]	0.03509[4]	0.03543[5]	0.03420[3]
	$\sum$ Ranks	22[2]	23[3]	37[4]	52[6]	16[1]	39[5]
70	BIAS(ψ_1)	0.065665[3]	0.064812[2]	0.077676[6]	0.071321[4]	0.061420[1]	0.073118[5]
	BIAS(ψ_2)	0.071675[1]	0.081711[3]	0.092987[5]	0.090495[4]	0.076576[2]	0.096953[6]
	MSE(ψ_1)	0.006796[3]	0.006810[4]	0.009406[6]	0.007897[2]	0.006070[1]	0.008390[5]
	MSE(ψ_2)	0.009175[2]	0.010650[3]	0.013651[5]	0.013634[4]	0.008975[1]	0.014994[6]
	MRE(ψ_1)	0.072961[3]	0.072014[2]	0.086306[6]	0.079246[4]	0.068244[1]	0.081243[5]
	MRE(ψ_2)	0.059729[1]	0.068092[3]	0.077489[5]	0.075413[4]	0.063813[2]	0.080794[6]
	D_{abs}	0.02905[2]	0.03003[3]	0.03364[6]	0.03167[4]	0.02878[1]	0.03317[5]
	$D_{\max}$	0.04508[1]	0.04723[3]	0.05333[6]	0.05045[4]	0.04460[2]	0.05222[5]
	ASAE	0.02093[6]	0.01941[3]	0.01835[1]	0.01990[2]	0.02021[4]	0.02064[5]
	$\sum$ Ranks	22[2]	26[3]	46[5]	32[4]	15[1]	48[6]
100	BIAS(ψ_1)	0.052513[2]	0.053802[3]	0.058269[4]	0.063104[6]	0.051315[1]	0.061077[5]
	BIAS(ψ_2)	0.057221[1]	0.064936[3]	0.074116[4]	0.080300[6]	0.063665[2]	0.077341[5]
	MSE(ψ_1)	0.004391[2]	0.004535[3]	0.005397[4]	0.006287[6]	0.004142[1]	0.006093[5]
	MSE(ψ_2)	0.005466[1]	0.006885[3]	0.008805[4]	0.010786[6]	0.006066[2]	0.009575[5]
	MRE(ψ_1)	0.058348[2]	0.059780[3]	0.064743[4]	0.070116[6]	0.057017[1]	0.067864[5]
	MRE(ψ_2)	0.047684[1]	0.054114[3]	0.061763[4]	0.066916[5]	0.053054[2]	0.080794[6]
	D_{abs}	0.02332[1]	0.02435[3]	0.02632[4]	0.02834[6]	0.02401[2]	0.02789[5]
	$D_{\max}$	0.03611[1]	0.03831[3]	0.04146[4]	0.04504[6]	0.03762[2]	0.04386[5]
	ASAE	0.01686[6]	0.01555[2]	0.01476[1]	0.01639[4]	0.01665[5]	0.01603[3]
	$\sum$ Ranks	17[1]	26[3]	33[4]	51[6]	18[2]	44[5]
200	BIAS(ψ_1)	0.035462[1]	0.038700[3]	0.045018[6]	0.041725[5]	0.038129[2]	0.040537[4]
	BIAS(ψ_2)	0.040430[1]	0.045905[3]	0.052530[4]	0.056755[5]	0.043849[2]	0.057045[6]
	MSE(ψ_1)	0.002042[1]	0.002490[3]	0.003087[6]	0.002715[5]	0.002288[2]	0.002605[4]
	MSE(ψ_2)	0.002622[1]	0.003366[3]	0.004390[4]	0.005097[5]	0.002969[2]	0.005224[6]
	MRE(ψ_1)	0.039402[1]	0.043000[3]	0.050020[6]	0.046361[5]	0.042366[2]	0.045042[4]
	MRE(ψ_2)	0.033692[1]	0.038254[3]	0.043775[4]	0.047296[5]	0.036541[2]	0.047538[6]
	D_{abs}	0.01593[1]	0.01770[3]	0.01952[6]	0.01914[5]	0.01734[2]	0.01889[4]
	$D_{\max}$	0.02492[1]	0.02760[3]	0.03070[6]	0.03065[5]	0.02679[2]	0.03018[4]
	ASAE	0.01067[4]	0.01024[2]	0.00955[1]	0.01046[3]	0.01086[6]	0.01075[5]
	$\sum$ Ranks	12[1]	26[3]	43[5]	43[5]	22[2]	43[5]
300	BIAS(ψ_1)	0.029958[2]	0.032943[3]	0.035304[6]	0.033956[5]	0.028826[1]	0.033259[4]
	BIAS(ψ_2)	0.033418[1]	0.036504[3]	0.042492[4]	0.045432[6]	0.036423[2]	0.045406[5]
	MSE(ψ_1)	0.001404[2]	0.001631[3]	0.001891[6]	0.001848[5]	0.001317[1]	0.001783[4]
	MSE(ψ_2)	0.001787[1]	0.002185[3]	0.002783[4]	0.003318[5]	0.002062[2]	0.003282[6]
	MRE(ψ_1)	0.033286[2]	0.036604[3]	0.039227[6]	0.037729[5]	0.032029[1]	0.036954[4]
	MRE(ψ_2)	0.027849[1]	0.030420[3]	0.035410[4]	0.037860[6]	0.030352[2]	0.037838[5]
	D_{abs}	0.01321[1]	0.01476[3]	0.01558[6]	0.01557[5]	0.01357[2]	0.01566[4]
	$D_{\max}$	0.02065[1]	0.02288[4]	0.02456[5]	0.02481[3]	0.02125[2]	0.02485[6]
	ASAE	0.00834[5]	0.00795[2]	0.00746[1]	0.00824[3]	0.00843[6]	0.00825[4]
	$\sum$ Ranks	16[1]	27[4]	42[5.5]	38[3]	19[2]	42[5.5]
400	BIAS(ψ_1)	0.025496[1]	0.029506[4]	0.029586[5]	0.028330[3]	0.027468[2]	0.029599[6]
	BIAS(ψ_2)	0.030431[1]	0.032646[3]	0.034910[4]	0.039947[6]	0.030991[2]	0.039385[5]
	MSE(ψ_1)	0.000990[1]	0.001363[5]	0.001389[6]	0.001306[3]	0.001180[2]	0.001334[4]
	MSE(ψ_2)	0.001448[1]	0.001646[3]	0.002037[4]	0.002635[6]	0.001499[2]	0.002337[5]
	MRE(ψ_1)	0.028328[1]	0.032784[4]	0.032874[5]	0.031478[3]	0.030519[2]	0.032887[6]
	MRE(ψ_2)	0.025359[1]	0.027205[3]	0.029092[4]	0.033289[6]	0.025826[2]	0.032821[5]
	D_{abs}	0.01146[1]	0.01300[3]	0.01301[4]	0.01333[5]	0.01229[2]	0.01340[6]
	$D_{\max}$	0.01801[1]	0.02032[3]	0.02044[4]	0.02130[5]	0.01910[2]	0.02145[6]
	ASAE	0.00704[6]	0.00635[1]	0.00638[2]	0.00686[4]	0.00703[5]	0.00676[3]
	$\sum$ Ranks	14[1]	29[3]	38[4]	41[5]	21[2]	46[6]

Table 4. Numerical values of simulation evaluation for $\psi_1 = 0.7,\ \psi_2 = 1.1$.

n	Est.	∇_1	∇_2	∇_3	∇_4	∇_5	∇_6
30	BIAS(ψ_1)	0.079201[1]	0.081250[3]	0.093778[6]	0.090610[4]	0.079847[2]	0.091350[5]
	BIAS(ψ_2)	0.112783[2]	0.114497[3]	0.135115[5]	0.151140[6]	0.108745[1]	0.134603[4]
	MSE(ψ_1)	0.010058[1]	0.010786[3]	0.013750[6]	0.013386[4]	0.010584[2]	0.013505[5]
	MSE(ψ_2)	0.023746[3]	0.021938[2]	0.030767[5]	0.041082[6]	0.017647[1]	0.029501[4]
	MRE(ψ_1)	0.113144[1]	0.116072[3]	0.133968[6]	0.129442[4]	0.114068[2]	0.130500[5]
	MRE(ψ_2)	0.102530[2]	0.104088[3]	0.122832[5]	0.137400[6]	0.098859[1]	0.122366[4]
	D_{abs}	0.04269[1]	0.04439[2]	0.04826[4]	0.04997[5]	0.04498[3]	0.05058[6]
	D_{max}	0.04269[1]	0.06961[3]	0.07645[4]	0.08157[6]	0.06875[2]	0.07984[5]
	ASAE	0.03686[6]	0.03250[2]	0.03151[1]	0.03493[5]	0.03490[4]	0.03393[3]
	$\sum$ Ranks	18[1.5]	24[3]	42[5]	46[6]	18[1.5]	41[4]
70	BIAS(ψ_1)	0.051382[2]	0.057029[3]	0.066726[6]	0.058323[4]	0.049704[1]	0.061499[5]
	BIAS(ψ_2)	0.065124[1]	0.070270[2]	0.084821[5]	0.091135[6]	0.073417[3]	0.082290[4]
	MSE(ψ_1)	0.004120[1]	0.005019[3]	0.007076[6]	0.005335[4]	0.004144[2]	0.005948[5]
	MSE(ψ_2)	0.006881[1]	0.007780[2]	0.011432[5]	0.012825[6]	0.008123[3]	0.010971[4]
	MRE(ψ_1)	0.073403[2]	0.081470[3]	0.095324[6]	0.083319[4]	0.071005[1]	0.087855[5]
	MRE(ψ_2)	0.059203[1]	0.063882[2]	0.077110[5]	0.082850[6]	0.066742[3]	0.074809[4]
	D_{abs}	0.02812[1]	0.03073[3]	0.03309[5]	0.03230[4]	0.02896[2]	0.03322[6]
	D_{max}	0.04381[1]	0.04764[3]	0.05249[6]	0.05232[5]	0.04529[2]	0.05185[4]
	ASAE	0.02110[6]	0.01902[2]	0.01877[1]	0.01993[4]	0.01987[3]	0.02007[5]
	$\sum$ Ranks	16[1]	23[3]	45[6]	43[5]	20[2]	42[4]
100	BIAS(ψ_1)	0.043495[1]	0.046247[3]	0.050964[6]	0.050990[5]	0.044867[2]	0.048470[4]
	BIAS(ψ_2)	0.053087[1]	0.058107[2]	0.067640[4]	0.071513[6]	0.058768[3]	0.069748[5]
	MSE(ψ_1)	0.002926[1]	0.003485[3]	0.004075[6]	0.004016[5]	0.003252[2]	0.003624[4]
	MSE(ψ_2)	0.004493[1]	0.005566[2]	0.007480[4]	0.008714[6]	0.005300[3]	0.008094[5]
	MRE(ψ_1)	0.062136[1]	0.066067[3]	0.072806[5]	0.072843[6]	0.064096[2]	0.069243[4]
	MRE(ψ_2)	0.048261[1]	0.052825[2]	0.061491[4]	0.065012[6]	0.053425[3]	0.063407[5]
	D_{abs}	0.02351[1]	0.02504[3]	0.02576[4]	0.02700[6]	0.02489[2]	0.02615[5]
	D_{max}	0.03652[1]	0.03905[3]	0.04086[4]	0.04282[6]	0.03860[2]	0.04139[5]
	ASAE	0.01689[6]	0.01532[2]	0.01435[1]	0.01604[3]	0.01606[4]	0.01624[5]
	$\sum$ Ranks	14[1]	23[2.5]	38[4]	49[6]	23[2.5]	42[5]
200	BIAS(ψ_1)	0.028900[1]	0.031410[2]	0.037080[6]	0.036155[5]	0.031887[3]	0.034297[4]
	BIAS(ψ_2)	0.037966[1]	0.041888[3]	0.045302[4]	0.052373[6]	0.039924[2]	0.050940[5]
	MSE(ψ_1)	0.001287[1]	0.001577[3]	0.002135[6]	0.002068[5]	0.001561[2]	0.001860[4]
	MSE(ψ_2)	0.002393[1]	0.002837[3]	0.003253[4]	0.004421[6]	0.002502[2]	0.004050[5]
	MRE(ψ_1)	0.041286[1]	0.044871[2]	0.052971[6]	0.051650[5]	0.045553[3]	0.048995[4]
	MRE(ψ_2)	0.034515[1]	0.038080[3]	0.041184[4]	0.047612[6]	0.036294[2]	0.046309[5]
	D_{abs}	0.01590[1]	0.01702[2]	0.01877[5]	0.01967[6]	0.01726[3]	0.01873[4]
	D_{max}	0.02499[1]	0.02675[2]	0.02943[4]	0.03139[6]	0.02687[3]	0.02989[5]
	ASAE	0.01079[6]	0.00979[2]	0.00946[1]	0.01048[5]	0.01030[4]	0.010240[3]
	$\sum$ Ranks	14[1]	22[2]	40[5]	50[6]	24[3]	39[4]
300	BIAS(ψ_1)	0.024238[1]	0.026155[3]	0.029893[6]	0.026118[4]	0.024592[2]	0.027734[5]
	BIAS(ψ_2)	0.029988[1]	0.036050[3]	0.039147[5]	0.040614[6]	0.031593[2]	0.038705[4]
	MSE(ψ_1)	0.000948[2]	0.001092[4]	0.001389[6]	0.001056[3]	0.000941[1]	0.001213[5]
	MSE(ψ_2)	0.001445[1]	0.002007[3]	0.002386[5]	0.002608[6]	0.001529[2]	0.002311[4]
	MRE(ψ_1)	0.034626[1]	0.037365[4]	0.042705[6]	0.037312[3]	0.035131[2]	0.039620[5]
	MRE(ψ_2)	0.027262[1]	0.032773[3]	0.035588[5]	0.036922[6]	0.028721[2]	0.035187[4]
	D_{abs}	0.01349[1]	0.01435[4]	0.01531[5]	0.01434[3]	0.01355[2]	0.01539[6]
	D_{max}	0.02097[1]	0.02257[3]	0.02424[5]	0.02310[4]	0.02112[2]	0.02439[6]
	ASAE	0.00820[5]	0.00773[2]	0.00738[1]	0.00797[4]	0.00823[6]	0.00783[3]
	$\sum$ Ranks	14[1]	29[3]	44[6]	39[4]	21[2]	42[5]
400	BIAS(ψ_1)	0.021251[2]	0.022782[3]	0.027032[6]	0.024434[4]	0.020536[1]	0.025178[5]
	BIAS(ψ_2)	0.026804[1]	0.028565[2]	0.035312[5]	0.036960[6]	0.029195[3]	0.034541[4]
	MSE(ψ_1)	0.000734[2]	0.000794[3]	0.001163[6]	0.000926[4]	0.000649[1]	0.000980[5]
	MSE(ψ_2)	0.001148[1]	0.001363[3]	0.001915[5]	0.002110[6]	0.001312[2]	0.001885[4]
	MRE(ψ_1)	0.030358[2]	0.032546[3]	0.038617[6]	0.034906[4]	0.029338[1]	0.035968[5]
	MRE(ψ_2)	0.024368[1]	0.025968[2]	0.032102[5]	0.033600[6]	0.026541[3]	0.031401[4]
	D_{abs}	0.01173[2]	0.01240[3]	0.01401[6]	0.01350[4]	0.01132[1]	0.01395[5]
	D_{max}	0.01824[2]	0.01935[3]	0.02208[6]	0.02170[4]	0.01789[1]	0.02195[5]
	ASAE	0.00665[4]	0.00629[2]	0.00611[1]	0.00671[5]	0.00686[6]	0.00664[3]
	$\sum$ Ranks	17[1]	24[3]	41[5]	43[6]	19[2]	40[4]

Table 5. Numerical values of simulation evaluation for $\psi_1 = 1.2,\ \psi_2 = 0.8$.

n	Est.	∇_1	∇_2	∇_3	∇_4	∇_5	∇_6
30	BIAS(ψ_1)	0.138493$^{\{3\}}$	0.134011$^{\{2\}}$	0.143351$^{\{4\}}$	0.155671$^{\{6\}}$	0.120471$^{\{1\}}$	0.146109$^{\{5\}}$
	BIAS(ψ_2)	0.076590$^{\{2\}}$	0.085570$^{\{3\}}$	0.096592$^{\{4\}}$	0.105372$^{\{6\}}$	0.079104$^{\{1\}}$	0.100957$^{\{5\}}$
	MSE(ψ_1)	0.032817$^{\{3\}}$	0.029235$^{\{2\}}$	0.034828$^{\{4\}}$	0.042063$^{\{6\}}$	0.023085$^{\{1\}}$	0.036903$^{\{5\}}$
	MSE(ψ_2)	0.010062$^{\{2\}}$	0.011583$^{\{3\}}$	0.017062$^{\{5\}}$	0.020811$^{\{6\}}$	0.009454$^{\{1\}}$	0.016068$^{\{4\}}$
	MRE(ψ_1)	0.115411$^{\{3\}}$	0.111676$^{\{2\}}$	0.119459$^{\{4\}}$	0.129726$^{\{6\}}$	0.100392$^{\{1\}}$	0.121758$^{\{5\}}$
	MRE(ψ_2)	0.095737$^{\{1\}}$	0.106962$^{\{3\}}$	0.120740$^{\{4\}}$	0.131715$^{\{6\}}$	0.098881$^{\{2\}}$	0.126196$^{\{5\}}$
	D_{abs}	0.04448$^{\{1\}}$	0.04646$^{\{3\}}$	0.04835$^{\{4\}}$	0.05027$^{\{6\}}$	0.04535$^{\{2\}}$	0.04982$^{\{5\}}$
	$D_{\max}$	0.06921$^{\{2\}}$	0.07232$^{\{3\}}$	0.07702$^{\{4\}}$	0.08145$^{\{6\}}$	0.06918$^{\{1\}}$	0.07944$^{\{5\}}$
	ASAE	0.03596$^{\{5\}}$	0.03393$^{\{2\}}$	0.03093$^{\{1\}}$	0.03606$^{\{6\}}$	0.03454$^{\{3\}}$	0.03516$^{\{4\}}$
	$\sum$ Ranks	22$^{\{2\}}$	23$^{\{3\}}$	36$^{\{4\}}$	54$^{\{6\}}$	13$^{\{1\}}$	43$^{\{5\}}$
70	BIAS(ψ_1)	0.086321$^{\{2\}}$	0.086687$^{\{3\}}$	0.096321$^{\{6\}}$	0.091759$^{\{4\}}$	0.079816$^{\{1\}}$	0.093088$^{\{5\}}$
	BIAS(ψ_2)	0.047780$^{\{1\}}$	0.054473$^{\{3\}}$	0.061992$^{\{5\}}$	0.060330$^{\{4\}}$	0.051060$^{\{2\}}$	0.064636$^{\{6\}}$
	MSE(ψ_1)	0.011819$^{\{2\}}$	0.012097$^{\{3\}}$	0.014688$^{\{6\}}$	0.013176$^{\{4\}}$	0.010348$^{\{1\}}$	0.014381$^{\{5\}}$
	MSE(ψ_2)	0.004078$^{\{2\}}$	0.004733$^{\{3\}}$	0.006067$^{\{5\}}$	0.006060$^{\{4\}}$	0.003990$^{\{1\}}$	0.006664$^{\{6\}}$
	MRE(ψ_1)	0.071934$^{\{2\}}$	0.072239$^{\{3\}}$	0.080267$^{\{6\}}$	0.076466$^{\{4\}}$	0.066514$^{\{1\}}$	0.077573$^{\{5\}}$
	MRE(ψ_2)	0.059726$^{\{1\}}$	0.068092$^{\{3\}}$	0.077490$^{\{5\}}$	0.075413$^{\{4\}}$	0.063824$^{\{2\}}$	0.080794$^{\{6\}}$
	D_{abs}	0.02905$^{\{1\}}$	0.03003$^{\{2\}}$	0.03364$^{\{5\}}$	0.03167$^{\{3\}}$	0.04535$^{\{6\}}$	0.03317$^{\{4\}}$
	$D_{\max}$	0.04508$^{\{1\}}$	0.04723$^{\{2\}}$	0.05333$^{\{5\}}$	0.05045$^{\{3\}}$	0.06918$^{\{6\}}$	0.05222$^{\{4\}}$
	ASAE	0.01977$^{\{4\}}$	0.01896$^{\{2\}}$	0.01721$^{\{1\}}$	0.01965$^{\{3\}}$	0.03454$^{\{6\}}$	0.02065$^{\{5\}}$
	$\sum$ Ranks	16$^{\{1\}}$	24$^{\{2\}}$	44$^{\{5\}}$	33$^{\{4\}}$	26$^{\{3\}}$	46$^{\{6\}}$
100	BIAS(ψ_1)	0.068804$^{\{1\}}$	0.072297$^{\{2\}}$	0.073475$^{\{3\}}$	0.082866$^{\{6\}}$	0.079816$^{\{4\}}$	0.080396$^{\{5\}}$
	BIAS(ψ_2)	0.038135$^{\{1\}}$	0.043293$^{\{2\}}$	0.049410$^{\{3\}}$	0.053532$^{\{6\}}$	0.051060$^{\{4\}}$	0.051560$^{\{5\}}$
	MSE(ψ_1)	0.007753$^{\{1\}}$	0.008310$^{\{2\}}$	0.008732$^{\{3\}}$	0.010784$^{\{5\}}$	0.067622$^{\{6\}}$	0.010484$^{\{4\}}$
	MSE(ψ_2)	0.002428$^{\{1\}}$	0.003060$^{\{2\}}$	0.003913$^{\{3\}}$	0.004794$^{\{5\}}$	0.042445$^{\{6\}}$	0.004255$^{\{4\}}$
	MRE(ψ_1)	0.057336$^{\{2\}}$	0.060248$^{\{3\}}$	0.061229$^{\{4\}}$	0.069055$^{\{6\}}$	0.056351$^{\{1\}}$	0.066996$^{\{5\}}$
	MRE(ψ_2)	0.047669$^{\{1\}}$	0.054116$^{\{3\}}$	0.061762$^{\{4\}}$	0.066915$^{\{6\}}$	0.053056$^{\{2\}}$	0.064450$^{\{5\}}$
	D_{abs}	0.02331$^{\{1\}}$	0.02435$^{\{3\}}$	0.02632$^{\{4\}}$	0.02834$^{\{6\}}$	0.02402$^{\{2\}}$	0.02789$^{\{5\}}$
	$D_{\max}$	0.03610$^{\{1\}}$	0.03831$^{\{2\}}$	0.05333$^{\{6\}}$	0.04504$^{\{5\}}$	0.03762$^{\{3\}}$	0.04386$^{\{4\}}$
	ASAE	0.01569$^{\{5\}}$	0.01493$^{\{2\}}$	0.01377$^{\{1\}}$	0.01605$^{\{6\}}$	0.01528$^{\{3\}}$	0.01567$^{\{4\}}$
	$\sum$ Ranks	14$^{\{1\}}$	21$^{\{2\}}$	31$^{\{3.5\}}$	41$^{\{5.5\}}$	31$^{\{3.5\}}$	41$^{\{5.5\}}$
200	BIAS(ψ_1)	0.003688$^{\{1\}}$	0.051478$^{\{3\}}$	0.055240$^{\{6\}}$	0.054960$^{\{5\}}$	0.049060$^{\{2\}}$	0.053140$^{\{4\}}$
	BIAS(ψ_2)	0.026944$^{\{1\}}$	0.030603$^{\{3\}}$	0.035019$^{\{4\}}$	0.037837$^{\{5\}}$	0.029243$^{\{2\}}$	0.038030$^{\{6\}}$
	MSE(ψ_1)	0.003688$^{\{2\}}$	0.004440$^{\{3\}}$	0.004584$^{\{5\}}$	0.004739$^{\{6\}}$	0.003826$^{\{1\}}$	0.004449$^{\{4\}}$
	MSE(ψ_2)	0.001165$^{\{1\}}$	0.001496$^{\{3\}}$	0.001951$^{\{4\}}$	0.002265$^{\{5\}}$	0.001321$^{\{2\}}$	0.002322$^{\{6\}}$
	MRE(ψ_1)	0.039590$^{\{1\}}$	0.042898$^{\{3\}}$	0.046033$^{\{6\}}$	0.045800$^{\{5\}}$	0.040883$^{\{2\}}$	0.044283$^{\{3\}}$
	MRE(ψ_2)	0.033680$^{\{1\}}$	0.038254$^{\{3\}}$	0.043774$^{\{4\}}$	0.047296$^{\{5\}}$	0.036554$^{\{2\}}$	0.047538$^{\{6\}}$
	D_{abs}	0.01594$^{\{1\}}$	0.01770$^{\{3\}}$	0.01952$^{\{6\}}$	0.01914$^{\{5\}}$	0.01734$^{\{2\}}$	0.01889$^{\{4\}}$
	$D_{\max}$	0.02493$^{\{1\}}$	0.02760$^{\{3\}}$	0.03070$^{\{6\}}$	0.03065$^{\{5\}}$	0.02679$^{\{2\}}$	0.03018$^{\{4\}}$
	ASAE	0.00960$^{\{1\}}$	0.00966$^{\{2\}}$	0.00869$^{\{3\}}$	0.00993$^{\{5\}}$	0.00975$^{\{4\}}$	0.01026$^{\{6\}}$
	$\sum$ Ranks	10$^{\{1\}}$	26$^{\{3\}}$	44$^{\{5\}}$	46$^{\{6\}}$	19$^{\{2\}}$	43$^{\{4\}}$
300	BIAS(ψ_1)	0.038799$^{\{2\}}$	0.042989$^{\{4\}}$	0.044219$^{\{3\}}$	0.044126$^{\{5\}}$	0.038252$^{\{1\}}$	0.044210$^{\{6\}}$
	BIAS(ψ_2)	0.022280$^{\{1\}}$	0.024336$^{\{3\}}$	0.028328$^{\{4\}}$	0.030287$^{\{6\}}$	0.024280$^{\{2\}}$	0.030270$^{\{5\}}$
	MSE(ψ_1)	0.002355$^{\{2\}}$	0.002782$^{\{3\}}$	0.002987$^{\{4\}}$	0.003100$^{\{6\}}$	0.002325$^{\{1\}}$	0.003075$^{\{5\}}$
	MSE(ψ_2)	0.000794$^{\{1\}}$	0.000971$^{\{3\}}$	0.001237$^{\{4\}}$	0.001474$^{\{6\}}$	0.000917$^{\{2\}}$	0.001459$^{\{5\}}$
	MRE(ψ_1)	0.032333$^{\{2\}}$	0.035824$^{\{3\}}$	0.036849$^{\{6\}}$	0.036772$^{\{4\}}$	0.031876$^{\{1\}}$	0.036841$^{\{5\}}$
	MRE(ψ_2)	0.027850$^{\{1\}}$	0.030420$^{\{3\}}$	0.035410$^{\{4\}}$	0.037859$^{\{6\}}$	0.030350$^{\{2\}}$	0.037838$^{\{5\}}$
	D_{abs}	0.01321$^{\{1\}}$	0.01476$^{\{3\}}$	0.01558$^{\{5\}}$	0.01557$^{\{4\}}$	0.01358$^{\{2\}}$	0.01566$^{\{6\}}$
	$D_{\max}$	0.02065$^{\{1\}}$	0.02288$^{\{3\}}$	0.02456$^{\{4\}}$	0.02481$^{\{5\}}$	0.02126$^{\{2\}}$	0.02485$^{\{6\}}$
	ASAE	0.00744$^{\{3.5\}}$	0.00735$^{\{2\}}$	0.00670$^{\{1\}}$	0.00775$^{\{6\}}$	0.00744$^{\{3.5\}}$	0.00772$^{\{5\}}$
	$\sum$ Ranks	14.5$^{\{1\}}$	27$^{\{3\}}$	35$^{\{4\}}$	48$^{\{6\}}$	16.5$^{\{2\}}$	43$^{\{5\}}$
400	BIAS(ψ_1)	0.032927$^{\{1\}}$	0.038213$^{\{6\}}$	0.037063$^{\{3\}}$	0.037679$^{\{4\}}$	0.035147$^{\{2\}}$	0.037879$^{\{5\}}$
	BIAS(ψ_2)	0.020280$^{\{1\}}$	0.021764$^{\{3\}}$	0.023273$^{\{4\}}$	0.026632$^{\{6\}}$	0.020653$^{\{2\}}$	0.026256$^{\{5\}}$
	MSE(ψ_1)	0.001686$^{\{1\}}$	0.002275$^{\{5\}}$	0.002188$^{\{3\}}$	0.002376$^{\{6\}}$	0.001995$^{\{2\}}$	0.002269$^{\{4\}}$
	MSE(ψ_2)	0.000643$^{\{1\}}$	0.000732$^{\{3\}}$	0.000905$^{\{4\}}$	0.001171$^{\{6\}}$	0.000666$^{\{2\}}$	0.001039$^{\{5\}}$
	MRE(ψ_1)	0.027439$^{\{1\}}$	0.031844$^{\{6\}}$	0.030886$^{\{3\}}$	0.031399$^{\{4\}}$	0.029289$^{\{2\}}$	0.031566$^{\{5\}}$
	MRE(ψ_2)	0.025350$^{\{1\}}$	0.027205$^{\{3\}}$	0.029092$^{\{4\}}$	0.033290$^{\{6\}}$	0.025817$^{\{2\}}$	0.032820$^{\{5\}}$
	D_{abs}	0.01146$^{\{1\}}$	0.01300$^{\{3\}}$	0.01301$^{\{4\}}$	0.01333$^{\{5\}}$	0.01230$^{\{2\}}$	0.01340$^{\{6\}}$
	$D_{\max}$	0.01801$^{\{1\}}$	0.02032$^{\{3\}}$	0.02044$^{\{4\}}$	0.02130$^{\{5\}}$	0.01911$^{\{2\}}$	0.02145$^{\{6\}}$
	ASAE	0.00621$^{\{4\}}$	0.00580$^{\{2\}}$	0.00570$^{\{1\}}$	0.00641$^{\{6\}}$	0.00613$^{\{3\}}$	0.00626$^{\{5\}}$
	$\sum$ Ranks	12$^{\{1\}}$	34$^{\{4\}}$	30$^{\{3\}}$	48$^{\{6\}}$	19$^{\{2\}}$	46$^{\{5\}}$

Table 6. Relative and comprehensive rankings of all estimation techniques for the proposed distribution across varying model parameter values.

Parameter	n	∇_1	∇_2	∇_3	∇_4	∇_5	∇_6
$\psi_1 = 0.6,\ \psi_2 = 0.7$	30	2.0	3.0	4.5	6.0	1.0	4.5
	70	1.0	3.0	6.0	5.0	2.0	4.0
	100	1.0	3.0	4.0	6.0	2.0	5.0
	200	1.0	2.0	5.0	6.0	3.0	4.0
	300	1.0	3.0	5.5	4.0	2.0	5.5
	400	2.0	3.0	6.0	5.0	1.0	4.0
$\psi_1 = 0.9,\ \psi_2 = 1.2$	30	2.0	3.0	4.0	6.0	1.0	5.0
	70	2.0	3.0	5.0	4.0	1.0	6.0
	100	1.0	3.0	4.0	6.0	2.0	5.0
	200	1.0	3.0	5.0	5.0	2.0	5.0
	300	1.0	4.0	5.5	3.0	2.0	5.5
	400	1.0	3.0	4.0	5.0	2.0	6.0
$\psi_1 = 0.7,\ \psi_2 = 1.1$	30	1.5	3.0	5.0	6.0	1.5	4.0
	70	1.0	3.0	6.0	5.0	2.0	4.0
	100	1.0	2.5	4.0	6.0	2.5	5.0
	200	1.0	2.0	5.0	6.0	3.0	4.0
	300	1.0	3.0	6.0	4.0	2.0	5.0
	400	1.0	3.0	5.0	6.0	2.0	4.0
$\psi_1 = 1.2,\ \psi_2 = 0.8$	30	2.0	3.0	4.0	6.0	1.0	5.0
	70	1.0	2.0	5.0	5.0	3.0	6.0
	100	1.0	2.0	3.5	5.5	3.5	5.5
	200	1.0	3.0	5.0	6.0	2.0	4.0
	300	1.0	3.0	4.0	6.0	2.0	5.0
	400	1.0	4.0	3.0	6.0	2.0	5.0
$\sum$ Ranks		29.5	69.0	114.0	128.5	47.5	116.0
Overall Rank		1.0	3.0	4.0	6.0	2.0	5.0

Although various estimation techniques are discussed in this paper, the aim here is not to rank all of the estimation techniques universally but to investigate their finite sample behavior for the NCWD distribution. As seen from the simulation tables, the MLE technique always offers the most precise parameter estimations and the highest rank in general. Therefore, MLE can be viewed as the most appropriate technique for estimation in practice when using the NCWD distribution. All other techniques discussed are merely used for comparative purposes as benchmarks for the investigation of the NCWD distribution in different estimation frameworks. Theoretical investigations of asymptotic properties, computational efficiency, and estimator-selection criteria are beyond the scope of the present study and remain topics for future research.

4.8. Bayesian analysis

Bayesian estimation is applied to estimate the NCWD model's unknown parameters. This approach evaluates parameters as random variables rather than definite quantities and assigns them a prior distribution based on existing beliefs. Given that such previous knowledge is frequently unavailable, selecting an acceptable prior becomes an important challenge. We use a joint conjugate prior distribution for the ψ_1 and ψ_2 parameters, thereby assuming a gamma distribution for each. Hence $\psi_1 \sim \text{Gamma}(\alpha_1, \alpha_2)$ and $\psi_2 \sim \text{Gamma}(\alpha_3, \alpha_4)$. The prior distributions for the parameters ψ_1 and ψ_2 are specified as follows: $\varrho_1(\psi_1)$ and $\varrho_2(\psi_2)$, respectively,

$$\varrho_1(\psi_1) = \frac{\alpha_2^{\alpha_1}}{\Gamma(\alpha_1)} \psi_1^{\alpha_1 - 1} e^{-\alpha_2 \psi_1}, \qquad \alpha_1, \alpha_2 > 0,\ \psi_1 > 0, \tag{4.2}$$

and

$$\varrho_2(\psi_2) = \frac{\alpha_4^{\alpha_3}}{\Gamma(\alpha_3)} \psi_2^{\alpha_3 - 1} e^{-\alpha_4 \psi_2}, \qquad \alpha_3, \alpha_4 > 0,\ \psi_2 > 0 \tag{4.3}$$

where α_j ; $j = 1, 2, 3, 4$ serve as hyperparameters in this context.

The joint probability density function that defines $\varphi(\psi_1, \psi_2)$ is as follows:

$$\varrho(\varphi) = \varrho_1(\psi_2)\, \varrho_2(\psi_2). \tag{4.4}$$

By incorporating Eqs (4.2) and (4.3) into Eq (4.4), we obtain the following:

$$\varrho(\varphi) \propto \psi_1^{\alpha_1 - 1} \psi_2^{\alpha_3 - 1} e^{-(\alpha_2 \psi_1 + \alpha_4 \psi_2)}.$$

The joint posterior density is obtained by applying Bayes' theorem as follows:

$$\varrho(\varphi \mid z) = \frac{L(z \mid \varphi) \varrho(\varphi)}{\int_0^\infty \int_0^\infty L(z \mid \varphi) \varrho(\varphi)\, d\varphi}.$$

Our present technique leverages three different loss functions: squared error loss (SELF), linear-exponential loss (LELF), and generalized entropy loss (GELF).

The SELF is a mostly applied loss function in statistical estimation and Bayesian inference. It evaluates the difference between the real parameter value and its estimate by calculating the square of their difference. Because the error function is squared, bigger estimating errors incur a much higher penality than the smaller ones which making SELF susceptible to significant deviations. Mathematically, if φ denotes the real parameter and $\hat{\varphi}$ denotes its estimate, then the SELF is defined as follows:

$$L(\varphi, \hat{\varphi}) = (\varphi - \hat{\varphi})^2.$$

When employing a SELF, the posterior mean is the closest Bayesian estimate:

$$\hat{\varphi}_{SELF} = \mathbb{E}\left[\varphi \mid Z\right] = \int \varphi\, \varrho(\varphi \mid z)\, d\varphi. \tag{4.5}$$

Varian [31], established a LELF to solve estimates where there are unequal consequences associated with overestimation and underestimation. Linex differs from SELF because it penalizes each estimate equally, whereas LELF takes asymmetric penalties in estimate errors into consideration and therefore assigns different weights to negative and positive error terms, based on penalties of the errors, in order to compute a corresponding overall estimation error. The key characteristic of LELF is that it exponentially grows in one direction and approximately linear in other direction. The LELF is defined as follows:

$$L(\varphi, \hat{\varphi}) = e^{c(\varphi-\hat{\varphi})} - c(\varphi - \hat{\varphi}) - 1, \qquad c \neq 0.$$

The parameter c determines the degree and direction of asymmetry in the LINEX loss function. Throughout this study, two values, $v_1 = -0.5$ and $v_1 = 0.5$, are considered for c to investigate the performance of the estimators under different asymmetric loss structures. The Bayes estimate, which compensates for this, appears as follows:

$$\hat{\varphi}_{LELF} = -\frac{1}{c} \ln(\mathbb{E}[e^{-c\varphi} \mid z]) = -\frac{1}{c} \ln \int e^{-c\varphi}\, \varrho(\varphi \mid z)\, d\varphi. \tag{4.6}$$

The GELF is a versatile asymmetric loss function that can be employed to generate Bayesian estimates. Its versatility stems from a parameter that enables it to change the level of asymmetry, thus making it appropriate for situations where overestimation and underestimation have distinct repercussions. The GELF is described as follows when estimating a parameter φ with an estimator $\hat{\varphi}$:

$$L(\varphi, \hat{\varphi}) = [\left(\frac{\hat{\varphi}}{\varphi}\right)^{\omega} - k \ln\left(\frac{\hat{\varphi}}{\varphi}\right) - 1],$$

for which $\omega \neq 0$ is the shape (asymmetry) parameter controlling the degree of penalty imposed on estimation errors. The hyperparameters for the above mentioned loss functions used in this work have been set to $p_1 = -0.5$ and $p_2 = 0.5$ for the GELF. The Bayesian estimator derived under GELF is expressed as follows:

$$\hat{\varphi}_{GELF} = \left(\mathbb{E}\left[(\varphi|z)^{-\omega}\right]\right)^{-\frac{1}{\omega}} = \left[\int (\varphi|z)^{-\omega}\, \varrho(\varphi \mid z)\, d\varphi\right]^{-\frac{1}{\omega}}. \tag{4.7}$$

To overcome the analytical challenge of Eqs (4.5)–(4.7), we implemented Bayesian estimation with R in Markov Chain Monte Carlo (MCMC) simulation. The MCMC approach produced samples from the posterior distributions of the unknown parameters, thus permitting us to derive reliable Bayesian estimates. This method's primary benefit is its ability to handle complicated models and provide precise conclusions based on the posterior distribution. The Bayesian estimates for the parameter vector $\varphi^i = (\psi_1^i, \psi_2^i)$ have been determined based on three specific loss functions: SELF, LELF, and GELF. The estimations are described as follows:

$$\hat{\varphi}_{SELF} = \frac{1}{M-B} \sum_{k=B+1}^{M} \varphi_k^i,$$

$$\hat{\varphi}_{LELF} = -\frac{1}{c} \ln\left(\frac{1}{M-B} \sum_{k=B+1}^{M} e^{-c\varphi_k^i}\right),$$

$$\hat{\varphi}_{GELF} = \left(\frac{1}{M-B} \sum_{k=B+1}^{M} (\varphi_k^i)^{-\omega}\right)^{-\frac{1}{\omega}}.$$

Here, $M = 3000$ presents the total number of MCMC iterations and $B = 500$ presents the number of burn-in iterations that were discarded in order to achieve convergence.

4.9. Metropolis-Hastings within Gibbs sampling algorithm

We adopt a Metropolis-Hastings embedding within the Gibbs sampler to generate samples from the joint posterior distribution of the parameter vector:

(1) Consider the initial values

$$\psi_1^{(0)}, \psi_2^{(0)}.$$

(2) Iterations $t = 1, 2, \dots, T$

(i) Sample $\psi_1^{(t)}$ given $\psi_2^{(t-1)}$

(a) Propose $\psi_1^* \sim q_1(\psi_1^* \mid \psi_1^{(t-1)})$.

(b) Compute the acceptance probability

$$\alpha_1 = \min\Big(1,\ \frac{\pi(\psi_1^*, \psi_2^{(t-1)} \mid z)}{\pi(\psi_1^{(t-1)}, \psi_2^{(t-1)} \mid z)} \times \frac{q_1(\psi_1^{(t-1)} \mid \psi_1^*)}{q_1(\psi_1^* \mid \psi_1^{(t-1)})}\Big).$$

(c) Accept ψ_1^* with probability α_1, otherwise, set

$$\psi_1^{(t)} = \psi_1^{(t-1)}.$$

(ii) Sample $\psi_2^{(t)}$ given $\psi_1^{(t)}$

(a) Propose $\psi_2^* \sim q_2(\psi_2^* \mid \psi_2^{(t-1)})$.

(b) Compute

$$\alpha_2 = \min\Big(1,\ \frac{\pi(\psi_1^{(t)}, \psi_2^* \mid z)}{\pi(\psi_1^{(t)}, \psi_2^{(t-1)} \mid z)} \times \frac{q_2(\psi_2^{(t-1)} \mid \psi_2^*)}{q_2(\psi_2^* \mid \psi_2^{(t-1)})}\Big).$$

(c) Accept ψ_2^* with probability α_2; otherwise set

$$\psi_2^{(t)} = \psi_2^{(t-1)}.$$

(3) Repeat steps (i) and (ii) for T iterations.

(4) Posterior estimation after obtaining the Markov chain samples $(\psi_1^{(t)}, \psi_2^{(t)})$, discard the burn-in period B. The remaining $T - B$ samples are used to compute the Bayesian estimates under the specified loss functions.

4.10. Simulation evaluation under Bayesian estimation

In this section, an extensive simulation study is carried out to investigate the behavior of Bayesian estimates of the parameters of the NCWD distribution. This simulation study aims to assess the efficiency and consistency of the Bayesian estimates of the parameters based on various loss functions and sample sizes. In order to examine the performance of Bayesian estimation method, a Monte Carlo simulation study was conducted by generating ($N_{\text{sim}} = 500$) random samples from the NCWD distribution using two pairs of specified parameter values, that is, $(\psi_1, \psi_2) = (1.5, 1.8)$ and $(\psi_1, \psi_2) = (1.7, 2.0)$. Four sample sizes, specifically $n = 30, 50, 100$, and 200, were taken into account to study the effect of Bayesian estimation for the NCWD distribution under small, medium, and large sample sizes. In the Bayesian method, a Bayesian estimation is done using the MCMC procedure through the Metropolis-Hastings algorithm. In each simulation run, 3000 MCMC iterations were generated and the first 500 draws were discarded as burn-in. Independent Gamma priors were assumed for the parameters with hyperparameters fixed at ($\alpha_1 = \alpha_2 = \alpha_3 = \alpha_4 = 1.2$). Bayesian estimates were considered under SELF, LELF and GELF. The effectiveness of the rival estimators was investigated using relative bias (RBIAS), MSE, root mean square error (RMSE), highest posterior density intervals (HPD), average interval length (AIL), and coverage probability (CP). In addition to these measures, the Gelman-Rubin Potential Scale Reduction Factor ($\hat{R}$) was used to investigate the convergence of the MCMC chain.

Tables 7 and 8 provide the results of the simulation evaluation that comprehensively assesses the finite sample properties of MLE and Bayesian estimators based on BE_{SELF}, BE_{LELF1}, BE_{LELF2}, BE_{GELF1}, and BE_{GELF2} loss functions to estimate the parameters ψ_1 and ψ_2 of the NCWD distribution. Such comparisons were done on the basis of a number of statistical measures which include RBIAS, MSE, RMSE, HPD intervals, AIL, and CP. The consistency in estimation can be clearly observed in both simulations. As the number of observations increases from $n = 30$ to $n = 200$, the performance of all the estimators greatly improves. This observation can be seen from the decreasing values of RBIAS, MSE, RMSE, and widths of confidence intervals.

- In both cases, the Bayesian estimators exhibit better performances compared to the MLE estimators in terms of the estimation efficiency and accuracy. The BE_{LELF2} and BE_{GELF2} loss function estimators tend to provide the minimum values for RBIAS, MSE, and RMSE criteria. For instance, if $(\psi_1, \psi_2) = (1.5, 1.8)$ and $n = 200$, then the BE_{GELF2} estimator exhibits the minimum RBIAS (1.2201) and MSE (1.4885) for ψ_1 as opposed to 1.2292 and 1.5109, respectively, of the MLE. Similar improvements are observed under the second parameter configuration $(1.7, 2.0)$.
- The findings regarding the interval estimation also provide evidence that Bayesian approaches are superior. First, it can be noted that the HPD intervals are narrowing with the increase in sample sizes, whereas the AIL values are greatly reducing. Thus, for ψ_1 within $(1.7, 2.0)$, the AIL value of BE_{GELF2} estimator is decreasing from 0.7808 when $n = 30$ to 0.3617 when $n = 200$. Second, the coverage probability values of all methods stay close to 95%.
- From Tables 8–10, which displays the Gelman-Rubin diagnostics, we can observe that the chains have successfully converged in their simulations. The potential scale reduction factor (PSRF), denoted as $\hat{R}$, statistics for both parameters are very close to unity, varying from about 1.0004 to 1.0043, and all upper confidence intervals lie below the recommended value. The multivariate PSRFs are also close to unity.
- Generally, the results of the simulation study indicate that the performance of the Bayesian estimators, especially when using the BE_{LELF2} and BE_{GELF2} loss functions, are better in terms of both the precision of the point estimates and the intervals than that of the MLE, and therefore, meets the required coverage probability.
- Graphical diagnostics for the parameters of NCWD are presented in Figures 4–5 through Bayesian diagnostic plots at various sample sizes. From the above graphs, it is clear that the fitted probability density function histograms and the Q-Q plots have a good fit with the simulated data and the fitted models. In addition, from the trace plots, it is evident that there is good convergence of the MCMC algorithm. Moreover, the posterior and joint posterior density plots have improved focus as the sample size increases.

Table 7. Simulation values for $\psi_1 = 1.5$, $\psi_2 = 1.8$ including Bias, RMSE, HPD intervals, and coverage.

Parameter	Metric	MLE	BE_{SELF}	BE_{LELF1}	BE_{LELF2}	BE_{GELF1}	BE_{GELF2}
ψ_1	RBIAS (n = 30)	1.2533	1.2381	1.2415	1.2347	1.2362	1.2324
	RBIAS (n = 50)	1.2432	1.2303	1.2332	1.2275	1.2287	1.2255
	RBIAS (n = 100)	1.2360	1.2259	1.2280	1.2238	1.2247	1.2223
	RBIAS (n = 200)	1.2292	1.2225	1.2238	1.2211	1.2216	1.2201
	MSE (n = 30)	1.5706	1.5329	1.5414	1.5245	1.5282	1.5188
	MSE (n = 50)	1.5457	1.5137	1.5207	1.5067	1.5097	1.5018
	MSE (n = 100)	1.5278	1.5028	1.5079	1.4977	1.4999	1.4940
	MSE (n = 200)	1.5109	1.4944	1.4978	1.4910	1.4924	1.4885
	RMSE (n = 30)	1.2417	1.2174	1.2207	1.2141	1.2155	1.2117
	RMSE (n = 50)	1.2364	1.2172	1.2200	1.2144	1.2156	1.2124
	RMSE (n = 100)	1.2326	1.2259	1.2280	1.2171	1.2180	1.2156
	RMSE (n = 200)	1.2278	1.2199	1.2213	1.2211	1.2191	1.2175
	HPD_lower (n = 30)	1.5746	1.5562	1.5678	1.5448	1.5489	1.5236
	HPD_lower (n = 50)	1.6735	1.6423	1.6503	1.6343	1.6374	1.6277
	HPD_lower (n = 100)	1.7571	1.7401	1.7409	1.7357	1.7376	1.7326
	HPD_lower (n = 200)	1.7993	1.7867	1.7894	1.7840	1.7852	1.7822
	HPD_upper (n = 30)	2.4578	2.3033	2.3382	2.2697	2.2885	2.2474
	HPD_upper (n = 50)	2.3049	2.2096	2.2271	2.1934	2.2022	2.1876
	HPD_upper (n = 100)	2.2036	2.1663	2.1714	2.1577	2.1623	2.1544
	HPD_upper (n = 200)	2.1283	2.1050	2.1087	2.1013	2.1032	2.0997
	AIL (n = 30)	0.8832	0.7472	0.7704	0.7249	0.7396	0.7239
	AIL (n = 50)	0.6314	0.5673	0.5768	0.5591	0.5648	0.5599
	AIL (n = 100)	0.4465	0.4263	0.4305	0.4219	0.4247	0.4219
	AIL (n = 200)	0.3290	0.3183	0.3193	0.3173	0.3180	0.3175
	CP (n = 30)	95.00	95.00	95.00	95.00	95.00	95.00
	CP (n = 50)	95.00	95.00	95.00	95.00	95.00	95.00
	CP (n = 100)	95.00	95.00	95.00	95.00	95.00	95.00
	CP (n = 200)	95.00	95.00	95.00	95.00	95.00	95.00
ψ_2	RBIAS (n = 30)	0.5292	0.5332	0.5331	0.5333	0.5335	0.5342
	RBIAS (n = 50)	0.5112	0.5327	0.5316	0.5329	0.5310	0.5326
	RBIAS (n = 100)	0.5035	0.5239	0.5308	0.5320	0.5308	0.5265
	RBIAS (n = 200)	0.4348	0.3361	0.3360	0.3261	0.4362	0.4364
	MSE (n = 30)	0.2801	0.2843	0.2842	0.2844	0.2847	0.2854
	MSE (n = 50)	0.2800	0.2840	0.2838	0.2831	0.2833	0.2849
	MSE (n = 100)	0.2800	0.2812	0.2821	0.2812	0.2824	0.2828
	MSE (n = 200)	0.1860	0.1874	0.1573	0.1874	0.1675	0.2878
	RMSE (n = 30)	0.5287	0.5320	0.5318	0.5321	0.5323	0.5330
	RMSE (n = 50)	0.5110	0.5241	0.5240	0.5242	0.5244	0.5250
	RMSE (n = 100)	0.5034	0.5159	0.5058	0.5157	0.5158	0.5162
	RMSE (n = 200)	0.3348	0.3059	0.3259	0.1361	0.1161	0.1263
	HPD_upper (n = 30)	0.8415	0.7990	0.8009	0.7970	0.7965	0.7914
	HPD_upper (n = 50)	0.7634	0.7429	0.7439	0.7418	0.7415	0.7386
	HPD_upper (n = 100)	0.6836	0.6727	0.6732	0.6722	0.6720	0.6706
	HPD_upper (n = 200)	0.6456	0.6431	0.6433	0.6430	0.6429	0.6423
	AIL (n = 30)	0.4557	0.4285	0.4301	0.4270	0.4272	0.4246
	AIL (n = 50)	0.3685	0.3551	0.3560	0.3543	0.3543	0.3527
	AIL (n = 100)	0.2667	0.2566	0.2570	0.2563	0.2562	0.2554
	AIL (n = 200)	0.1920	0.1955	0.1956	0.1954	0.1954	0.1953
	CP (n = 30)	95.00	95.00	95.00	95.00	95.00	95.00
	CP (n = 50)	95.00	95.00	95.00	95.00	95.00	95.00
	CP (n = 100)	95.00	95.00	95.00	95.00	95.00	95.00
	CP (n = 200)	95.00	95.00	95.00	95.00	95.00	95.00

Table 8. Simulation values for $\psi_1 = 1.7$, $\psi_2 = 2.0$ including Bias, RMSE, HPD intervals, and coverage.

Parameter	Metric	MLE	BE_{SELF}	BE_{LELF1}	BE_{LELF2}	BE_{GELF1}	BE_{GELF2}
ψ_1	RBIAS (n = 30)	0.9795	0.9466	0.9535	0.9398	0.9439	0.9385
	RBIAS (n = 50)	0.9562	0.8878	0.9272	0.9155	0.9190	0.9143
	RBIAS (n = 100)	0.9489	0.8162	0.9206	0.9118	0.9144	0.9108
	RBIAS (n = 200)	0.9391	0.8058	0.9190	0.9027	0.9045	0.9019
	MSE (n = 30)	0.9594	0.8960	0.9091	0.8832	0.8909	0.8808
	MSE (n = 50)	0.9144	0.8489	0.8597	0.8382	0.8446	0.8360
	MSE (n = 100)	0.9004	0.8394	0.8475	0.8315	0.8362	0.8296
	MSE (n = 200)	0.8820	0.8387	0.8445	0.8229	0.8263	0.8116
	RMSE (n = 30)	0.9625	0.8984	0.9052	0.8917	0.8957	0.8901
	RMSE (n = 50)	0.9562	0.8878	0.8936	0.8821	0.8854	0.8807
	RMSE (n = 100)	0.9442	0.8798	0.9041	0.8955	0.8980	0.8944
	RMSE (n = 200)	0.9368	0.8087	0.9018	0.8055	0.8074	0.8048
	HPD_lower (n = 30)	1.7036	1.6729	1.6860	1.6601	1.6652	1.6499
	HPD_lower (n = 50)	1.8175	1.7677	1.7783	1.7573	1.7618	1.7499
	HPD_lower (n = 100)	1.8637	1.8448	1.8504	1.8390	1.8416	1.8353
	HPD_lower (n = 200)	1.9367	1.9028	1.9058	1.8998	1.9012	1.9170
	HPD_upper (n = 30)	2.6774	2.4806	2.5223	2.4403	2.4640	2.4307
	HPD_upper (n = 50)	2.5024	2.3765	2.3991	2.3556	2.3674	2.3500
	HPD_upper (n = 100)	2.3682	2.3205	2.3303	2.3107	2.3162	2.3079
	HPD_upper (n = 200)	2.3065	2.2658	2.2704	2.2613	2.2638	2.2787
	AIL (n = 30)	0.9738	0.8077	0.8364	0.7802	0.7988	0.7808
	AIL (n = 50)	0.6849	0.6088	0.6208	0.5983	0.6056	0.6001
	AIL (n = 100)	0.5045	0.4757	0.4799	0.4718	0.4746	0.4726
	AIL (n = 200)	0.3698	0.3630	0.3646	0.3615	0.3626	0.3617
	CP (n = 30)	95.00	95.00	95.00	95.00	95.00	95.00
	CP (n = 50)	95.00	95.00	95.00	95.00	95.00	95.00
	CP (n = 100)	95.00	95.00	95.00	95.00	95.00	95.00
	CP (n = 200)	95.00	95.00	95.00	95.00	95.00	95.00
ψ_2	RBIAS (n = 30)	0.7159	0.7379	0.7371	0.7387	0.7387	0.7404
	RBIAS (n = 50)	0.7129	0.7376	0.7311	0.7324	0.7324	0.7338
	RBIAS (n = 100)	0.7083	0.7214	0.7309	0.7318	0.7318	0.7328
	RBIAS (n = 200)	0.7013	0.7189	0.7286	0.7292	0.7292	0.7298
	MSE (n = 30)	0.5125	0.5444	0.5432	0.5456	0.5457	0.5482
	MSE (n = 50)	0.5116	0.5402	0.5422	0.5412	0.5412	0.5433
	MSE (n = 100)	0.5105	0.5396	0.5420	0.5403	0.5403	0.5417
	MSE (n = 200)	0.5048	0.5260	0.5406	0.5364	0.5365	0.5374
	RMSE (n = 30)	0.7110	0.7303	0.7295	0.7312	0.7312	0.7329
	RMSE (n = 50)	0.7029	0.7276	0.7209	0.7303	0.7303	0.7317
	RMSE (n = 100)	0.7014	0.7254	0.7190	0.7299	0.7299	0.7309
	RMSE (n = 200)	0.7008	0.7231	0.7078	0.7184	0.7185	0.7291
	HPD_lower (n = 30)	0.3857	0.3706	0.3710	0.3701	0.3694	0.3672
	HPD_lower (n = 50)	0.3949	0.3868	0.3871	0.3866	0.3862	0.3849
	HPD_lower (n = 100)	0.4375	0.4159	0.4160	0.4157	0.4155	0.4145
	HPD_lower (n = 200)	0.4536	0.4472	0.4473	0.4471	0.4470	0.4466
	HPD_upper (n = 30)	0.8415	0.7962	0.7983	0.7942	0.7936	0.7885
	HPD_upper (n = 50)	0.7634	0.7392	0.7402	0.7382	0.7378	0.7351
	HPD_upper (n = 100)	0.7008	0.6726	0.6730	0.6721	0.6719	0.6705
	HPD_upper (n = 200)	0.6460	0.6418	0.6420	0.6417	0.6416	0.6410
	AIL (n = 30)	0.4557	0.4256	0.4272	0.4240	0.4242	0.4213
	AIL (n = 50)	0.3685	0.3524	0.3532	0.3517	0.3517	0.3502
	AIL (n = 100)	0.2633	0.2567	0.2570	0.2564	0.2564	0.2560
	AIL (n = 200)	0.1924	0.1946	0.1947	0.1946	0.1946	0.1944
	CP (n = 30)	95.00	95.00	95.00	95.00	95.00	95.00
	CP (n = 50)	95.00	95.00	95.00	95.00	95.00	95.00
	CP (n = 100)	95.00	95.00	95.00	95.00	95.00	95.00
	CP (n = 200)	95.00	95.00	95.00	95.00	95.00	95.00

Table 9. Gelman-Rubin diagnostic: Potential scale reduction factors (PSRF).

Sample Size	Parameter ψ_1		Parameter ψ_2		Multivariate PSRF
	Point Est.	Upper C.I.	Point Est.	Upper C.I.	
$n = 30$	1.0029	1.2035	1.0013	1.1455	1.0029
$n = 50$	1.0021	1.1766	1.0006	1.1119	1.0021
$n = 100$	1.0018	1.1662	1.0007	1.1151	1.0018
$n = 200$	1.0008	1.1245	1.0025	1.1905	1.0025

Table 10. Gelman-Rubin diagnostic: Potential scale reduction factors (PSRF).

Sample Size	Parameter ψ_1		Parameter ψ_2		Multivariate PSRF
	Point Est.	Upper C.I.	Point Est.	Upper C.I.	
$n = 30$	1.0043	1.2442	1.0021	1.1790	1.0043
$n = 50$	1.0007	1.1188	1.0004	1.0971	1.0007
$n = 100$	1.0018	1.1664	1.0016	1.1590	1.0018
$n = 200$	1.0012	1.1434	1.0014	1.1512	1.0014

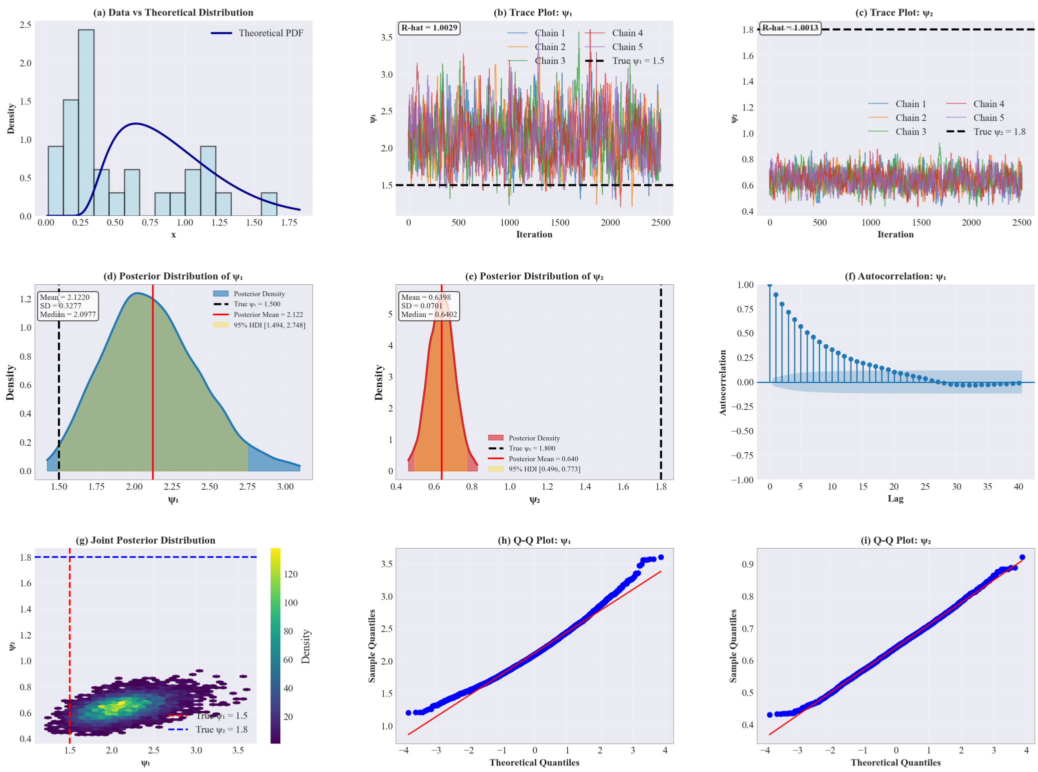

(a) $n = 30$

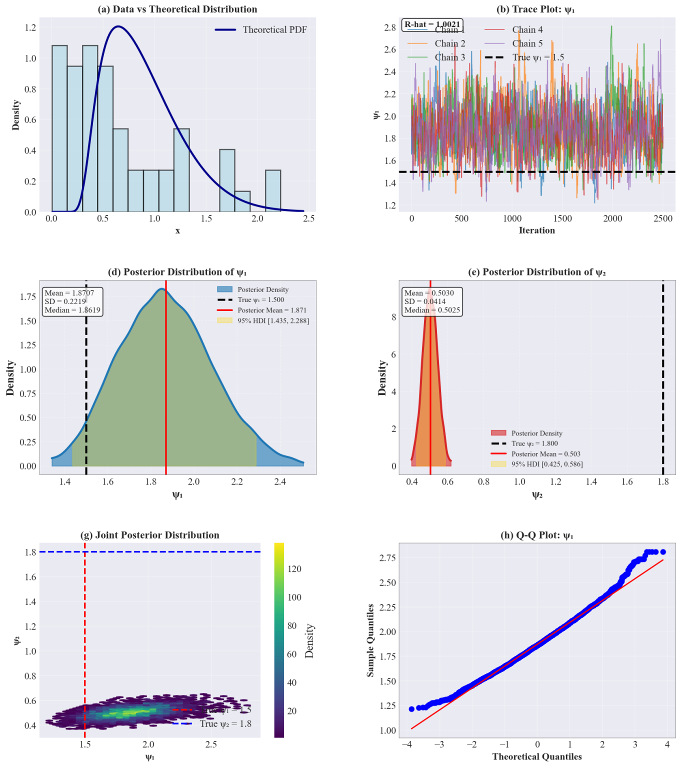
(a) Data vs Theoretical Distribution
Theoretical PDF
(b) Trace Plot: ψ₁
R-hat = 1.0021
(c) Trace Plot: ψ₂
R-hat = 1.0006
(d) Posterior Distribution of ψ₁
Mean = 1.8707
SD = 0.2219
Median = 1.8619
(e) Posterior Distribution of ψ₂
Mean = 0.5030
SD = 0.0414
Median = 0.5025
(f) Autocorrelation: ψ₁
(g) Joint Posterior Distribution
(h) Q-Q Plot: ψ₁
(i) Q-Q Plot: ψ₂

(b) $n = 50$

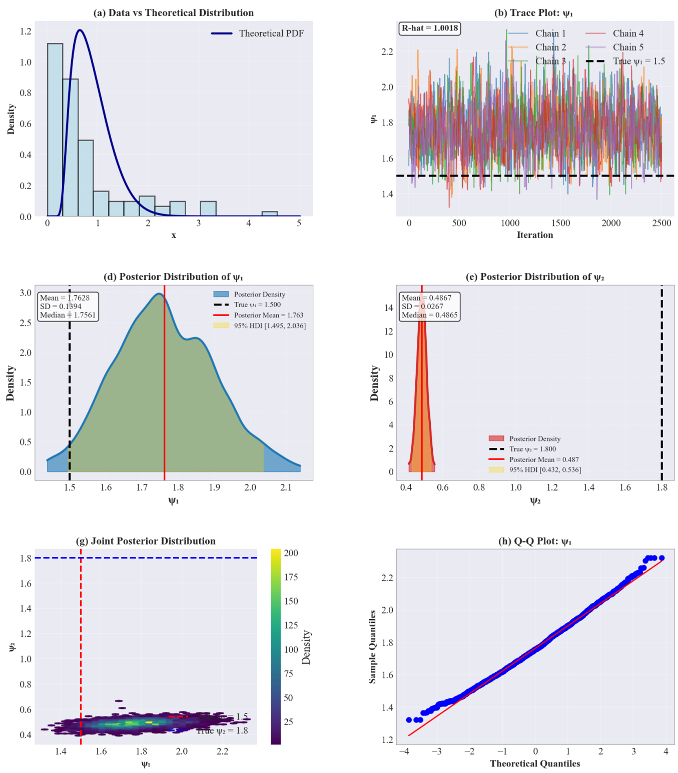
(a) Data vs Theoretical Distribution
Theoretical PDF
(b) Trace Plot: ψ₁
R-hat = 1.0018
(c) Trace Plot: ψ₂
R-hat = 1.0007
(d) Posterior Distribution of ψ₁
Mean = 1.7628
SD = 0.1394
Median = 1.7561
(e) Posterior Distribution of ψ₂
Mean = 0.4867
SD = 0.0267
Median = 0.4865
(f) Autocorrelation: ψ₁
(g) Joint Posterior Distribution
(h) Q-Q Plot: ψ₁
(i) Q-Q Plot: ψ₂

(c) $n = 100$

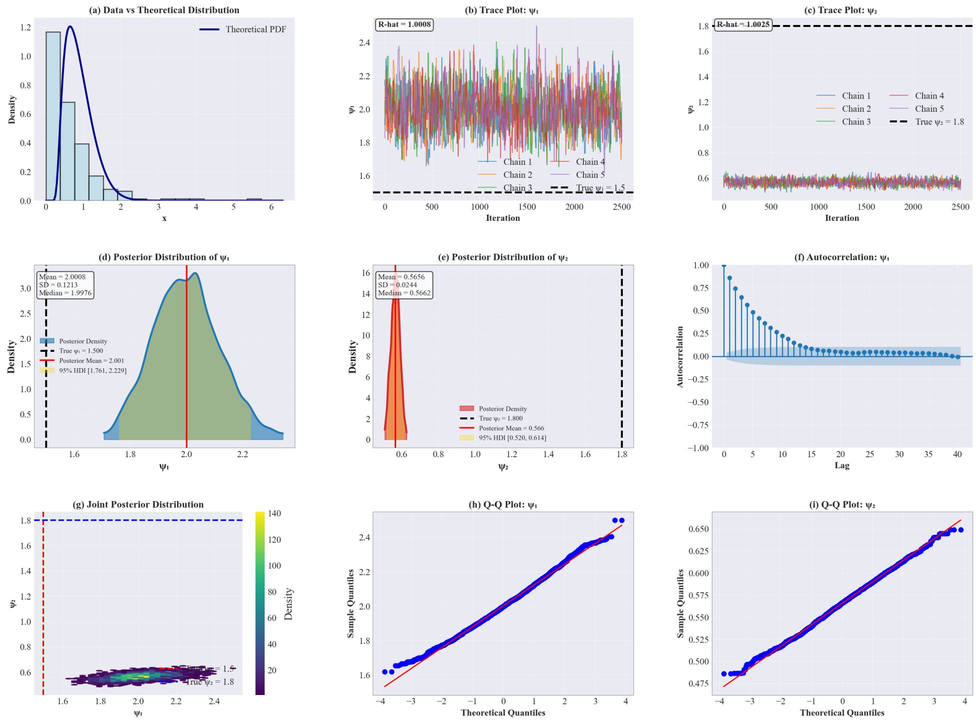

(d) $n = 200$

Figure 4. Bayesian diagnostic plots of the NCWD parameters for different sample sizes $n = 30, 50, 100$, and 200 fitted PDF histograms, trace plots, posterior densities, joint posterior densities, and Q-Q plots Table 7.

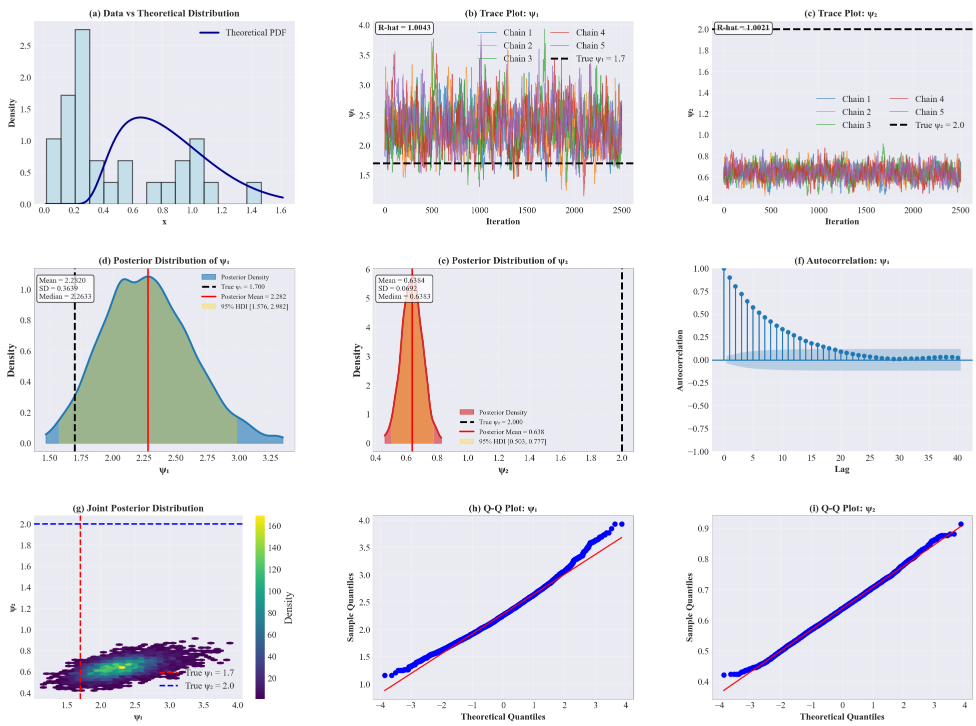

(a) $n = 30$

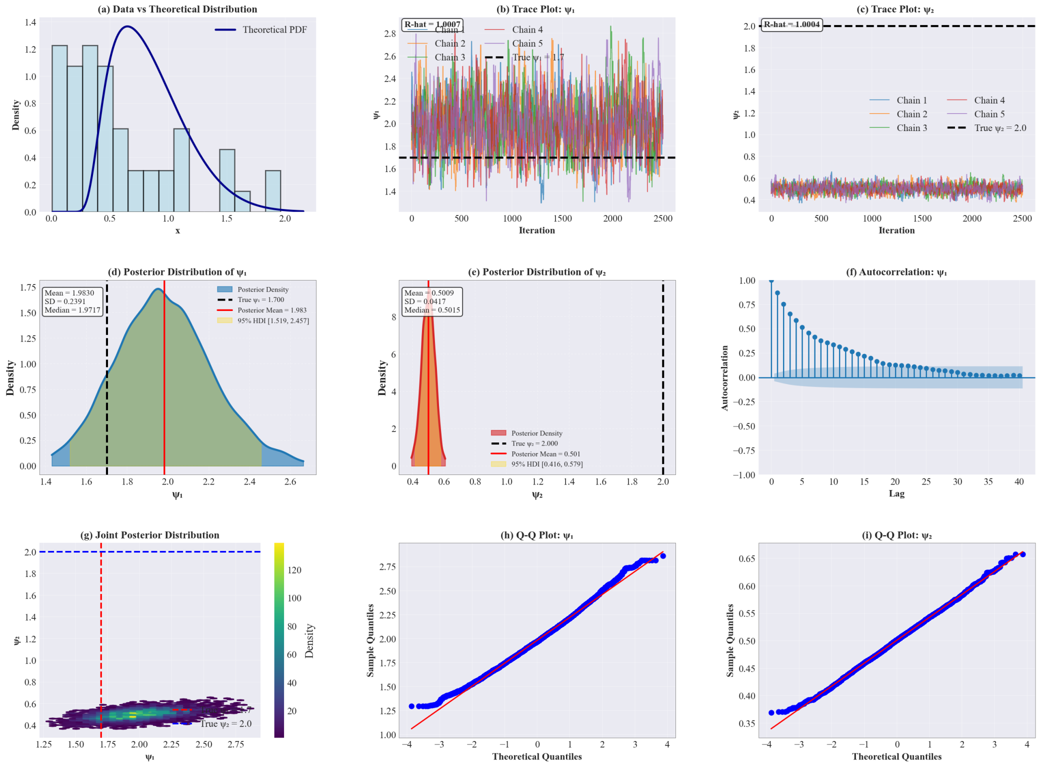

(b) n = 50

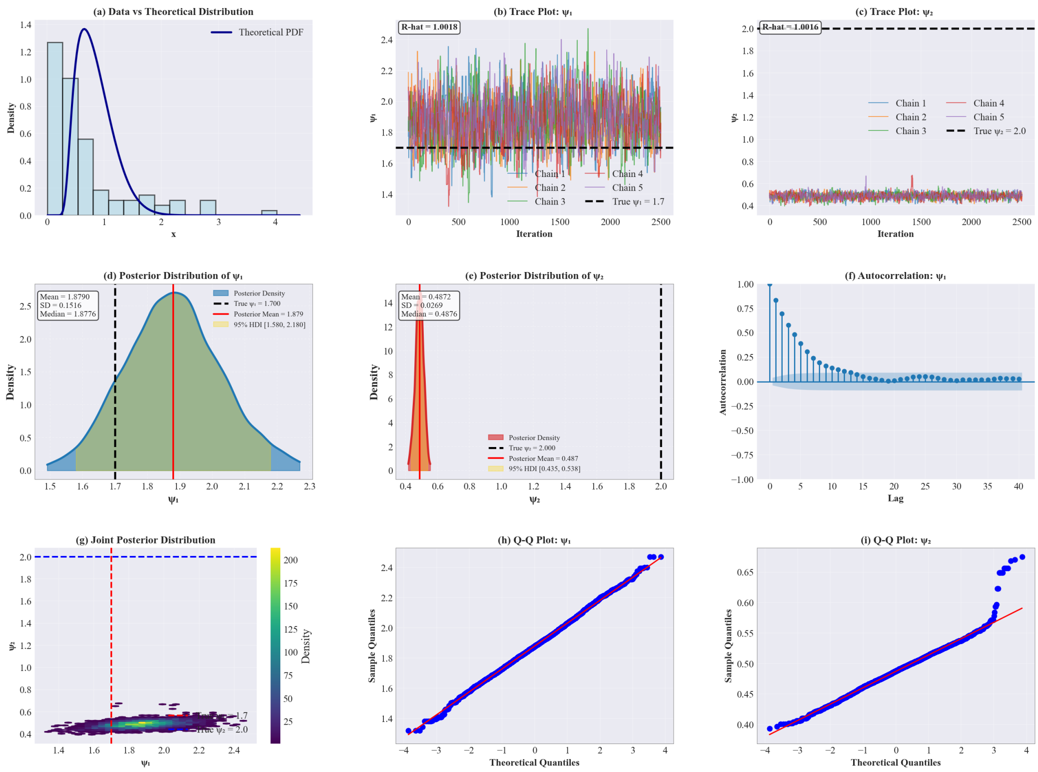

(c) n = 100

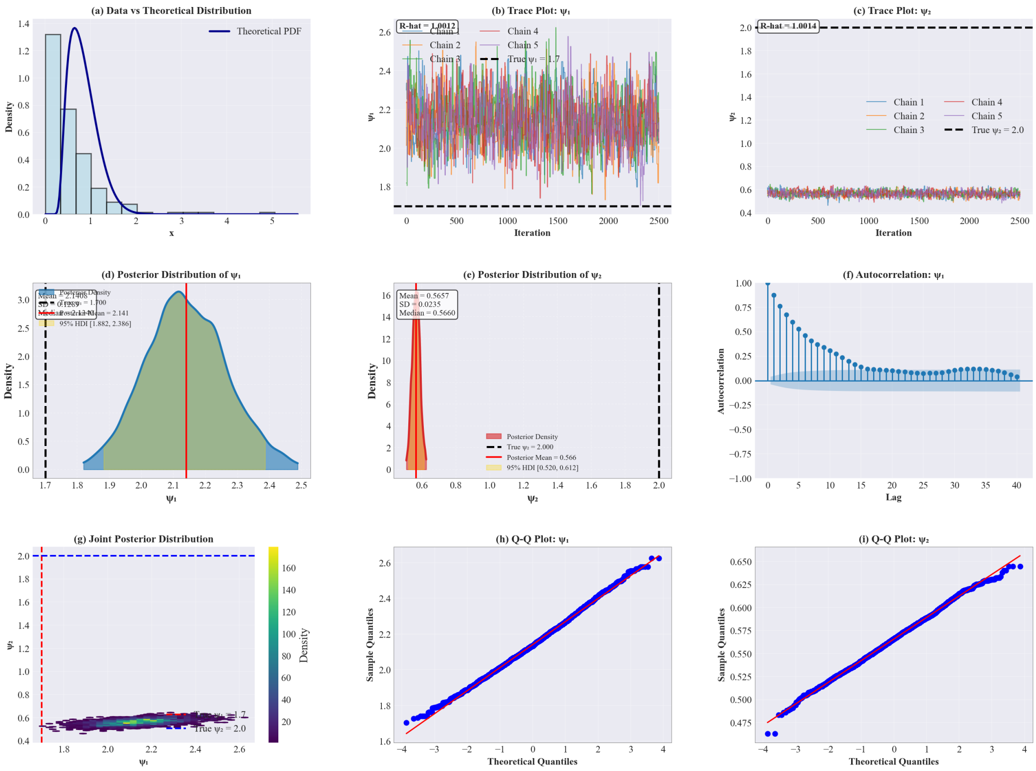

(d) $n = 200$

Figure 5. Bayesian diagnostic plots of the NCWD parameters for different sample sizes $n = 30, 50, 100,$ and 200 fitted PDF histograms, trace plots, posterior densities, joint posterior densities, and Q-Q plots from Table 8.

5. Data analysis

The appealing aspect of this portion rests in its evaluation of real data, which demonstrates the adaptability of the developed novel cotangent-Φ family of generator. To demonstrate this, we applied the standard Weibull distribution (from Section 2) as a baseline model to create the NCWD. Then we investigated numerous aspects of this newly developed distribution. Our analysis included two major datasets: The first dataset relates to an aerial communication transceiver, while the second includes measurements of the inter-arrival times of automobiles at a specified roadside site. To show the flexibility of the established model, we compare its PDF to that of the other distributions.

(1) Weibull distribution (WD):

$$f(z;\psi_1,\psi_2) = \psi_1\psi_2\, z^{\psi_2-1}e^{-\psi_1 z^{\psi_2}}, \qquad z>0,\ \psi_1,\psi_2>0.$$

(2) Sin-Weibull distribution (Sin-WD):

$$f(z;\psi_1,\psi_2) = \frac{\pi}{2}\,\psi_1\psi_2\, z^{\psi_2-1}e^{-\psi_1 z^{\psi_2}}\, \sin\left(\frac{\pi}{2}\left(1-e^{-\psi_1 z^{\psi_2}}\right)\right), \qquad z>0,\ \psi_1,\psi_2>0.$$

(3) Cos-Weibull distribution (Cos-WD):

$$f(z;\psi_1,\psi_2) = \frac{\pi}{2}\,\psi_1\psi_2\, z^{\psi_2-1}e^{-\psi_1 z^{\psi_2}}\, \cos\left(\frac{\pi}{2}\left(1-e^{-\psi_1 z^{\psi_2}}\right)\right), \qquad z>0,\ \psi_1,\psi_2>0.$$

(4) Tan-Weibull distribution (TWD):

$$f(z;\psi_1,\psi_2)=\frac{\pi}{4}\,\psi_1\psi_2\,z^{\psi_2-1}e^{-\psi_1 z^{\psi_2}}\sec^2\left(\frac{\pi}{4}\left(1-e^{-\psi_1 z^{\psi_2}}\right)\right),\qquad z>0,\ \psi_1,\psi_2>0.$$

(5) Novel arctan-Weibull distribution (NATWD):

$$f(z;\psi_1,\psi_2)=\frac{\log(16)}{\pi}\,\frac{\psi_1\psi_2\,z^{\psi_2-1}e^{-\psi_1 z^{\psi_2}}\,2^{1-e^{-\psi_1 z^{\psi_2}}}}{1+\left(2^{1-e^{-\psi_1 z^{\psi_2}}}-1\right)^2},\quad z>0,\ \psi_1\psi_2>0.$$

(6) Novel Sin-Lomax distribution (NSLD):

$$f(z;\psi_1,\psi_2)=\frac{\pi}{2}\,\log\left(\frac{1}{2}\right)\psi_1\psi_2\,(1+\psi_1 z)^{-\psi_2-1}\,2^{(1+\psi_1 z)^{-\psi_2}}\cos\left(\frac{\pi}{2}\left(3-2^{(1+\psi_1 z)^{-\psi_2}}\right)\right),\quad z;\ \psi_1,\psi_2>0.$$

(7) Lomax distribution (LD):

$$f(z;\psi_1,\psi_2)=\psi_1\psi_2\,(1+\psi_1 z)^{-\psi_2-1},\qquad z>0,\ \psi_1,\psi_2>0.$$

(8) Power Fréchet distribution (PFD):

$$f(z;\psi_1,\psi_2,\psi_3)=\psi_1\psi_2\psi_3\,z^{-\psi_3-1}(1+\psi_1 z^{-\psi_3})^{-\psi_2-1}e^{1-(1+\psi_1 z^{-\psi_3})^{\psi_2}},\qquad z>0,\ \psi_1,\psi_2,\psi_3>0.$$

(9) Kumarasawamy power Fréchet distribution (KPFD):

$$\begin{aligned}f(z;\psi_1,\psi_2,\psi_3,\psi_4)&=\psi_1\psi_2\psi_3\psi_4\,z^{-\psi_1-1}(1+z^{-\psi_1})^{\psi_2-1}e^{-\psi_3(1+z^{-\psi_1})^{\psi_2}+\psi_3}\\&\quad\times\left(1-e^{-\psi_3(1+z^{-\psi_1})^{\psi_2}+\psi_3}\right)^{\psi_4-1},\qquad z>0,\ \psi_1,\psi_2,\psi_3,\psi_4>0.\end{aligned}$$

Several criteria are implemented to examine the appropriateness of fitted distributions. These include information criteria such as the Akaike information criterion (AIC), consistent Akaike information criterion (CAIC), Bayesian information criterion (BIC), and Hannan-Quinn information criterion (HQIC), which have lower values and suggest a better match. This approach is reinforced with goodness-of-fit tests Kolmogorov-Smirnov (K-S), Anderson-Darling (A*), and Cramér-von Mises (W*), which show that a superior model has lower test statistics and higher associated p-values.

Standard information criterion and goodness-of-fit test statistics are as follows, where ℓ represents the log-likelihood function, k is the number of parameters, and n is the sample size:

$$\text{AIC}=-2\ell+2k,\quad \text{AICC}=-2\ell+\frac{2kn}{n-k-1},\quad \text{BIC}=-2\ell+k\log(n),$$
$$\text{HQIC}=-2\ell+2k\log(\log n),\quad \text{K-S}=\max_{1\le j\le n}\left\{F(z_{(j)})-\frac{j-1}{n},\ \frac{j}{n}-F(z_{(j)})\right\},$$
$$\text{W*}=\frac{1}{12n}+\sum_{j=1}^{n}\left(\frac{2j-1}{2n}-F(z_{(j)})\right)^2,\quad \text{A*}=-n-\frac{1}{n}\sum_{j=1}^{n}(2j-1)\Big[\log F(z_{(j)})+\log\left(1-F(z_{(n-j+1)})\right)\Big].$$

Data set 1: The first dataset we look at is an authentic set of active repair periods (in hours) for an aerial communication transceiver. The following information is supplied by Jorgensen [32]:

2.50, 2.60, 2.60, 2.70, 2.80, 2.80, 2.90, 3.00, 3.00, 3.10, 3.20, 3.40, 3.70, 3.90, 3.90, 3.90, 4.60, 4.70, 5.00, 5.60, 5.70, 6.00, 6.00, 6.10, 6.60, 6.90, 6.90, 7.30, 7.60, 7.90, 8.00, 8.30, 8.80, 8.80, 9.30, 9.40, 9.50, 10.1, 11.0, 11.3, 11.9, 11.9, 12.3, 12.9, 12.9, 13.0, 13.8, 14.5, 14.9, 15.3, 15.4, 15.9, 16.2, 17.6, 20.1, 20.3, 20.6, 21.4, 22.8, 23.7, 23.7, 24.7, 29.7, 30.6, 31.0, 34.1, 34.7, 36.8, 40.1, 40.2, 41.3, 42.0, 44.8, 49.8, 51.7, 55.7, 56.5, 58.1, 70.5, 72.6, 87.1, 88.6, 91.7, 119.8.

The data exhibits a strong right-skewed distribution (skewness 1.915498), with the majority of values grouped on the left and a large tail of high values to the right. The high kurtosis (6.580869) indicates a highly peaked distribution with heavy tails, suggesting that extreme values occur more frequently than in a normal distribution.

Data set 2: The second data set that we investigate consists of the lengths between the periods in which cars pass a spot on a road. The data are shown below, and their source is Jorgensen [32]:

0.50, 0.60, 0.60, 0.70, 0.70, 0.70, 0.80, 0.80, 1.00, 1.00, 1.00, 1.00, 1.10, 1.30, 1.50, 1.50, 1.50, 1.50, 2.00, 2.00, 2.20, 2.50, 2.70, 3.00, 3.00, 3.30, 4.00, 4.00, 4.50, 4.70, 5.00, 5.40, 5.40, 7.00, 7.50, 8.80, 9.00, 10.20, 22.00, 24.50.

The distribution is highly right-skewed (2.717118), meaning most data points are clustered at lower values, with a long tail extending toward exceptionally high values. Its high kurtosis (10.54327) reveals a distribution that is more peaked and has fatter tails than a normal distribution, thus indicating a pronounced tendency for extreme values.

Data set 3: The original dataset, developed by Abdelfattah and Sayed in [33], investigated the effects of gamma and microwave irradiation on peppermint packaging. They designed four categories for comparison: choice packages, choice non-packages, non-choice packages, and non-choice non-packages. For our study, we will concentrate on the non-choice package category. This subset includes 21 observations, each measuring the susceptibility index (SI) of peppermint packages exposed to gamma radiation (6, 8, and 10 kGy) or microwave irradiation (1, 2, and 3 minutes) when threatened by adult infestation of Stegobium panicum L. (drugstore beetle). The SI measurements recorded are as follows:

2.342985965 2.342985965 2.34913 2.33606 2.04988 1.91295 2.15892 1.69393 1.60347 1.61141 1.32852, 1.26452 1.31174 2.01959 2.08279 1.95425 1.62188 1.64787 1.64908 1.33791 1.33791 1.29013.

The facts from the dataset articulate that the minimum (0.500) and first quartile (1.000) are so low, thus revealing a strong concentration of data points at smaller values. The mean (4.013) is well above the median (2.100), indicating the impact of larger data points. Although 75% of the data fall below 4.775, the maximum (24.500) indicates the presence of extreme right-tail data points. The strong positive skewness (2.717) reinforces the presence of strong right skewness, and the high kurtosis (10.543) indicates a sharply peaked and heavy-tailed distribution.

The descriptive statistics of the three datasets used for analysis perposes of NCWD are shown in Tables 11–13, whereas Tables 14–16 provide the maximum likelihood estimate and the standard errors of the parameters. Tables 17–19 show the goodness-of-fit criteria and model selection criteria. It is evident from the results that the proposed model NCWD provides a better fit compared to all other competing models. The model produces the smallest value of AIC, CAIC, HQIC, BIC, KS, Hazard Discrepancy using Kaplan-Meier estimator, Cramér-von Mises (W^*), statistic and Anderson-Darling (A^*), statistic along with the largest corresponding (p)-value. Additionally, the minimum value of the hazard discrepancy with respect to the non-parametric Kaplan-Meier hazard function proves the capability of the NCWD to capture the hazard function of the data well. In order to analyze the appropriateness of the proposed NCWD further, various graphical methods shown in Figures 6, 7 and 9 were applied, which include the histogram, empirical cumulative distribution function (ECDF), survival function, probability-probability (PP) plot, Quantile-Quantile (QQ) plot, total time on test (TTT) plot, log-log survival plot, box plot, and violin plot for all the three data sets. Histograms, ECDF, and the survival function demonstrate that the NCWD is an appropriate distribution model to describe the data set behavior. PP and QQ plots clearly show that there is a close fit of the empirical data with the theoretical quantiles and probabilities of the NCWD. TTT plots demonstrate the hazard rate shape and help to validate the flexibility of the proposed model in fitting various types of hazard rates. Moreover, log–log survival plots, box plots, and violin plots demonstrate the ability of the model in modeling the characteristics, skewness, variability, and tail behavior of the datasets also Figures 8 and 10 provides insights about the estimated pdf's of the fitted models across all datasets. Figure 11 shows the patterns of the hazard rates in each of the three data sets via non-parametric estimation of the hazard functions for Datasets 1-3 using the Kaplan-Meier estimator. It can be seen from the figures that the new NCWD model approximates the hazard rate patterns and performs much better than the other models because of the non-monotonicity of the hazard rates.

Table 11. Descriptive statistics for aerial communication transceiver repair periods (hours).

Min	1st Qu.	Median	Mean	3rd Qu.	Max.	Skewness	Kurtosis
2.500	5.925	12.100	21.602	29.925	119.800	1.915498	6.580869

Table 12. Descriptive statistics for inter-car interval lengths.

Min	1st Qu.	Median	Mean	3rd Qu.	Max.	Skewness	Kurtosis
0.500	1.000	2.100	4.013	4.775	24.500	2.717118	10.54327

Table 13. Descriptive statistics for gamma and microwave irradiation.

Min	1st Qu.	Median	Mean	3rd Qu.	Max.	Skewness	Kurtosis
1.265	1.404	1.672	1.784	2.075	2.349	0.1335679	1.65369

Table 14. Maximum likelihood estimates (with standard errors) for aerial communication transceiver repair periods (hours).

Model	$\widehat{\psi}_1$	$\widehat{\psi}_2$	$\widehat{\psi}_3$	$\widehat{\psi}_4$
NCWD	0.15849392	0.73002520	⋯	⋯
	(0.02415895)	(0.04876709)	⋯	⋯
WD	0.04674872	0.99720159	⋯	⋯
	(0.01432535)	(0.08076216)	⋯	⋯
TWD	0.06756672	0.94122320	⋯	⋯
	(0.02066147)	(0.07885026)	⋯	⋯
SWD	0.032035896	0.938479625	⋯	⋯
	(0.009418028)	(0.077395149)	⋯	⋯
CWD	0.17605051	0.72462576	⋯	⋯
	(0.03504459)	(0.05691676)	⋯	⋯
NATWD	0.05336350	0.95877082	⋯	⋯
	(0.01564728)	(0.07876552)	⋯	⋯
NSLD	0.03176183	2.60506465	⋯	⋯
	(0.01573132)	(1.00645124)	⋯	⋯
LXD	0.009131020	6.019652737	⋯	⋯
	(0.005351785)	(3.107942762)	⋯	⋯
PFD	3.3022880	1.3570415	1.1484449	⋯
	(9.2586180)	(2.5487344)	(0.2783791)	⋯
KPFD	0.4658314	2.2031195	2.3014153	4.3847118
	(0.3962383)	(2.3360430)	(4.5356022)	(5.9011651)

Table 15. Maximum likelihood estimates (with standard errors) for inter-car interval lengths.

Model	$\widehat{\psi}_1$	$\widehat{\psi}_2$	$\widehat{\psi}_3$	$\widehat{\psi}_4$
NCWD	0.53055469	0.74087213	⋯	⋯
	(0.07203004)	(0.07144541)	⋯	⋯
WD	0.26883647	0.96035422	⋯	⋯
	(0.06977278)	(0.10886148)	⋯	⋯
TWD	0.35840164	0.90222504	⋯	⋯
	(0.09238639)	(0.10594015)	⋯	⋯
SWD	0.02035334	5.02670933	⋯	⋯
	(0.01351863)	(0.84855958)	⋯	⋯
CWD	0.60992584	0.71788858	⋯	⋯
	(0.10258667)	(0.07969621)	⋯	⋯
NATWD	0.28491914	0.92792526	⋯	⋯
	(0.07011504)	(0.10628965)	⋯	⋯
NSLD	0.1814240	2.5363882	⋯	⋯
	(0.1203026)	(1.3094409)	⋯	⋯
LXD	0.06792873	4.66883588	⋯	⋯
	(0.06690863)	(3.85903188)	⋯	⋯
PFD	0.02845397	19.08910574	1.11829423	⋯
	(0.06790416)	(44.81384389)	(0.14322717)	⋯
KPFD	0.9905501	1.3975855	1.0691353	1.2250090
	(1.1306935)	(1.5569554)	(1.4920264)	(1.9154924)

Table 16. Maximum likelihood estimates (with standard errors) for gamma and microwave irradiation.

Model	$\widehat{\psi}_1$	$\widehat{\psi}_2$	$\widehat{\psi}_3$	$\widehat{\psi}_4$
NCWD	0.13911506	3.62663865	⋯	⋯
	(0.04298785)	(0.47707272)	⋯	⋯
WD	0.02945117	5.32689605	⋯	⋯
	(0.02042545)	(0.88937288)	⋯	⋯
TWD	0.04084384	5.11079537	⋯	⋯
	(0.02842060)	(0.87577855)	⋯	⋯
SWD	0.02035334	5.02670933	⋯	⋯
	(0.01351863)	(0.84855958)	⋯	⋯
CWD	0.12706713	3.75213391	⋯	⋯
	(0.05487522)	(0.59420017)	⋯	⋯
NATWD	0.03484157	5.07713982	⋯	⋯
	(0.02330648)	(0.86720978)	⋯	⋯
NSLD	0.009024795	63.346900715	⋯	⋯
	(0.008803283)	(62.411236729)	⋯	⋯
LXD	0.007377669	76.498786657	⋯	⋯
	(0.008010811)	(84.096426127)	⋯	⋯
PFD	9.516062	1.007656	145.065797	⋯
	(7.083697)	(1.634711)	(1269.343202)	⋯
KPFD	1.4343950	0.5447761	18.2960792	39.2103406
	(1.1390141)	(3.2690141)	(51.3003621)	(161.2003153)

Table 17. Comparison criterion, goodness-of-fit statistics, and hazard discrepancy rankings for aerial communication transceiver repair periods (hours).

Model	$-\ell$	AIC	CAIC	HQIC	BIC	K.S statistic (p-value)	A* (p-value)	W* (p-value)	Hazard MAE (KM)
NCWD	333.9830	671.9659	672.1141	673.9203	676.8276	0.06904 (0.8182)	0.71912 (0.5426)	0.10622 (0.5563)	0.06842
WD	342.1150	688.2300	688.3782	690.1843	693.0916	0.11003 (0.261)	1.4187 (0.1971)	0.21287 (0.2441)	0.07071
TWD	343.5869	691.1738	691.3220	693.1282	696.0355	0.11669 (0.2028)	1.7047 (0.1345)	0.27029 (0.1643)	0.07133
SWD	342.7387	689.4774	689.6256	691.4318	694.3391	0.11427 (0.2227)	1.4685 (0.1842)	0.21698 (0.237)	0.07083
CWD	384.0133	772.0266	772.1747	773.9809	776.8882	0.70907 (2.2e-16)	72.653 (7.143e-06)	14.24 (2.2e-16)	0.06951
NATWD	341.9912	687.9823	688.1305	689.9366	692.8439	0.11069 (0.2548)	1.2964 (0.2335)	0.17971 (0.3109)	0.07042
NSLD	337.25625	678.5125	678.6606	680.4668	683.3741	0.077473 (0.809)	0.73208 (0.4177)	0.20631 (0.449)	0.06860
LXD	341.6424	687.2847	687.4329	689.2390	692.1463	0.12704 (0.1328)	1.1373 (0.2925)	0.1236 (0.4819)	0.06980
PFD	412.1774	830.3549	830.6549	833.2864	837.6473	0.29947 (5.722e-07)	18.878 (7.143e-06)	3.54 (2.082e-09)	0.06847
KPFD	335.1643	678.3287	678.8350	682.2374	688.0520	0.073447 (0.7553)	0.60505 (0.6427)	0.065902 (0.7783)	0.06844

Table 18. Comparison criterion, goodness-of-fit statistics, and hazard discrepancy rankings for inter-car interval lengths.

Model	$-\ell$	AIC	CAIC	HQIC	BIC	K.S statistic (p-value)	W* (p-value)	A* (p-value)	Hazard MAE (KM)
NCWD	90.45398	184.90797	185.23229	186.12926	188.28573	0.0382 (0.9295)	0.06501 (0.8877)	0.0154 (0.8612)	0.21397
WD	95.51136	195.02272	195.34705	196.24402	198.40048	0.12904 (0.5181)	1.0211 (0.3459)	0.1359 (0.4371)	0.22246
TWD	96.42895	196.85790	197.18223	198.07919	200.23566	0.13792 (0.4321)	1.1635 (0.2816)	0.15875 (0.3651)	0.22371
SWD	95.78205	195.56410	195.88840	196.78540	198.94180	0.13347 (0.4743)	1.0308 (0.341)	0.13498 (0.4403)	0.22232
CWD	114.72340	233.44680	233.77110	234.66810	236.82460	0.7084 (2.2e-16)	35.102 (1.5e-05)	6.8701 (2.2e-16)	0.21920
NATWD	95.19697	194.39394	194.71826	195.61523	197.77170	0.12842 (0.5244)	0.9228 (0.3998)	0.11703 (0.5096)	0.22174
NSLD	91.40390	186.80780	187.13210	188.02910	190.18550	0.10786 (0.7407)	0.44301 (0.8043)	0.056228 (0.8405)	0.21845
LXD	94.50289	193.00578	193.33011	194.22707	196.38354	0.14515 (0.3683)	0.84963 (0.4458)	0.097715 (0.5985)	0.21682
PFD	125.45760	256.91510	257.58180	258.74710	261.98180	0.31508 (0.0007111)	9.0068 (4.783e-05)	1.6568 (5.746e-05)	0.21996
KPFD	89.40261	186.80522	187.94807	189.24780	193.56073	0.095305 (0.8606)	0.43028 (0.8174)	0.070627 (0.7505)	0.21965

Table 19. Comparison criterion, goodness-of-fit statistics, and hazard discrepancy rankings for gamma and microwave irradiation.

Model	$-\ell$	AIC	CAIC	HQIC	BIC	K.S statistic (p-value)	W* (p-value)	A* (p-value)	Hazard MAE (KM)
NCWD	8.537691	21.075382	21.706961	21.589415	23.257467	0.16965 (0.7511)	0.65406 (0.6437)	0.10038 (0.632)	14.12802
WD	9.819739	23.639477	24.271056	24.153511	25.821562	0.18932 (0.5318)	0.72466 (0.5368)	0.10224 (0.5781)	14.23975
TWD	9.873791	23.747581	24.379160	24.261615	25.929666	0.17357 (0.5214)	0.7505 (0.5164)	0.10845 (0.5488)	14.26805
SWD	9.954920	23.909840	24.541420	24.423880	26.091930	0.16254 (0.6063)	0.72661 (0.5353)	0.10306 (0.5741)	14.24717
CWD	9.673555	23.347110	23.978690	23.861140	25.529190	0.15256 (0.6852)	0.71201 (0.5471)	0.099212 (0.5929)	14.18590
NATWD	10.041440	24.082890	24.714470	24.596920	26.264970	0.18470 (0.6683)	0.72392 (0.5374)	0.10219 (0.5783)	14.23586
NSLD	29.994420	63.988840	64.620420	64.502880	66.170930	0.40987 (0.001232)	4.6299 (0.004429)	0.89301 (0.003908)	14.90519
LXD	34.872080	73.744170	74.375750	74.258200	75.926250	0.50854 (2.287e-05)	6.3542 (0.0007013)	1.3361 (0.0002957)	14.92780
PWD	9.537945	25.075890	26.409223	25.846940	28.349017	0.15953 (0.6301)	0.72104 (0.5398)	0.10036 (0.5872)	14.16840
KPFD	9.577077	27.154154	29.507095	28.182221	31.518324	0.16138 (0.6155)	0.72342 (0.5378)	0.10034 (0.5873)	14.23586

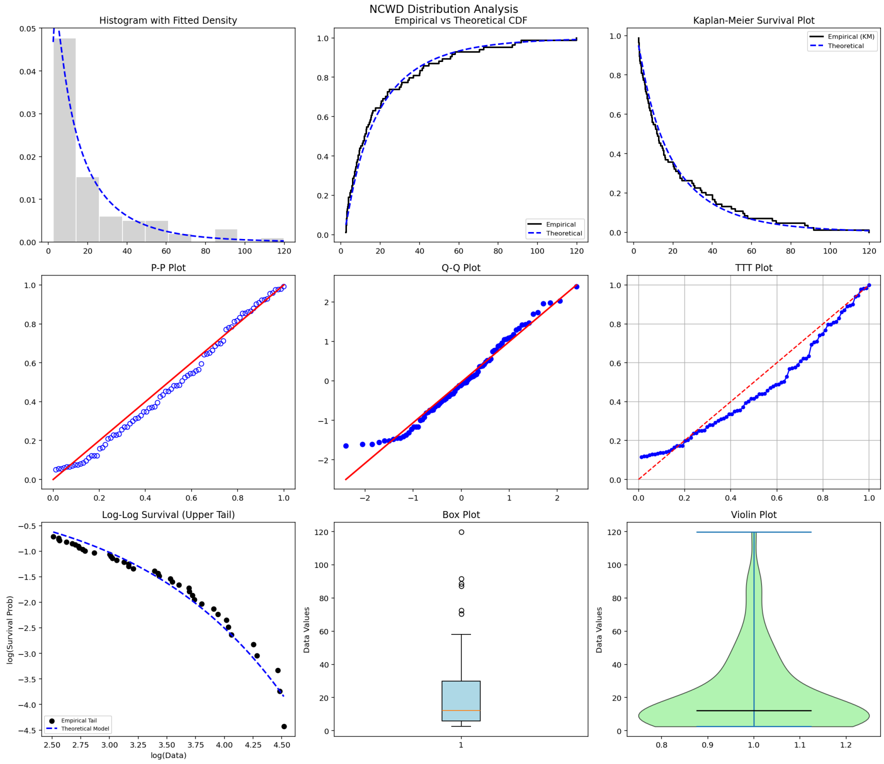

Figure 6. Histogram, empirical cdf, survival function, pp-plot, qq-plot, and ttt-plot, log-log survival, box plot, and violin plot of NCWD for aerial communication transceiver repair periods (hours).

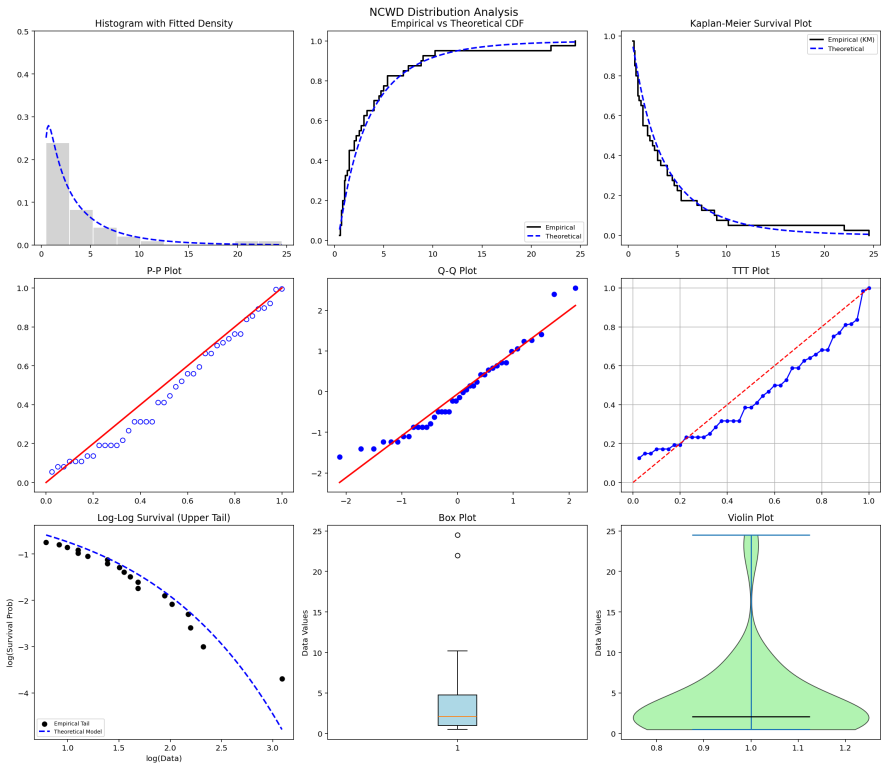

Figure 7. Histogram, empirical cdf, survival function, pp-plot, qq-plot, and ttt-plot, log-log survival, box plot, and violin plot for the NCWD for inter-car interval lengths.

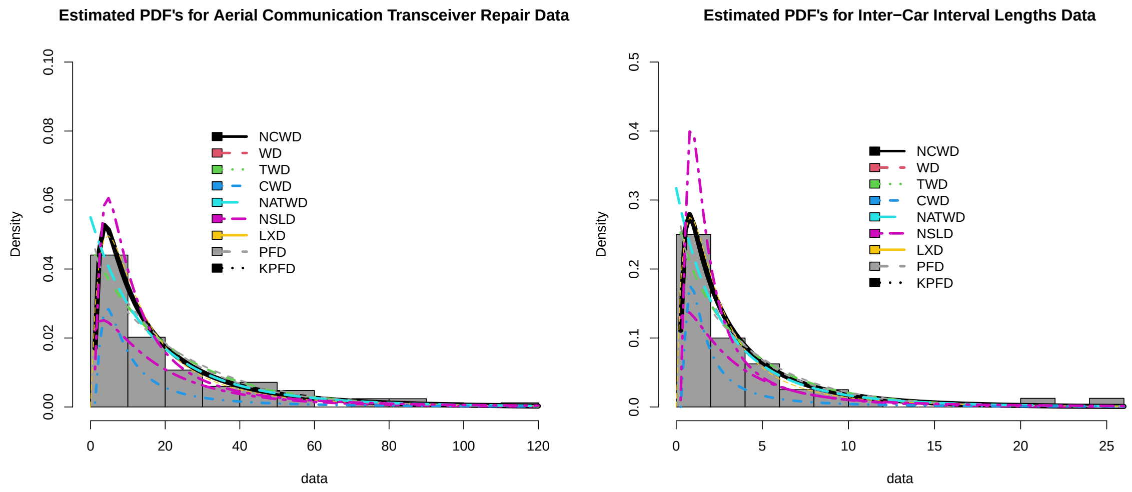

Figure 8. Estimated pdf's of the fitted models for dataset.

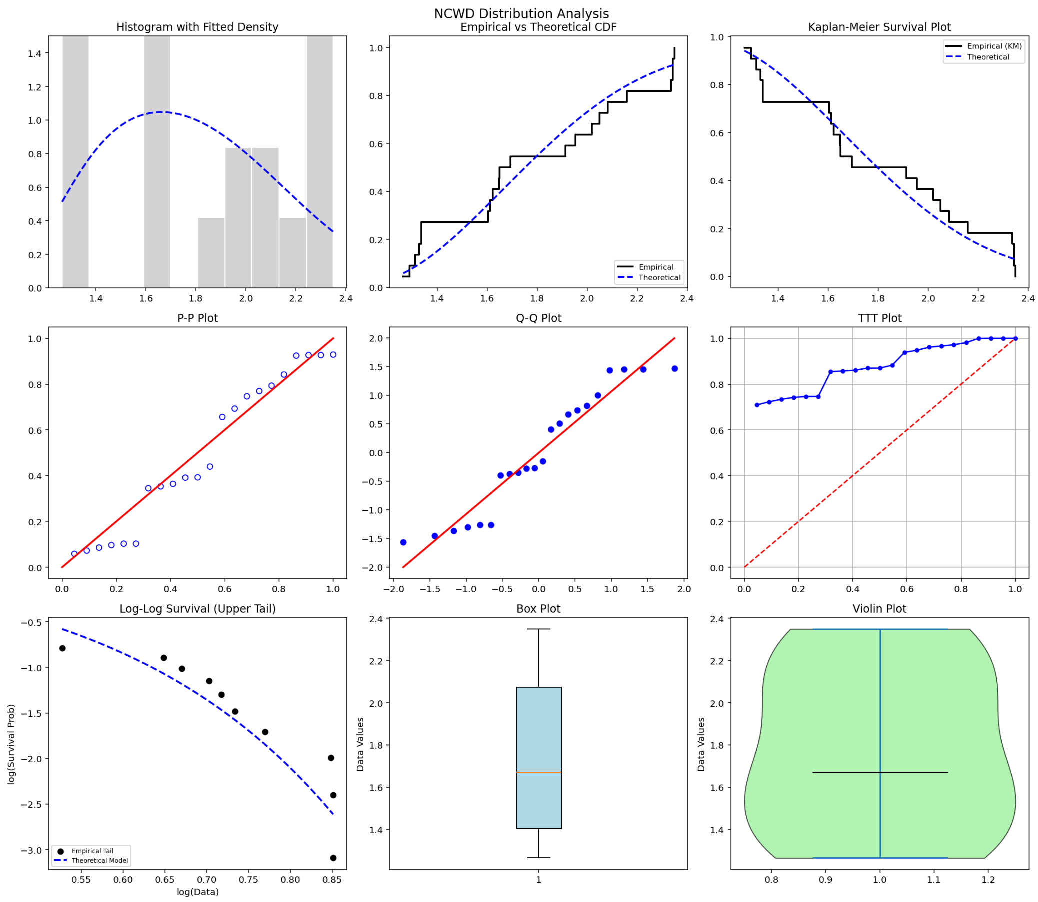

Figure 9. Histogram, empirical cdf, survival function, pp-plot, qq-plot, and ttt-plot, log-log survival, box plot, and violin plot for the NCWD for gamma and microwave irradiation.

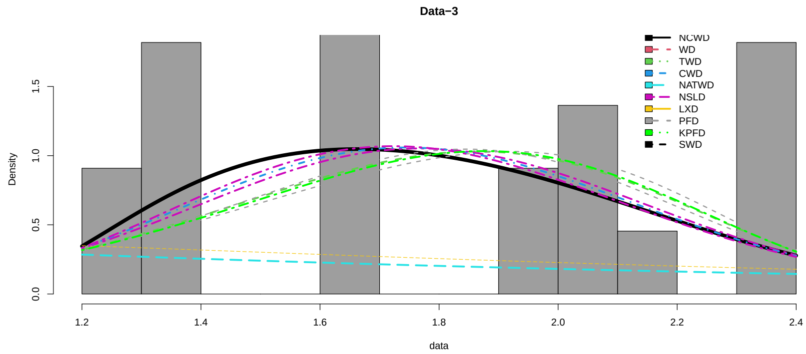

Figure 10. Estimated pdf's of the fitted models for dataset.

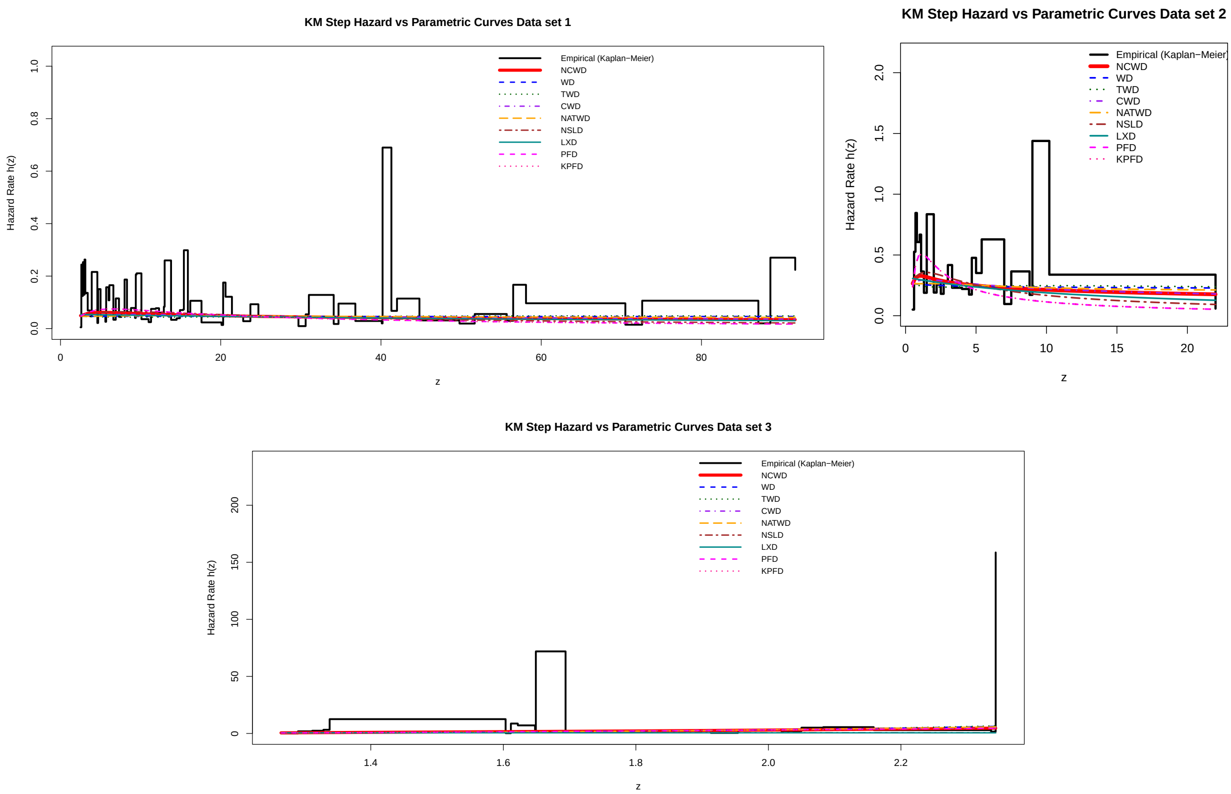

Figure 11. Kaplan-Meier hazard estimates for Datasets 1–3, showing the improved fit of the proposed NCWD.

6. XGBoost machine learning model development

Extreme gradient boosting (XGBoost) is a popular machine learning method that helps to solve regressions and classification tasks. For practical purposes, the data set is usually split into two parts, namely the training and testing data sets. The training data set is utilized to develop the prediction model by building regression trees, determining split points, and minimizing the required loss function. This procedure is accompanied by updating the parameters of the model in order to increase its prediction accuracy. Then, the testing data set, which is not applied in the training stage, is then used to test the prediction capabilities of the model. The XGBoost is a boosting method based on decision trees, which utilize gradient descent to optimize the loss function step by step. To achieve a better prediction accuracy and avoid overfitting, XGBoost adds the regularization term to its loss function. XGBoost tries to optimize an objective function that consists of two parts, namely loss and regularization [34]:

$$\mathcal{L}^{(t)} = \sum_{i=1}^{n} l\left(y_i, \hat{y}_i^{(t-1)} + f_t(x_i)\right) + \Omega(f_t). \tag{6.1}$$

Here, l represents the loss function employed to measure the difference between the true value y_i and the estimated value $\hat{y}_i$. f_t is the model for the (t)-th decision tree, and (t) is the number of iterations of the boosting algorithm. The definition of the regularization parameter $\Omega(f_t)$ is described as follows:

$$\Omega(f) = \gamma T + \frac{1}{2}\lambda \|w\|^2,$$

where T is the number of leaf nodes, γ and λ are regularization coefficients, and w represents the vector of leaf scores.

The similarity scores are as follows:

$$SS(I) = \frac{\left(\sum_{i\in I} g_i\right)^2}{\sum_{i\in I} h_i + \lambda},$$

where g_i denotes the first-order gradient, and h_i denotes the second-order gradient (Hessian) of the loss function with respect to the predicted value $\hat{y}_i$. The set I contains all observations assigned to a particular node. A comprehensive description of the XGBoost methodology is provided by Chen and Guestrin [34].

6.1. NCWD-inspired loss function

For this research, the standard XGBoost regression objective was substituted for a user-defined objective function by employing the novel NCWD distribution. In particular, the negative log-likelihood from the NCWD distribution was applied as the loss function, thus allowing for the optimization process to take place according to the probability structure of the response variable. Hence, the negative log-likelihood of PDF defined in Eq (2.2) is as follows:

$$\begin{aligned}\ell_i(\psi_1,\psi_2) = &-\log\left(\frac{\pi}{4}\right) - \log(\psi_1) - \log(\psi_2) - (\psi_2 - 1)\log(z_i) + 2\log\left(1 - e^{\psi_1 z_i^{\psi_2}}\right)\\ &+ \psi_1 z_i^{\psi_2} + \left(e^{\psi_1 z_i^{\psi_2}} - 1\right)^{-1} + 2\log\sin\left(\frac{\pi}{4}\left(2 - e^{-(e^{\psi_1 z_i^{\psi_2}} - 1)^{-1}}\right)\right).\end{aligned} \tag{6.2}$$

Both parameters must be positive, and we apply an exponential log-link function to the raw margin arrays predicted by the respective parallel tree branche's $\hat{y_1}$ and $\hat{y_2}$, as follows:

$$\psi_1 = e^{\hat{y}_1} > 0 \quad \text{and} \quad \psi_2 = e^{\hat{y}_2} > 0, \quad \text{where } y_1, y_2 \in \mathbb{R}.$$

Now, the negative log-likelihood becomes the following:

$$\ell_i(\psi_1,\psi_2) = -\log(z_i;\, e^{\hat{y}_1}, e^{\hat{y}_2}).$$

Therefore, the NCWD-XGBoost objective function at the boosting iteration t becomes the following:

$$\mathcal{L}^{(t)} = \sum_{i=1}^{n} \ell(\hat{y}_{1,i}^{(t-1)} + f_{1,t}(x_i),\, \hat{y}_{2,i}^{(t-1)} + f_{2,t}(x_i)) + \Omega(f_t), \tag{6.3}$$

where $\Omega(f_t)$ denotes the regularization penalty on the newly added tree.

According to the XGBoost methodology, the objective function given in Eq (6.3) is approximated through a second-order Taylor expansion based on the current prediction, which enables us to derive the split criteria and the optimal leaf weight parameters w_i as follows:

$$\mathcal{L}^{(t)} \approx \sum_{i=1}^{n} \left[\ell_i^{(t-1)} + g_{1i} f_{1,t}(x_i) + g_{2i} f_{2,t}(x_i) + \frac{1}{2} h_{1i} f_{1,t}^2(x_i) + \frac{1}{2} h_{22i} f_{2,t}^2(x_i) + \frac{1}{2} h_{2i} f_{2,t}^2(x_i) \right] + \Omega(f_t).$$

Therefore, gradients (g) and Hessians (h) for both parameters are

$$g_{1i} = \psi_1 \left(\frac{\partial \ell_i}{\partial \psi_1} \right), \quad g_{2i} = \psi_2 \left(\frac{\partial \ell_i}{\partial \psi_2} \right),$$

and

$$h_{1i} = \psi_1^2 \frac{\partial^2 \ell_i}{\partial \psi_1^2} + \psi_1 \frac{\partial \ell_i}{\partial \psi_1}, \quad h_{2i} = \psi_2^2 \frac{\partial^2 \ell_i}{\partial \psi_2^2} + \psi_2 \frac{\partial \ell_i}{\partial \psi_1}, \quad h_{22i} = \psi_1 \psi_2 \frac{\partial^2 \ell_i}{\partial \psi_1 \partial \psi_2}.$$

Thus, the second-order Taylor expansion reduces the objective function, defined with the help of NCWD, to an easy-to-handle form which only uses the first and second derivatives of the loss function. This method allows for the effective calculation of the leaf weights and splitting gains in the XGBoost system. As a result, the presented NCWD-XGBoost model is trainable via the same approach as the traditional XGBoost model but with an additional NCWD-based loss function.

For the empirical assessment of the custom loss parametric approach, we use the classical Miles per Gallon (MPG) benchmarking dataset that is provided by the StatLib library from Carnegie Mellon University [35]. The dataset includes structural and performance attributes of 398 automobiles produced within the 1970–1982 time frame and can be accessed via the Seaborn library. The response variable was MPG, while independent variables included car attributes such as cylinders, displacement, horsepower, weight, acceleration, model year, origin of manufacture attributes, and names of cars in one-hot encoded format. The datasets was randomly split into training and test datasets with a ratio of 80 : 20 (test_size = 0.20) and random state equal to 42 (random_state = 42). The predictive accuracy of the proposed NCWD-XGBoost model was compared with the standard XGBoost loss functions, which include squared error and absolute error. For the NCWD-XGBoost model, the MSE was found to be 6.8273, RMSE was calculated as 2.6129, MAE was determined as 1.8632, and R^2 was equal to 0.8662. On the other hand, the XGBoost model with squared error loss function gave an MSE of 7.6761, RMSE of 2.7706, MAE of 1.9984, and an R^2 value of 0.8496. The same way XGBoost model with absolute error loss function produced an MSE of 7.4704, RMSE of 2.7332, MAE of 2.0561, and an R^2 value of 0.8536. The results are summarized in Table 20.

Table 20. Comparative predictive performance of NCWD-XGBoost and standard XGBoost loss functions on the MPG dataset.

Model	MSE	RMSE	MAE	R^2
NCWD-XGBoost	6.8273	2.6129	1.8632	0.8662
XGBoost (squared error)	7.6761	2.7706	1.9984	0.8496
XGBoost (absolute error)	7.4704	2.7332	2.0561	0.8536

The findings from Table 20 reveal that the NCWD-based loss function is better than the standard squared error and absolute error loss functions on all the measures used for evaluation. In particular, the NCWD-XGBoost model has the least values for MSE, RMSE, and MAE, while having the highest coefficient of determination (R^2). Relative to the squared error objective, the proposed approach decreases the MSE value by approximately 11.06% and the RMSE by 5.69%.

Figure 12 illustrates the comparison between the real value and the predicted values through NCWD-XGBoost, squared-error XGBoost, and absolute-error XGBoost models. All these models show that their predicted values almost perfectly coincide with the line of perfect prediction, thus proving their successful predictions. However, among them, the newly proposed NCWD-XGBoost model shows the closest fit to the actual values by giving the highest ($R^2 = 0.8662$) value, then the absolute-error XGBoost ($R^2 = 0.8536$) and squared-error XGBoost ($R^2 = 0.8496$).

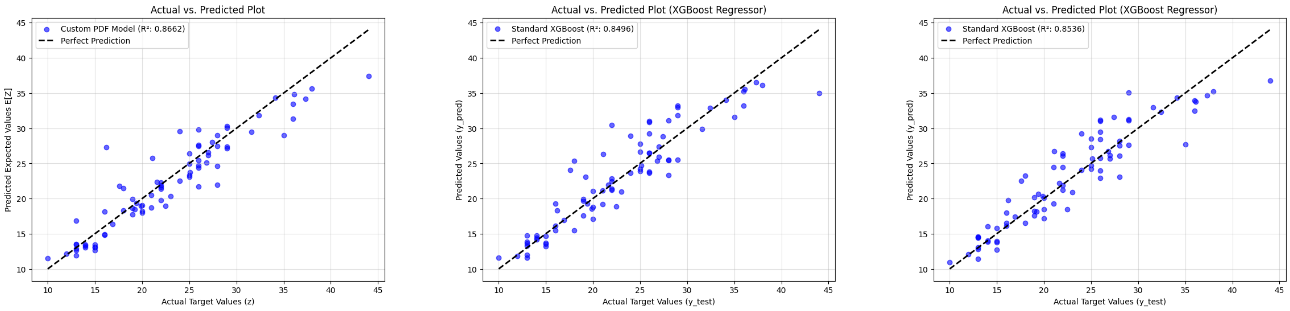

(a) NCWD-XGBoost. **(b)** Squared error. **(c)** Absolute error.

Figure 12. Actual versus predicted values obtained from XGBoost models using (a) NCWD loss, (b) squared-error loss, and (c) absolute-error loss. The proposed NCWD-XGBoost model exhibits the closest agreement with the observed values, thus indicating superior predictive performance.

The SHapley Additive exPlanations (SHAP) summary plot for the parameter ψ_1 is shown in Figure 13 panel (a). From the figure, weight was found to be the most important feature, while the other features were model year, horsepower, and displacement. The higher values of these features contributed to positive SHAP values, which led to the rise in estimation of ψ_1 . Conversely, the lower values resulted in negative values of SHAP values, thereby decreasing the estimation of ψ_1. The features of vehicle origin, number of cylinders, and vehicle names gave SHAP values near zero. This shows that the vehicle size and engine are the key factors affecting parameter ψ_1, and Figure 13 panel (b) shows the SHAP summary plot for the variable ψ_2. Engine displacement was the most important predictor variable, followed by vehicle weight, model year, and horsepower. Larger values of displacement, weight, and horsepower resulted in more positive SHAP values, and hence, increased the value of the estimated ψ_2 . Newer model years were associated with negative SHAP values, thus implying a decrease in the parameter estimate. The effect of acceleration, cylinders, and origin was found to have a comparatively insignificant effect, and that of name variables was the negligible. This means that the parameter ψ_2 in NCWD depends on the engine size and weight of the car.

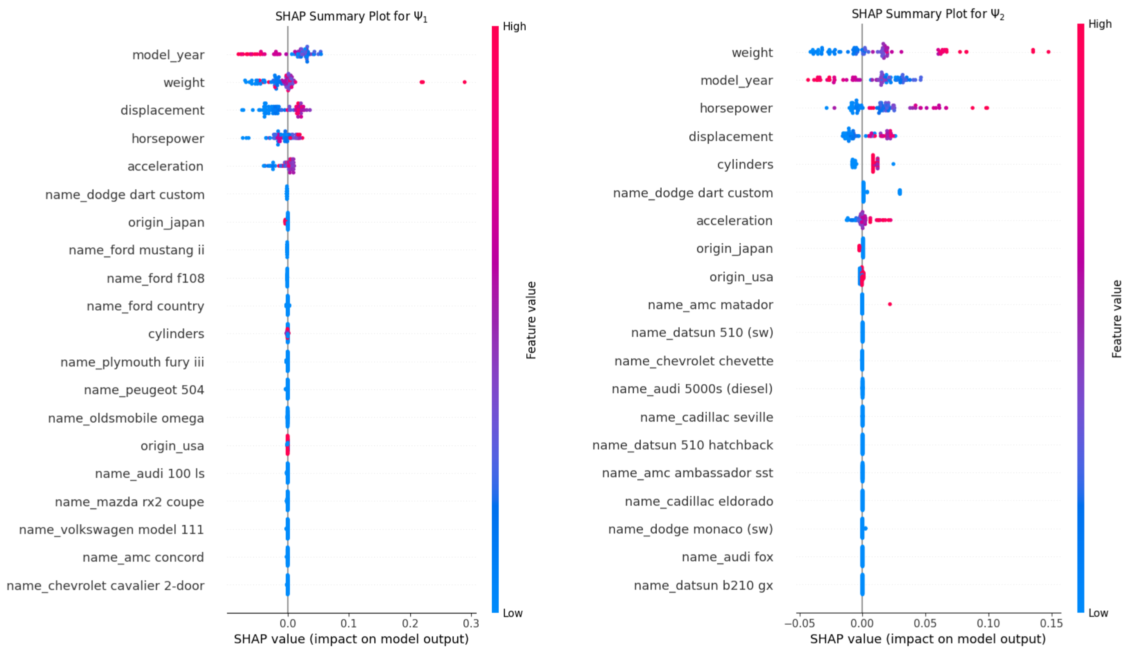

(a) ψ_1 **(b)** ψ_2

Figure 13. SHAP summary plots for the NCWD-XGBoost model. Panel (a) illustrates the contribution of explanatory variables to the estimation of parameter ψ_1, while panel (b) presents the corresponding effects on parameter ψ_2. Features are ranked according to their importance, and the color gradient indicates the magnitude of feature values.

7. Conclusions

This investigation offers the novel cotangent-Φ (NC-Φ) family, which is a new class of distributions based on the cotangent function. This technology makes it simpler to develop trigonometric distributions based on established baseline models, thereby exhibiting a greater flexibility in modeling complicated data than the original baselines. A comprehensive examination was provided for a specific member of this family: the NCWD. The study includes derivations of its fundamental statistical functions, such as the CDF and PDF, along with a detailed analysis of its moments. For robust parameter estimation, we employed both non-Bayesian and Bayesian techniques. To examine its functional significance, we fitted the suggested distribution to two real-world datasets: active maintenance periods for an aerial transceiver and vehicle inter-arrival times at a roadside position. The framework's capacity to capture complex data structures was validated by the empirical results, thus suggesting that it has important implications in fields including biology, actuarial science, and reliability engineering. We found that the NCWD provides a better fit to the data, a conclusion that is clearly supported by the results in Tables 17–19. We think that this distribution might be a viable option for a number of applications that require probabilistic models that are both theoretically tractable and adaptable. It is important to notice that the current analysis is restricted to the case of finite samples only, since no theoretical studies have been carried out on asymptotic properties of the estimators such as consistency, asymptotic normality, and efficiency. In addition, no consideration has been given to the computational properties of the estimators, (i.e, running time and speed of convergence). Consequently, the obtained results can only be used for particular settings in simulations; any general recommendations cannot be drawn from this research.

Data availability

All data supporting the findings of this study are fully available in the article and are clearly cited.

Author contributions

Aijaz Ahmad: Conceptualization, methodology, Theory development and formal analysis; Farouq Mohammad A. Alam: Formal analysis, simulations and data curation; Andaç Batur Çolak: Machine learning, formal analysis and interpretation of results; Aafaq A. Rather: Supervision, validation, manuscript review and editing of manuscripts; Mahmoud E. Bakr: Investigation, interpretation of results, interpretation and final manuscript. All authors have read and approved the final version of the manuscript for publication.

Use of Generative-AI tools declaration

The authors declare that they have not used Artificial Intelligence (AI) tools in the creation of this article.

Acknowledgments

The authors would like to thank the Ongoing Research Funding Program (ORF-2026-1004), King Saud University, Riyadh, Saudi Arabia, for funding this research.

Conflict of interest

There is no conflict of interest.

References

1. A. Aijaz, N. Alsadat, N. A. Mintode, S. Q. ul Ain, A. Afaq, M. G. Ahmed, et al., A new hyperbolic sine-generator with an example of Rayleigh distribution: simulation and data analysis in industry, *Alex. Eng. J.*, **73** (2023), 415–426.
2. A. Ahmad, Y. Tashkandy, A. A. Rather, M. E. Bakr, E. Hussam, A. M. Gemeay, Novel family of probability generating distributions: properties and data analysis, *Phys. Scr.*, **99** (2024), 125007. https://doi.org/10.1088/1402-4896/ad8821

3. A. Aijaz, A. A. Rather, Y. A. Tashkandy, M. E. Bakr, M. M. Mohie El-Din, Deriving the new cotangent Fréchet distribution with real data analysis, *Alex. Eng. J.*, **100** (2024), 12–24.
4. I. Ali, A. H. Khan, A. A. Rather, T. R. Jan, K. Osmanli, A. Volodin, On a transmuted distribution based on log-logistic and ailamujia hazard functions with application to lifetime data, *Lobachevskii J. Math.*, **45** (2024), 1557–1569. https://doi.org/10.1134/s1995080224601620
5. H. M. Almongy, E. M. Almetwally, A. E. Mubarak, Marshall-Olkin alpha power Lomax distribution: estimation methods, application on physics and economics, *Pak. J. Stat. Oper. Res.*, **17** (2021), 137–153.
6. R. L. Smith, J. C. Naylor, A comparison of maximum likelihood and Bayesian estimation for the three parameter Weibull distribution, *J. R. Stat. Soc. Ser. C Appl. Stat.*, **36** (1987), 358–369.
7. D. Kumar, U. Singh, S. K. Singh, A new distribution using sine function: its application to bladder cancer patients data, *J. Stat. Appl. Probab.*, **4** (2015), 417–427.
8. Y. Wang, S. Lv, Z. Zhuang, O. Albalawi, H. M. Alshanbari, A novel probabilistic model: simulation and modeling the time duration in musical education and engineering, *Alex. Eng. J.*, **106** (2024), 392–402. https://doi.org/10.1016/j.aej.2024.06.094
9. C. Deng, W. Chen, Weighted exponential parameters estimation using maximum ranked set sampling with unequal samples, *Commun. Stat. Simul. Comput.*, **55** (2026), 262–285.
10. C. Deng, W. Chen, Y. Zhou, S. K. Khosa, R. Yang, Maximum likelihood estimation of the parameters of weighted exponential distribution in simple random sampling and ranked set sampling, *Appl. Math. J. Chin. Univ. Ser. B*, **40** (2025), 818–832.
11. A. A. Rather, C. Subramanian, A new exponentiated distribution with engineering science applications, *J. Stat. Appl. Probab.*, **9** (2020), 127–137. https://doi.org/10.18576/jsap/090112
12. A. A. Rather, M. Azeem, M. Alam, C. Subramanian, G. Ozel, I. Ali, Weighted Erlang-truncated exponential distribution: system reliability optimization, structural properties, and simulation, *Lobachevskii J. Math.*, **45** (2024), 4311–4337. https://doi.org/10.1134/S1995080224605009
13. D. Qayoom, A. A. Rather, Weighted transmuted Mukherjee-Islam distribution with statistical properties, *Reliab. Theory Appl.*, **19** (2024), 124–137. https://doi.org/10.24412/1932-2321-2024-278-124-137
14. D. Qayoom, A. A. Rather, A comprehensive study of Length-Biased Transmuted distribution, *Reliab. Theory Appl.*, **19** (2024), 291–304. https://doi.org/10.24412/1932-2321-2024-278-291-304
15. E. S. Alotaibi, N. E. Alsubaie, D. Qayoom, A. A. Rather, A novel extension of Burhan distribution: theoretical properties, simulation study and practical application, *Lobachevskii J. Math.*, **45** (2025), 6224–6243. https://doi.org/10.1134/S1995080224607574
16. D. Qayoom, A. A. Rather, O. A. Alqasem, Z. Ahmad, M. Nagy, A. M. Yousuf, et al., Development of a novel extension of Rayleigh distribution with application to COVID-19 data, *Sci. Rep.*, **15** (2025), 18535. https://doi.org/10.1038/s41598-025-03645-w
17. D. Qayoom, A. A. Rather, E. S. Alotaibi, B. A. Shukr, A. A. Almazmomi, A. O. Alshammari, A novel extension of the power Lindley distribution with statistical properties and application to COVID-19 data, *Sci. Rep.*, **15** (2025), 30486. https://doi.org/10.1038/s41598-025-15256-6

18. B. Singh, I. Alam, A. A. Rather, M. Alam, Linear combination of order statistics of exponentiated Nadarajah-Haghighi distribution and their applications, *Lobachevskii J. Math.*, **44** (2023), 4839–4848. https://doi.org/10.1134/S1995080223110318
19. Z. Ahmad, Z. Almaspoor, F. Khan, M. El-Morshedy, On predictive modeling using a new flexible Weibull distribution and machine learning approach: analyzing the COVID-19 data, *Mathematics*, **10** (2022), 1792. https://doi.org/10.3390/math10111792
20. A. A. Rather, A. R. El-Saeed, D. Qayoom, Z. Ahmad, H. E. Semary, G. T. Mekiso, et al., Quality assurance through truncated life tests under the Lomax distribution, *Sci. Rep.*, **15** (2025), 24822. https://doi.org/10.1038/s41598-025-10164-1
21. D. Qayoom, A. A. Rather, A. Volodin, O. Supapueng, A. H. Khan, F. Danish, DUS exponential distribution: properties and applications, *Lobachevskii J. Math.*, **46** (2026), 5213–5228. https://doi.org/10.1134/S199508022560966X
22. A. Xu, Y. Miao, J. Sun, S. Zhou, Y. Tang, A hierarchical Bayesian multivariate Wiener process model with dependent degradation rates and volatilities, *IEEE Trans. Reliab.*, **75** (2026), 1420–1433. https://doi.org/10.1109/TR.2026.3674703
23. A. Xu, Y. Chen, B. Li, Q. Zhang, A bivariate Wiener degradation model with partially random scale weights, *Reliab. Eng. Syst. Saf.*, **275** (2026) 112684. https://doi.org/10.1016/j.ress.2026.112684
24. T. Liu, R. Xue, A convergent multi-step efficient iteration method to solve nonlinear equation systems, *J. Appl. Math. Comput.*, **71** (2025) 2571–2588. https://doi.org/10.1007/s12190-024-02324-9
25. T. Liu, B. Ding, A radial basis function neural network approach for solving a diffusion partial differential equation efficiently, *Appl. Math. Comput.*, **509** (2026) 129651. https://doi.org/10.1016/j.amc.2025.129651
26. Y. Liu, Y. Li, T. Liu, An RBF-FD method for pricing under the Bates model: handling stochastic volatility and jump processes, *Eng. Anal. Bound. Elem.*, **183** (2026) 106622. https://doi.org/10.1016/j.enganabound.2025.106622
27. H. Song, Q. Tan, A unified framework for high-order compact finite differences based on polyharmonic spline RBF, *Calcolo*, **63** (2026) 00684.
28. A. Aijaz, A. A. Rather, O. A. Alqasem, M. E. Bakr, G. T. Mekiso, O. S. Balogun, et al., Introducing novel arc cosine-Ψ class of distribution with theory and data evaluation related to coronavirus, *Sci. Rep.*, **15** (2025), 13069.
29. A. S. Alghamdi, M. M. Abd El-Raouf, A new alpha power cosine-Weibull model with applications to hydrological and engineering data, *Mathematics*, **11** (2023), 673. https://doi.org/10.3390/math11030673
30. S. Nanga, S. Nasiru, J. Dioggban, Tangent Topp-Leone family of distributions, *Sci. Afr.*, **17** (2022), e01363. https://doi.org/10.1016/j.sciaf.2022.e01363
31. H. R. Varian, *A Bayesian approach to real estate assessment*, Amsterdam: North-Holland Publishing Company, 1975, 195–208.

32. B. Jorgensen, *Statistical properties of the generalized inverse Gaussian distribution*, New York: Springer-Verlag, 1982.

33. N. A. H. Abdelfattah, R. M. Sayed, Comparative efficacy of gamma and microwave radiation in protecting peppermint from infestation by drugstore beetle (Stegobium paniceum) L., *Int. J. Trop. Insect Sci.*, **42** (2022), 1367–1372.

34. T. Chen, C. Guestrin, XGBoost: a scalable tree boosting system, *KDD'16: Proceedings of the 22nd ACM SIGKDD International Conference on Knowledge Discovery and Data Mining*, 2016, 785–794. https://doi.org/10.1145/2939672.2939785

35. J. R. Quinlan, Combining instance-based and model-based learning, *Proceedings of the Tenth International Conference on Machine Learning*, 1993, 236–243.

Appendix

Appendix A

To check that the CDF, $F(z;\zeta)$, defined in Eq (1.1) is valid when it satisfies the following properties:
(1) Non-decreasing monotonicity:

$$F(a;\zeta) \le F(b;\zeta) \quad \text{for all } a < b.$$

(2) Right-continuity:

$$\lim_{z\to z_0^+} F(z;\zeta) = F(z_0;\zeta).$$

(3) Boundary conditions:

$$\lim_{z\to-\infty} F(z;\zeta) = 0 \quad \text{and} \quad \lim_{z\to\infty} F(z;\zeta) = 1.$$

Proof of validity for the cotangent-Φ family CDF.
Step 1: Monotonicity

Let

$$g(z) = \frac{\pi}{4}\left(2 - e^{-\frac{\bar{\Phi}(z;\zeta)}{\Phi(z;\zeta)}}\right).$$

Since $\Phi(z;\zeta)$ is non-decreasing (property of CDFs), the ratio:

$$r(z) = \frac{\bar{\Phi}(z;\zeta)}{\Phi(z;\zeta)} = \frac{1-\Phi(z;\zeta)}{\Phi(z;\zeta)}$$

is non-increasing. Consequently, $e^{-r(z)}$ is non-decreasing, making $2-e^{-r(z)}$ non-increasing. Multiplying by $\pi/4$ preserves the monotonicity, so $g(z)$ is non-increasing. The cotangent function, $\cot(x)$, is strictly decreasing on $(0,\pi)$. Since $g(z) \in (\pi/4, \pi/2]$, the composition $\cot(g(z))$ is non-decreasing. Thus, $F(z;\zeta)$ is non-decreasing.
Step 2: Right-Continuity

The baseline $\Phi(z;\zeta)$ is right-continuous by definition. The functions e^{-x}, $\cot(x)$, and rational combinations preserve right-continuity. Therefore, $F(z;\zeta)$ is right-continuous.
Step 3: Boundary conditions As $z \to -\infty$,

$$\Phi(z;\zeta) \to 0^+ \Rightarrow r(z) \to \infty \Rightarrow e^{-r(z)} \to 0 \Rightarrow g(z) \to \frac{\pi}{4}\cdot 2 = \frac{\pi}{2}.$$

Thus, $F(z;\zeta) \to \cot(\pi/2) = 0$. As $z \to \infty$,

$$\Phi(z;\zeta) \to 1^- \Rightarrow r(z) \to 0^+ \Rightarrow e^{-r(z)} \to 1 \Rightarrow g(z) \to \frac{\pi}{4} \cdot (2-1) = \frac{\pi}{4}.$$

Thus, $F(z;\zeta) \to \cot(\pi/4) = 1$.

Step 4: Range of $g(z)$

Since $r(z) > 0$ for finite z, we have $0 < e^{-r(z)} < 1$, so

$$1 < 2 - e^{-r(z)} < 2 \quad \Rightarrow \quad \frac{\pi}{4} < g(z) < \frac{\pi}{2}.$$

Thus, $g(z)$ lies within the interval where cot is continuous and strictly decreasing. $F(z;\zeta)$ satisfies all properties of a valid CDF. □

Appendix B

$$\begin{aligned}
\frac{\partial \ell_i}{\partial \psi_1} &= -\frac{1}{\psi_1} + z_i^{\psi_2} + \frac{2z_i^{\psi_2}}{e^{\psi_1 z_i^{\psi_2}} - 1} - \frac{z_i^{\psi_2} e^{\psi_1 z_i^{\psi_2}}}{(e^{\psi_1 z_i^{\psi_2}} - 1)^2} \\
&\quad - \frac{\pi}{2} \cot\left(\frac{\pi}{4}\left(2 - e^{-(e^{\psi_1 z_i^{\psi_2}} - 1)^{-1}}\right)\right) e^{-(e^{\psi_1 z_i^{\psi_2}} - 1)^{-1}} \frac{z_i^{\psi_2} e^{\psi_1 z_i^{\psi_2}}}{(e^{\psi_1 z_i^{\psi_2}} - 1)^2}, \\
\frac{\partial \ell_i}{\partial \psi_2} &= -\frac{1}{\psi_2} - \log(z_i) + \psi_1 z_i^{\psi_2} \log(z_i) + \frac{2\psi_1 z_i^{\psi_2} \log(z_i)}{e^{\psi_1 z_i^{\psi_2}} - 1} \\
&\quad - \frac{\psi_1 z_i^{\psi_2} \log(z_i)\, e^{\psi_1 z_i^{\psi_2}}}{(e^{\psi_1 z_i^{\psi_2}} - 1)^2} \\
&\quad - \frac{\pi}{2} \cot\left(\frac{\pi}{4}\left(2 - e^{-(e^{\psi_1 z_i^{\psi_2}} - 1)^{-1}}\right)\right) e^{-(e^{\psi_1 z_i^{\psi_2}} - 1)^{-1}} \frac{\psi_1 z_i^{\psi_2} \log(z_i)\, e^{\psi_1 z_i^{\psi_2}}}{(e^{\psi_1 z_i^{\psi_2}} - 1)^2}, \\
\frac{\partial^2 \ell_i}{\partial \psi_1^2} &= \frac{1}{\psi_1^2} + z_i^{2\psi_2} \frac{\partial}{\partial(\psi_1 z_i^{\psi_2})}\Bigg[1 + \frac{2}{e^{\psi_1 z_i^{\psi_2}} - 1} - \frac{e^{\psi_1 z_i^{\psi_2}}}{(e^{\psi_1 z_i^{\psi_2}} - 1)^2} \\
&\quad - \frac{\pi}{2} \cot\left(\frac{\pi}{4}\left(2 - e^{-(e^{\psi_1 z_i^{\psi_2}} - 1)^{-1}}\right)\right) e^{-(e^{\psi_1 z_i^{\psi_2}} - 1)^{-1}} \frac{e^{\psi_1 z_i^{\psi_2}}}{(e^{\psi_1 z_i^{\psi_2}} - 1)^2}\Bigg].
\end{aligned}$$

Likewise,

$$\frac{\partial^2 \ell_i}{\partial \psi_2^2} = \frac{1}{\psi_2^2} + \psi_1 z_i^{\psi_2} \log^2 z_i\, A_i + \left(\psi_1 z_i^{\psi_2} \log z_i\right)^2 A_i',$$

and

$$\frac{\partial^2 \ell_i}{\partial \psi_1 \partial \psi_2} = z_i^{\psi_2} \log(z_i)\, A_i + \psi_1 z_i^{2\psi_2} \log(z_i)\, A_i',$$

where

$$
\begin{aligned}
A_i = 1 &+ \frac{2}{e^{\psi_1 z_i^{\psi_2}} - 1} - \frac{e^{\psi_1 z_i^{\psi_2}}}{(e^{\psi_1 z_i^{\psi_2}} - 1)^2} \\
&- \frac{\pi}{2} \cot\left(\frac{\pi}{4}\left(2 - e^{-(e^{\psi_1 z_i^{\psi_2}}-1)^{-1}}\right)\right) e^{-(e^{\psi_1 z_i^{\psi_2}}-1)^{-1}} \frac{e^{\psi_1 z_i^{\psi_2}}}{(e^{\psi_1 z_i^{\psi_2}} - 1)^2},
\end{aligned}
$$

and

$$A_i' = \frac{\partial A_i}{\partial(\psi_1 z_i^{\psi_2})}.$$